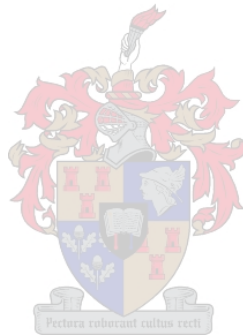


# Thermal Characteristics of a Greenhouse for Aquaculture

G.R. Branfield



Thesis presented in partial fulfilment of the requirements for the degree of  
Master of Science in Mechanical Engineering at the University of  
Stellenbosch.

Thesis supervisor: Prof. D.G. Kröger

April 2006

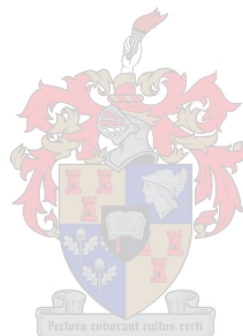
# Declaration

---

I, the undersigned, hereby declare that the work contained in this thesis is my own original work and that I have not previously in its entirety or part submitted it at any university for a degree.

Signature: .....

Date: .....



# Abstract

---

Successful housing and breeding of exotic animals or plants often requires an environment that is quite different to the ambient conditions present. The current study approached the problem of sub-optimal water temperatures experienced by Central African Bream (*Tilapia*) housed within a South African greenhouse during winter months. A theoretical and experimental study of fundamental heat and mass transfer processes relevant to an aquacultural greenhouse was conducted. Experimental results were generally in agreement with those of previous researchers; while evaporation tests were found to concur particularly well with an analytical equation developed. The experimental results were used to develop a simple glass greenhouse model to evaluate the expected thermal behaviour during the coldest time of the year. Manipulation of the model revealed that water has the ability to absorb large quantities of solar radiation and regulate temperature fluctuations within such a system, and that the appropriate use of thermal insulation during both the night and day can maintain acceptable water temperatures for extended periods of time. With the conclusions drawn from the experimentation and modelling done, an optimised conceptual greenhouse design was presented, along with associated guidelines and principles for attaining the required water temperatures, and consequently providing the exotic fish specie with a healthy environment.

# Opsomming

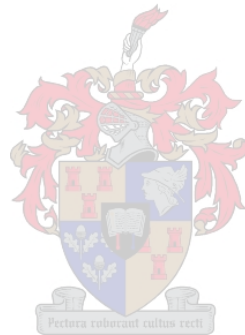
---

Daar bestaan dikwels omgewings toestande wat verskil van die wat ideaal is vir die teel en aanhou van eksotiese plante en diere, daarom is dit partykeer noodsaaklik om deur middel van tegniese innovasie die regte toestande na te streef vir suksesvolle resultate. Die huidige studie benader die probleem ondervind deur Kurpers van Sentrale Afrika wat bloodgestel is aan sub-optimale water temperature binne 'n Suid Afrikaanse kweekhuis gedurende winter maande. 'n Teoretiese en eksperimentele studie van fundamentele hitte en massa oordrag prosesse relevant tot aquakultuur kweekhuise is onderneem. Eksperimentele resultate het in die algemeen met die van vorige navorsers saamgestem en verdampingstoetse het veral goed gepas by 'n nuut ontwikkelde vergelyking. Die eksperimentele resultate is gebruik om 'n eenvoudige glas kweekhuis te ontwikkel wat die verwagte termiese gedrag kan evalueer gedurende die koudste maande van die jaar. Manipulasie van die model het gewys dat water die vermoë het om groot hoeveelhede sonstraling te absorbeer en om temperatuur veranderinge te reguleer in so 'n stelsel. Dit is verder gewys dat die regte gebruik van termiese insulasie gedurende dae en nagte 'n aanvaarbare water temperature oor lang periodes kan waarborg. 'n Optimeerde kweekhuis konsep ontwerp is voorgestel deur gebruik te maak van eksperimentele resultate en van analitiese modelle. Riglyne is ook voorgestel vir die behaling van korrekte water temperature wat 'n gesonde omgewing vir eksotiese plante en diere waarborg.

# Dedication

---

This thesis is dedicated to those who make it all worthwhile, my loving and supportive family and my insanely crazy friends, with an insatiable zest for life.



# Acknowledgements

---

The financial assistance of the National Research Foundation (NRF) towards this research is hereby acknowledged. Opinions expressed and presented conclusions are those of the author and are not necessarily to be attributed to the National Research Foundation.

The author wishes to acknowledge the contributions of the following people:

Prof. D.G. Kröger, for supervising this study and providing invaluable guidance during both undergraduate and postgraduate projects, for promoting great aspirations and the long discussions about the “important things in life.”

Dr. D. Brink, for organising financial assistance towards the current research; also for introducing the author to the field of Aquaculture and for help and friendship throughout the duration of this study.

Mr. C. Zietsman, for his enthusiasm towards this project and assistance with the associated experimental work.

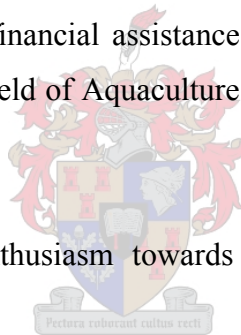


# Table of Contents

---

Declaration	
Abstract	i
Opsomming ( <i>Afrikaans</i> )	ii
Dedication	iii
Acknowledgements	iv
Table of Contents	v
List of Tables	viii
List of Figures	ix
Nomenclature	xii

## **Chapter 1: Introduction**

1.1	Background	1
1.2	Problem statement and objectives	2
1.3	Engineering approach	4
1.4	Literature study	5
1.5	Overview of chapters	8



## **Chapter 2: Convective- and evaporative heat transfer from a horizontal surface**

2.1	An analytical approach	9
2.2	Experimental convective heat transfer coefficient from a horizontal surface exposed to the natural environment	9
2.2.1	Experimental apparatus and procedure	10
2.2.2	Results obtained	12
2.3	Evaporation from a water surface exposed to the natural environment	13
2.3.1	Analysis	14
2.3.2	Experimental apparatus and procedure	16
2.3.3	Results and discussion	17
2.4	Conclusion	23

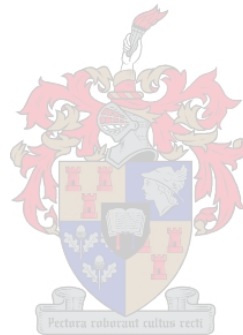
<b>Chapter 3:</b>	<b>Thermal behaviour and energy storage of water</b>	
3.1	Storage of solar energy in water	25
3.2	Open body of water exposed to the natural environment	26
3.2.1	Analysis	26
3.2.2	Experimental setup and procedure	28
3.2.3	Results and discussion	29
3.3	Solar collector with plastic covered water tank	33
3.3.1	Analysis	33
3.3.2	Experimental apparatus and procedure	34
3.3.3	Results and discussion	36
3.4	Solar collector with condensation	40
3.5	Conclusion	46
<b>Chapter 4:</b>	<b>Thermal behaviour and energy storage of water</b>	
4.1	Modelling objectives	48
4.2	Fundamental system	49
4.2.1	Analysis	49
4.2.1.1	Flat glass roof	52
4.2.1.2	Vertical glass walls	54
4.2.1.3	Concrete floor	56
4.2.1.4	Enclosed air	57
4.2.2	Simulation results	57
4.3	Night-time insulation usage	60
4.4	Day and night-time insulation usage	62
4.5	Conclusion	63
<b>Chapter 5:</b>	<b>Aspects of greenhouse design</b>	
5.1	System considerations	65
5.2	Proposed improved design	65
5.3	Aspects of optimal design analysis	68
5.4	Welgevallen system analysis	73
<b>Chapter 6:</b>	<b>Conclusion</b>	
6.1	Research findings	78

6.2	Greenhouse conclusions	80
6.3	Further investigation	82
<b>References</b>		83
<b>Appendix A: Solar Radiation</b>		
A.1	Direction of beam radiation	A.1
A.2	Ratio of beam radiation on tilted surface to that on horizontal surface	A.4
<b>Appendix B: Evaporation</b>		
B.1	Analysis – Evaporation from a water surface	B.1
B.2	Analysis – Temperature gradient within water layer	B.9
B.3	Evaporation pan photograph	B.10
B.4	Numerical example (section 2.3)	B.11
<b>Appendix C: Water tank experiments</b>		
C.1	Open water tank photograph and spindle drawing	C.1
C.2	Numerical example (section 3.2)	C.2
C.3	Solar collector with plastic-covered water tank: Photograph and analysis	C.9
C.4	Numerical example (section 3.3)	C.15
<b>Appendix D: Water tank solar characteristics</b>		
D.1	Cover solar characteristics	D.1
D.2	Absorber plate effective absorptivity	D.4
<b>Appendix E: Greenhouse sunlight properties</b>		
E.1	Area of transmitted sunlight	E.1

# List of Tables

---

Table 2.1:	Comparison between cumulative evaporation rates.	22
Table B.1:	Evaporation pan experimental data on April 14 <sup>th</sup> 2005 at 12.494 h.	B.11
Table C.1:	Experimental data and physical parameters of water tank.	C.2
Table C.2:	Experimental data and physical parameters of plastic covered water tank.	C.15



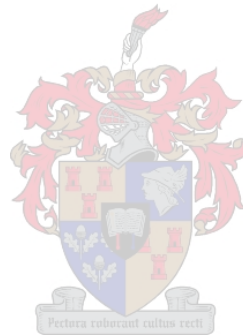
# List of Figures

---

Figure 1.1: Author at Welgevallen tilapia system.	3
Figure 2.1: Experimental apparatus used for determining convection heat transfer coefficient.	11
Figure 2.2: Comparison between predicted and measured dimensionless convective heat transfer coefficients.	13
Figure 2.3: Heat fluxes present on water surface exposed to natural environment.	14
Figure 2.4: Absorptivity of water.	15
Figure 2.5: Front and top views of evaporation pan.	16
Figure 2.6: Solar irradiation and wind speed readings on 13/14 April 2005	20
Figure 2.7: Measured water-, ambient air and dew point temperatures.	21
Figure 2.8: Comparative evaporation rates during daytime operation.	22
Figure 2.9: Predicted evaporation rates compared over period of 24 hours.	23
Figure 3.1: Drawing of water tank with associated heat fluxes.	27
Figure 3.2: Front and top views of experimental setup.	29
Figure 3.3: Solar irradiation and wind speed readings	30
Figure 3.4: Ambient air-, water surface- and dew-point temperatures.	31
Figure 3.5: Water temperature distribution.	31
Figure 3.6: Comparative evaporation rates.	32
Figure 3.7: Schematic drawing of solar collector with plastic-covered water tank.	33
Figure 3.8: Experimental apparatus.	35
Figure 3.9: Total solar irradiation and wind speed readings.	36
Figure 3.10: Water temperature profile.	37
Figure 3.11: Ambient air temperature and predicted- and measured glass cover and mean water temperatures.	38
Figure 3.12: Results from same analysis as above, including effect of glass cover stored energy.	38
Figure 3.13: Ambient air temperature and predicted- and measured glass cover and mean water temperatures during the night.	39
Figure 3.14: Ambient air temperature and predicted- and measured glass cover and mean water temperatures with Sisalation usage.	40

Figure 3.15: Condensation of fine droplets.	41
Figure 3.16: Size of droplets attained once system became stabilised.	42
Figure 3.17: Water temperature distribution.	44
Figure 3.18: Measured- and predicted glass and mean water temperatures.	44
Figure 3.19: Results attained for night-time operation.	45
Figure 3.20: Measured- predicted temperatures with Sisalation usage.	45
Figure 4.1: Sketch of fundamental greenhouse.	48
Figure 4.2: Path of the sun from above on the 1 <sup>st</sup> of January and the 1 <sup>st</sup> of July.	51
Figure 4.3: Energy balance on the roof of the greenhouse.	52
Figure 4.4: Heat fluxes imposed on vertical glass window.	54
Figure 4.5: Heat fluxes associated with concrete floor.	56
Figure 4.6: Beam- and diffuse solar irradiation profiles.	58
Figure 4.7: Relative humidity- and wind speed readings.	58
Figure 4.8: Predicted temperatures within greenhouse with concrete floor.	59
Figure 4.9: Predicted temperatures in greenhouse with 100 mm water floor.	60
Figure 4.10: Predicted temperatures in greenhouse with concrete floor and thermal insulation usage at night.	61
Figure 4.11: Predicted temperatures in greenhouse with water floor and thermal insulation usage at night.	62
Figure 4.12: Predicted greenhouse temperatures.	63
Figure 5.1: Side and plan views of the proposed greenhouse structure.	66
Figure 5.2: Simplified greenhouse model.	69
Figure 5.3: Mean water tank temperature on June 21 <sup>st</sup> .	70
Figure 5.4: Comparative glass cover temperatures.	71
Figure 5.5: Predicted glass greenhouse temperatures on December 21.	72
Figure 5.6: Side view of greenhouse structure.	73
Figure 5.7: Plan view of Welgevallen greenhouse layout.	74
Figure 5.8: Profile of corrugated polycarbonate	75
Figure A.1: Randomly orientated surface in direct sunlight with associated angles.	A.1
Figure B.1: Concentration or temperature distribution.	B.1
Figure B.2: Flow development on surface.	B.4
Figure B.3: Photograph of evaporation pan.	B.10

Figure C.1: Photograph of open water tank	C.1
Figure C.2: Thermocouple spindle used to determine water temperature profile	C.2
Figure C.3: Solar collector with plastic-covered water tank.	C.14
Figure D.1: Solar radiation striking a cover of thickness $t_c$ and being either transmitted, absorbed or reflected.	D.2
Figure D.2: Effective transmittance-absorptance product.	D.5
Figure E.1: Relative orientation of glass greenhouse.	E.1
Figure E.2: Sketch of condition 1.	E.2
Figure E.3: Sketch of condition 2.	E.3
Figure E.4: Sketch of condition 3.	E.4



# Nomenclature

---

A	Area, m <sup>2</sup>
a	Absorption coefficient, m <sup>-1</sup>
C	Coefficient
C <sub>e</sub>	Extinction coefficient, m <sup>-1</sup>
C <sub>f</sub>	Friction factor
c <sub>p</sub>	Specific heat capacity, J.kg <sup>-1</sup> .K <sup>-1</sup>
D	Diffusion coefficient, m <sup>2</sup> .s <sup>-1</sup>
DOY	Day of the year
g	Gravitational acceleration, 9.81 m.s <sup>-2</sup>
h	Convective heat transfer coefficient, W.m <sup>-2</sup> .K <sup>-1</sup>
I	Incident solar irradiation, W.m <sup>-2</sup>
i <sub>fg</sub>	Latent heat of vaporization, J.kg <sup>-1</sup>
k	Thermal conductivity, W.m <sup>-1</sup> .K <sup>-1</sup>
m	Mass or mass flowrate, kg or kg.s <sup>-1</sup>
n	Refraction index
P	Annual phase angle
p	Pressure, Pa
q	Heat flux, W.m <sup>-2</sup>
R	Gas constant, kJ.kg <sup>-1</sup> .K <sup>-1</sup>
T	Temperature, °C or K
t	Thickness or time, m or s
v	Velocity, m.s <sup>-1</sup>
x	Distance, m
Y	Year
YADJ	Leap year adjustment
z	Depth, m

## Dimensionless numbers

Gr	Grashof number, $\beta \Delta T g L^3 / \nu^2$
----	--

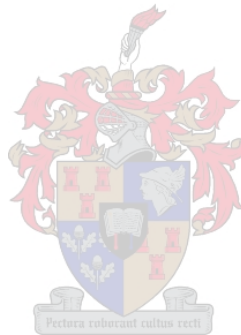
Le	Lewis number, $k/(D \mu c_p)$
Nu	Nusselt number, $h x / k$
Pr	Prandtl number, $\mu c_p / k$
Sc	Schmidt number, $\mu / (\rho D)$

## Greek symbols

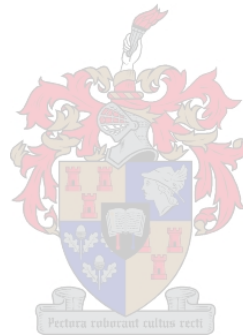
$\alpha$	Solar absorptivity or solar altitude angle, $^\circ$ Thermal diffusivity, $k/(\rho c_p)$ , $m^2/s$
$\alpha'$	Effective absorptivity
$\beta$	Slope angle, $^\circ$ or fraction of solar energy absorbed at open water surface
$\gamma$	Psychrometric constant or surface azimuth angle, $^\circ$
$\gamma_s$	Solar azimuth angle, $^\circ$
$\gamma_s'$	Pseudo solar azimuth angle, $^\circ$
$\gamma^*$	Adjusted psychrometric constant
$\Delta$	Slope of saturation pressure line, $dP/dT$ , $Pa.K^{-1}$
$\delta$	Declination angle, $^\circ$
$\varepsilon$	Emissivity
$\theta$	Incidence angle, $^\circ$
$\mu$	Dynamic viscosity, $N.s.m^{-2}$
$\rho$	Reflectivity or density, $kg.m^{-3}$
$\rho'$	Effective reflectivity
$\sigma$	Stefan-Boltzman's constant, $5.67 \cdot 10^{-8} W.m^{-2}.K^{-4}$
$\tau_a$	Transmissivity due to absorption
$\tau_e$	Effective transmissivity
$\nu$	Kinematic viscosity, $m^2.s^{-1}$
$\varphi$	Latitude angle, $^\circ$
$\varphi_l$	Longitude angle, $^\circ$
$\varphi_m$	Local meridian, $^\circ$
$\Psi$	Local time, h
$\omega$	Hour angle or specific, $^\circ$ or $kg H_2O / kg$ dry air

## Subscripts

a	Ambient air
af	Air-film
av	Air-vapour mixture
ave	Average
b	Beam
c	Cover
ca	Convection to ambient air
ce	Convection from enclosure
col	Colburn
cw	Convection from water surface
D	Mass diffusion
d	Diffuse
dp	Dew-point
e	Enclosure
ea	Enclosed air
en	Energy
ev	Evaporation
exp	Experimental
f	Film or floor
fw	Film-water
g	Glass
ge	Glass surface facing east
gn	Glass surface facing north
gr	Glass surface facing roof
gs	Glass surface facing south
gw	Glass surface facing west
h	Horizontal
horiz	Horizontal
i	Ambient condition or iteration
m	Mean
mon	Monteith



o	Saturated condition
p	Plate
ra	Radiation to environment
re	Radiation from enclosure
rw	Radiation from water surface
s	Surface
sat	Saturated
sky	Sky
v	Vapour
vert	Vertical
w	Wind or water
wb	Wet-bulb
z	Zenith



## CHAPTER 1

# Introduction

- 1.1 Background
  - 1.2 Problem statement and objectives
  - 1.3 Engineering approach
  - 1.4 Literature study
  - 1.5 Overview of chapters
- 

### 1.1 Background

Aquaculture is defined as the controlled production of fish, shellfish and aquatic plants for human consumption, industrial use and recreational purposes.

The rapid expansion of the global population has put tremendous pressure on the food resources of the world; this high demand presents both a dire need to feed those without food, and a market for a cheap protein-rich food that is easily attainable. Aquaculture has not only got the ability to boost worldwide food resources and -security, but can also assist in an economic and socio-economic manner by increasing export income and reducing imports, while also creating a demand for technology and training, and generating employment.

Aquaculture is the fastest growing food industry in the world; since it is accepted that the quantity of fish supplied by traditional methods is unlikely to increase substantially in the future due to factors such as over-fishing, pollution and habitat destruction, aquaculture production will need to increase in an attempt to meet the growing demand for fisheries products.

According to the *United Nations' Food and Agriculture Organization* (FAO), world aquaculture production increased from 3.5 million tonnes in 1970 to a quantity in excess of 40 million tonnes in 2000, which relates to a compounded annual growth rate

of approximately 9.2%. This compares favourably to an increase of 1.4% and 2.8% for capture fisheries and terrestrial meat farming respectively (FAO 2003). Between 1995 and 2000, Africa was the continent that showed the largest increase in aquaculture production (30.8%), with South Africa being responsible for less than 1% of African production. The South African aquaculture industry amassed a total of 4383 tonnes in produce in 2003, valued at R237 million at farm gate level (FAO 2003).

## 1.2 Problem statement and objectives

The current study is concerned with the tilapia group of fish, in particular the species *Oreochromis mossambicus*. Tilapias are endemic to Africa, but their potential as an aquaculture species has led to a widespread distribution in the past 50 years. *O. mossambicus* was the first tilapia species to be exported from Africa to the Indonesian island of Java in 1939 (Popma and Lovshin, 1994), the success has been such that the current worldwide annual production has reached a value of 1,26 million tonnes (FAO, 2003). This is valued at US\$1 706 million and has led to tilapia being considered the third most important fish species group worldwide.

The South African tilapia industry is only in the introductory phase with approximately 15 producers nationwide, the majority of which are located in the warmer northern and eastern regions of the country.

Welgevallen Research Centre is situated in Stellenbosch in the Western Cape and houses a smaller quantity of tilapia (*O. mossambicus*) within an intensive recirculation system in a greenhouse environment. Figure 1.1 shows a photograph taken within greenhouse-covered aquaculture system.

The fact that tilapias are tolerant toward lower water quality and have the ability to utilize a wide variety of natural food sources render it a suitable species for use in aquaculture. They are also prolific breeders and generally disease resistant (Popma and Masser, 1999; Roberts and Sommerville, 1982).

The optimal temperature range for tilapia is between 25 – 36°C; but the main biological constraint to the development of commercial tilapia farming is their inability to withstand temperatures below 10°C (*Chervinski, 1982*) and early sexual maturation that results in fish spawning before reaching market size (*Philapaert and Ruvet, 1982*). The problem of precocious breeding and excessive population growth due to the early onset of sexual maturation is a well-known phenomenon in tilapia aquaculture (*Hepher and Pruginin, 1982; Mair et al., 1997; Mair and Abella, 1997*). A tilapia population that reaches sexual maturity at an earlier age will have an increased spawning frequency and stunted growth rates. Fish exposed to an optimal water temperature range may reach sexual maturity at sizes of 150 – 200g, while those kept at colder temperatures may breed at sizes as small as 10g (*Jalabert and Zohar, 1982*).



Figure 1.1: Author at Welgevallen tilapia system.

The cold winter climate experienced in the south-western region of South Africa results in sub-optimal water temperatures, which adversely influence the general health of the fish, breeding success, production and ultimately economic success of the species. The

primary objective of this study is to determine a way in which the environment enclosed within the greenhouse can be thermally controlled to meet the needs of the species of interest. This should preferably be done in an environmentally friendly manner, considering the current system and the construction of other such systems in the future.

If possible, the most likely manner in which this can be achieved during winter without external input, such as gas or electricity, is to maximise the solar input entering the system, while minimising the losses experienced from the system at night. The method in which the recirculating water is heated should be done in the most environmentally friendly manner, with little or no running costs and should in no way hinder the performance of any feature necessary for the well-being of the fish.

### 1.3 Engineering approach

Attempts have been made in the past to regulate temperatures within similar greenhouse systems on a purely superficial basis, without complete knowledge of all the interacting components present. Optimal thermal control of such a system requires that the problem be divided into the appropriate fundamental heat and mass transfer modes for a thorough understanding of the behaviour of the system to be designed.

Tests were performed on numerous experimental set-ups that replicated some of the physical situations found within the greenhouse system. These systems were then analysed theoretically and the results compared to those obtained through testing. Once satisfied that the heat and mass transfer modes present in the greenhouse were fully understood, mathematical modelling of the system could begin. Dynamic simulation is regarded as one of the most powerful approaches to understanding the interactions of a complex system (Cuenco, 1989).

Modelling began with a very fundamental glass system, having a high solar input coupled with large losses. Modifications could be made to the model with respect to orientation, size, construction materials, thermal insulation and others, from which conclusions could be drawn as to whether or not the required temperature range is

obtainable during periods of adverse weather conditions and recommendations formulated for the construction and maintenance of future systems of this nature.

Simulations associated with the modelling of greenhouses can be classified either as passive- or active systems. A passive simulation would be used to determine what temperatures could be expected within such a system during operation. If the predicted temperatures do not meet the design specifications, then an active system needs to be employed to determine the appropriate heating or cooling load required.

#### 1.4 Literature study

The most useful paper found in the literature with respect to the current study is by *Zhu et al.* (1998) and deals with the thermal modeling of greenhouse pond systems (GPS). As stated in section 1.3, this source confirms that greenhouse pond systems can indeed provide a good alternative for maintaining water temperature in aquacultural facilities. It also verifies the fact that the thermal characteristics of such systems are not properly understood and that many pond greenhouses are simply copied from those used in horticulture.

Numerous authors have modelled pond temperature, some of which are *Klemetson and Rogers* (1985), *Carthcart and Wheaton* (1987), *Losordo and Piedrahita* (1991) and *Zhu et al.* (1998). The model developed by *Klemetson and Rogers* (1985) assumes saturated air conditions and no wind across the water surface; the results indicate an increase in water temperature of between 2.8 – 4.4°C for any month in the year when compared to an open air pond. Conflicting results were obtained by *Little and Wheaton* (1987), who predict an increase of between 9 - 10°C in the pond water temperature with the use of a greenhouse cover.

This paper states, as expected, that the primary losses from such a system are due to radiation from within the enclosure to the cover, convection from the cover to the environment and radiation from the cover to the sky; also that reducing these 3 flux densities is the principle measure for maintaining water temperature. The model used by *Zhu et al.* (1998) is similar to that used in this study with the air and water being

considered as homogenous, with the exception that the former considers only one-dimensional heat flow in a vertical direction and ignores the influence of the sides of the greenhouse.

The manner in which the condensation on the inner surfaces of the greenhouse affects the transmission of light entering the system is not stated in the publication. However, as far as thermal radiation exchange between the inner surfaces is concerned, the area covered by condensation is determined as a fraction of total area and treated as having radiation parameters equivalent to that of water. It is also important to note that the internal relative humidity was always assumed to be near 100%.

The performance of polyethylene, PVC, standard glass and low-emissivity glass were compared as cover materials for the GPS. Polyethylene achieves a 5.2°C increase in temperature when compared to the outside air temperature, PVC and low-emissivity glass produce equally good results while that of standard glass is somewhat less.

Another publication of interest is by *Pieters and Deltour* (1999) and deals with the modelling of solar input in greenhouses. Its purpose was to determine the relative importance of constructional parameters that influence the solar collecting efficiency of greenhouses. Even though the greenhouse considered contained a tomato crop, interesting results of application to the current study were obtained. While the study by *Zhu et al.* (1998) is fairly comprehensive and of a very similar nature to this thesis, the fact that it neglected to mention how the light transmission was determined is of concern to the author and is the reason for the former publication being considered.

*Pieters and Deltour* (1999) state that increasing the solar transmittance of greenhouses has always been an important research topic in horticultural engineering, and thus is of importance to the current study. Condensation on glass products is theoretically expected to develop as a film, while dropwise condensation is expected on most plastic cladding materials. The drops in the latter case generally grow until a certain size, after which run-off occurs; this is however only applicable to non-horizontal glazing. Numerous simulations and experimental studies have been performed by *Pieters* (1995), *Pieters et al.* (1997) and *Pollet and Pieters* (1999) to mention just a few. They confirm that film condensation or flat droplets result in a small decrease or even an

increase in glazing transmissivity, while drops with high contact angles can give rise to transmittance reductions of up to 40%.

It is interesting to note that when condensation forms on polyethylene its radiative properties change significantly; it becomes practically opaque to thermal radiation and behaves like low-emissivity glass. As found by *Zhu et al.* (1998), polyethylene performs better than glass does; thus even with the significant decrease in light transmission, the gain in thermal radiation is greater. Note that the glass and polyethylene compared were not the same thickness, and were measured to be 0.004 m and 0.0001 m respectively.

*Pieters and Deltour* (1999) find that condensation is found only during low- or zero solar radiation levels, this is however for a tomato crop with far less available moisture than in an aquaculture facility and thus continual condensation is expected to occur on the cladding of a GPS. It was found that the presence of condensation has little or no effect on the absorptance of the cladding. Thus it could be concluded that a greenhouse of glass construction without any horizontal glass surfaces is unlikely to perform any worse due to internal condensation.

*Critten and Bailey* (2002) published a review of greenhouse engineering developments during the 1990's, which covers much of the progress made in this field in recent years. A point of interest is the use of a reflecting surface on the wall/s receiving the least solar radiation to enhance the light entering the system, and the use of movable screens to provide thermal insulation and minimise night-time radiative losses.

*Nijskens et al.* (1984) consider heat transfer through covering materials in greenhouses. This paper deals with the associated heat fluxes and considers the use of double walls to minimise convective heat losses. This is found to have definite benefits and is used extensively throughout much of Europe and North America in residential structures with great success. The application thereof is however quite expensive, and thus this form of convection suppression will be retained unless urgently required.

## 1.5 Overview of chapters

The content of this study is summarised in the paragraphs that follow.

Chapter 2 contains all experimental work not associated with water storage. Theoretical models are developed for convective heat transfer coefficients and evaporation from horizontal surfaces, which are then compared to results obtained through experimentation.

Further experimental work was considered in Chapter 3. This dealt with the theoretical modelling and experimentation with regard to the open water tank, the solar collector with plastic covered water tank and the solar collector with condensation. The influence of thermal insulation on the above systems is also investigated. As before, the results obtained through experimentation are then compared to those predicted by the theoretical models developed.

The modelling of a fundamental greenhouse is covered in chapter 4. A simple glass model is developed, and the thermal behaviour is then analysed on the day of the winter solstice with either a water or concrete layer serving as the floor. The effect of thermal insulation usage on the predicted system temperatures is then investigated during both the day and night.

Chapter 5 contains a conceptual greenhouse design that is expected to absorb the greatest quantity of solar radiation available, while simultaneously experiencing minimal losses to the environment. Recommended modifications are also supplied to enable the greenhouse system at Welgevallen to meet the necessary design specifications.

Chapter 6 concludes this study and briefly discusses the results obtained in each section, with suggestions on how further studies in this field could be directed.

## CHAPTER 2

# Convective- and evaporative heat transfer from a horizontal surface

- 2.1 An analytical approach
  - 2.2 Experimental convective heat transfer coefficient from a horizontal surface exposed to the natural environment
  - 2.3 Evaporation from a water surface exposed to the natural environment
  - 2.4 Conclusion
- 

### 2.1 An analytical approach

Any system not fully insulated and exposed to environmental conditions will experience a net loss or gain in energy, comprised of heat fluxes entering and/or leaving the system of interest. While significant effort has been put into understanding the possible modes of heat transfer, the calculation of convective and evaporative heat transfer still relies largely on the use of empirical correlations. These correlations are the result of experimental work performed by various researchers, with the result that opinions are often divided as to which specific correlation is in fact the most accurate. The lack of an analytical approach to the above issues presents a potential margin of error, and while inevitable in some cases, is highly undesirable.

### 2.2 Experimental convective heat transfer coefficient from a horizontal surface to the natural environment

Reviewing the content available in the literature on convective heat transfer coefficients between a horizontal surface and the environment revealed that a large degree of uncertainty exists in this field. *Lombaard* (2002) quotes numerous sources that verify the above statement, one of which is *Duffie and Beckman* (1991) who state that, “from

the preceding discussion it is apparent that the calculation of the wind induced heat transfer coefficient is not well established.”

A potential source of these discrepancies may be that the experimental apparatus and procedure is often poorly defined. Also it was found that the definition of the convective heat transfer coefficient is often inconsistent, with many researchers making use of correlations not in dimensionless form. This presents the problem that the variation in thermophysical properties of the air are not taken into account, and thus it is unlikely that a simple equation will accurately model the complex convective heat transfer process.

*Kröger* (2002) theoretically analysed the problem of convective heat transfer between a horizontal surface and the natural environment; his findings were later confirmed experimentally and refined by *Burger and Kröger* (2004).

Testing was performed on an apparatus similar to that employed by *Burger and Kröger* (2004) in an attempt to verify their results. The reader is referred to *Burger and Kröger* (2004) for a theoretical analysis of this system.

### 2.2.1 Experimental apparatus and procedure

Experiments were conducted on a polystyrene plate, with sides measuring 1.020 x 1.020 m and a thickness of 0.05 m. A simple drawing of the experimental apparatus used is shown in figure 2.1. The surface was covered in a matt black paint ( $\alpha_s \approx 0.93$ ,  $\epsilon_s \approx 0.90$ ) and was positioned such that the height of the upper surface was flush with the surrounding ground. The lower surface of the polystyrene plate was reinforced to resist warping while exposed to solar radiation.

Five type-T thermocouples were used to measure the temperature across the surface of the horizontal plate, while another four were used to measure the vertical ambient air temperature distribution until a height of 1 meter above the surface. Figure 2.1 shows a zoomed in view of a thermocouple at the polystyrene surface, which measures the

temperature as close to the surface as possible. A light layer a black paint covers the exposed wires and helps prevent inaccurate temperature readings.

A weather station (Davis Weather Monitor II) was used to measure the ambient air- and dew-point temperatures, as well as the wind speed at a height 1 m above the ground and the barometric pressure. A Kipp and Zonen pyranometer was used to measure the total solar radiation. Diffuse radiation readings were measured by shielding the pyranometer from direct sunlight for a period long enough for stable readings to be taken.

All data was collected in one-minute intervals and averaged over a period of ten minutes. The location of the University of Stellenbosch Solar Energy Laboratory is 100 m above sea level, at a latitude of  $33.98^\circ$  S and a longitude of  $18.85^\circ$  E.

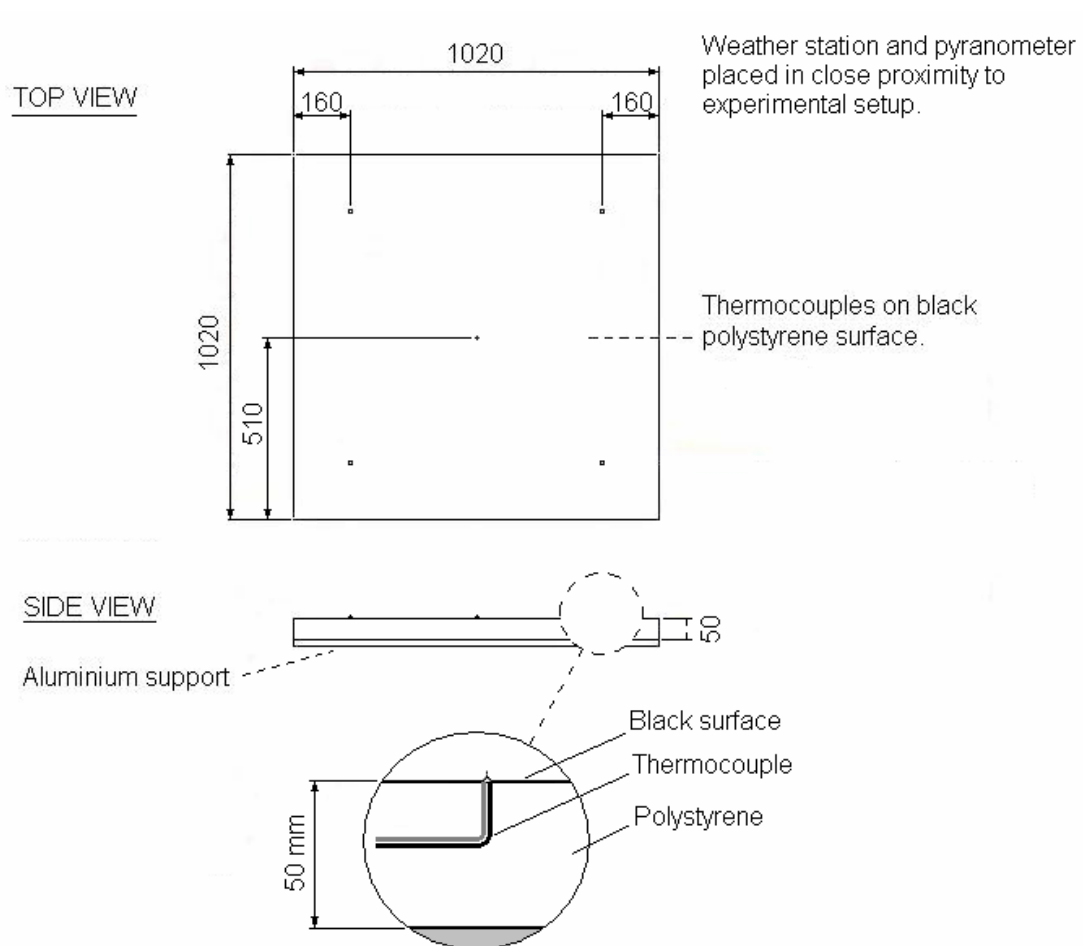


Figure 2.1: Experimental apparatus used for determining convection heat transfer coefficient.

## 2.2.2 Results obtained

*Burger and Kröger* (2004) present the two equations that follow to determine the experimental convective heat transfer coefficient between a horizontal surface and the natural environment under day- and night-time conditions respectively.

$$h_a = \frac{0.2106 + 0.0026 \cdot v_w \left[ \frac{\rho \cdot T_m}{\mu \cdot g \cdot (T_s - T_a)} \right]^{1/3}}{\left[ \frac{\mu \cdot T_m}{g \cdot (T_s - T_a) \cdot c_p \cdot k^2 \cdot \rho^2} \right]^{1/3}} \quad (2.1)$$

$$h_a = 3.87 + 0.0022 \frac{v_w \cdot \rho \cdot c_p}{(\mu \cdot c_p / k)^{2/3}} \quad (2.2)$$

The values of the thermophysical properties in the above equations are evaluated at the arithmetic mean temperature,  $T_m$  between the measured surface and ambient air temperatures,  $T_s$  and  $T_a$ . Equation (2.1) is applicable when the surface temperature  $T_s$  is greater than the ambient temperature  $T_a$ . While the use of equation (2.2) is recommended when the surface temperature  $T_s$  is less than the ambient temperature  $T_a$ , or when  $T_s$  is slightly larger than  $T_a$  when equation (2.2) is larger than equation (2.1).

Experimental data is not available to check the validity of equation (2.2), since the formation of dew occurs rapidly after sunset during the time of the year when testing was done at the given location, and condensation on the system changes the analysis entirely.

*Burger and Kröger* (2004) consider an energy balance on a horizontal surface exposed to the natural environment, and give equation (2.3) for the experimental convective heat transfer coefficient during daytime operation.

$$h_e = \frac{\alpha_s \cdot I_h - \varepsilon_s \cdot \sigma \left[ T_s^4 - \left[ (0.727 + 0.0060 T_{dp}) \cdot T_a^4 \right] \right]}{(T_s - T_a)} \quad (2.3)$$

Experimentally determined results are compared to values predicted by equations (2.1) in figure 2.2.

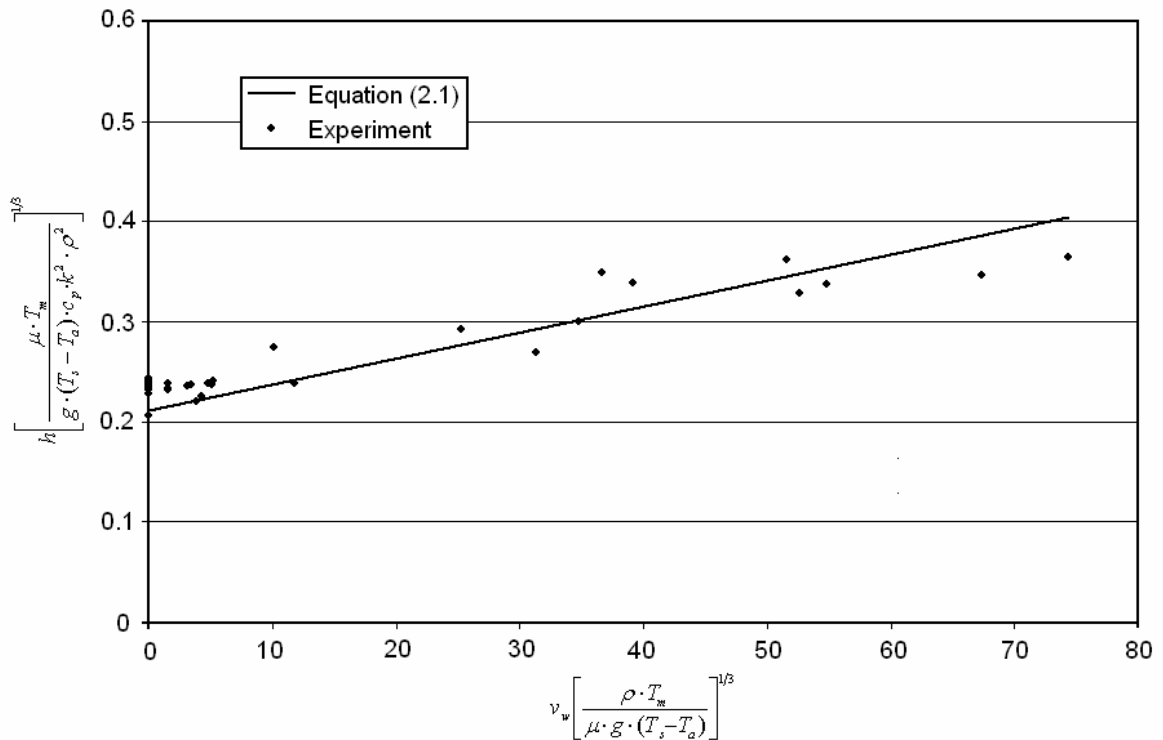


Figure 2.2: Comparison between predicted and measured dimensionless convective heat transfer coefficients.



### 2.3 Evaporation from a water surface exposed to the natural environment

Solar applications such as solar ponds, swimming pools or roof ponds with stringent energy or economic requirements demand that the associated heat fluxes be accurately determined. If it is considered that evaporation is responsible for more than half the energy loss from a free water surface, an inability to accurately determine the loss of energy from such a system could result in a significant error.

*Sartori (1999), Yilmaz (1999) and Shah (2002)* all made comparisons between the theoretical and experimental expressions available for the prediction of water evaporation rates from free water surfaces. They all indicated that significant discrepancies exist between the available expressions.

Many authors in the literature refer to work published by *Dalton* (1802); he states that the rate of evaporation from a water surface is proportional to the difference in vapour pressure between the water surface and the surrounding air, he also goes on to say that this proportionality is influenced by wind speed.

Based on the analogy between heat- and mass transfer, the majority of the expressions available have a format similar to  $m_{ev} = (A + B \cdot v_w) \cdot (p_w - \phi p_a) / i_{fg}$ , where  $A$  and  $B$  are coefficients that are simply determined through repetitive experimental work. The analysis, experimental procedure and results obtained in the present study will be discussed in the section that follows, with a full numerical example available in Appendix B.4.

### 2.3.1 Analysis

By applying a steady state energy balance to the surface of a film of water on an insulated base that is exposed to the natural environment as shown schematically in figure 2.3, it is possible to obtain an expression for the rate of evaporation per unit surface area i.e.

$$m_{en} = [\alpha_w I_h - \varepsilon_w \sigma (T_w^4 - T_{sky}^4) - h_a (T_w - T_a)] / i_{fg} \quad (2.4)$$

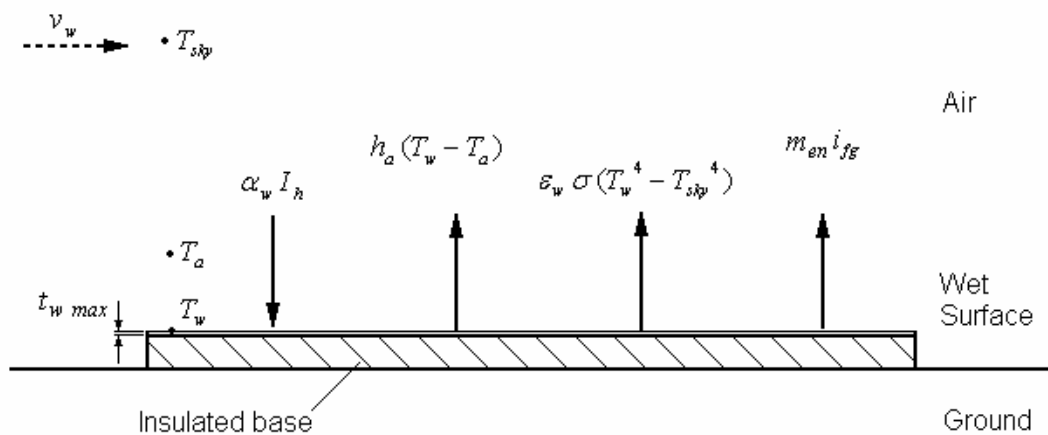


Figure 2.3: Heat fluxes present on water surface exposed to natural environment.

The term  $\alpha_w I_h$  represents the net solar radiation absorbed by the surface,  $h_a(T_w - T_a)$  is the convective heat transfer,  $m_{en} i_{fg}$  the evaporative heat transfer, with the subscript *en* referring to the above energy balance, while  $\epsilon_w \sigma(T_w^4 - T_{sky}^4)$  is the radiative heat transfer from the water surface.

The absorptivity of the water surface  $\alpha_w$  is given by *Holman* (1986) as a function of the zenith angle  $\theta_z$ . This relationship is shown graphically in figure 2.4.

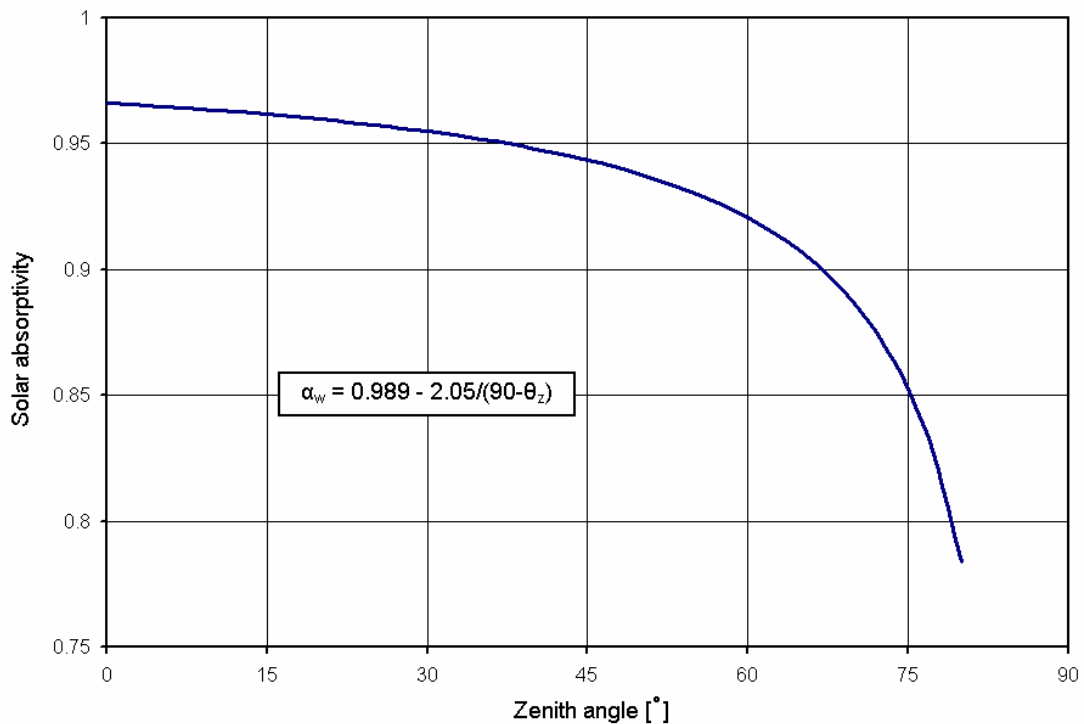


Figure 2.4: Absorptivity of water.

One could argue that the above relationship is only valid for a large expanse of water and that a very thin film of water is essentially transparent, absorbing practically no solar radiation. The equation above has been rewritten for the current application and was originally a relationship between solar altitude and albedo. All solar radiation incident on a large body of water and not reflected at the surface will be absorbed. Similarly if a thin film of water covers an insulated black surface, it is assumed that all solar radiation not reflected at the water surface will be absorbed upon striking the highly absorptive surface.

The convective heat transfer coefficient  $h_a$  is represented by equation (2.1), while the sky temperature  $T_{sky}$  is determined according to *Berdahl and Fromberg* (1982) for daytime- and night-time operation in equations (2.5) and (2.6) respectively.

$$T_{sky} = \left[ (0.727 + 0.0060 T_{dp}) \cdot T_a^4 \right]^{1/4} \quad (2.5)$$

$$T_{sky} = \left[ (0.741 + 0.0062 T_{dp}) \cdot T_a^4 \right]^{1/4} \quad (2.6)$$

Where  $T_{dp}$  is the dew-point temperature measured in degrees Celsius.

### 2.3.2 Experimental apparatus and procedure

The evaporation pan used to experimentally determine the rate of evaporation from a water surface is shown in figure 2.5.

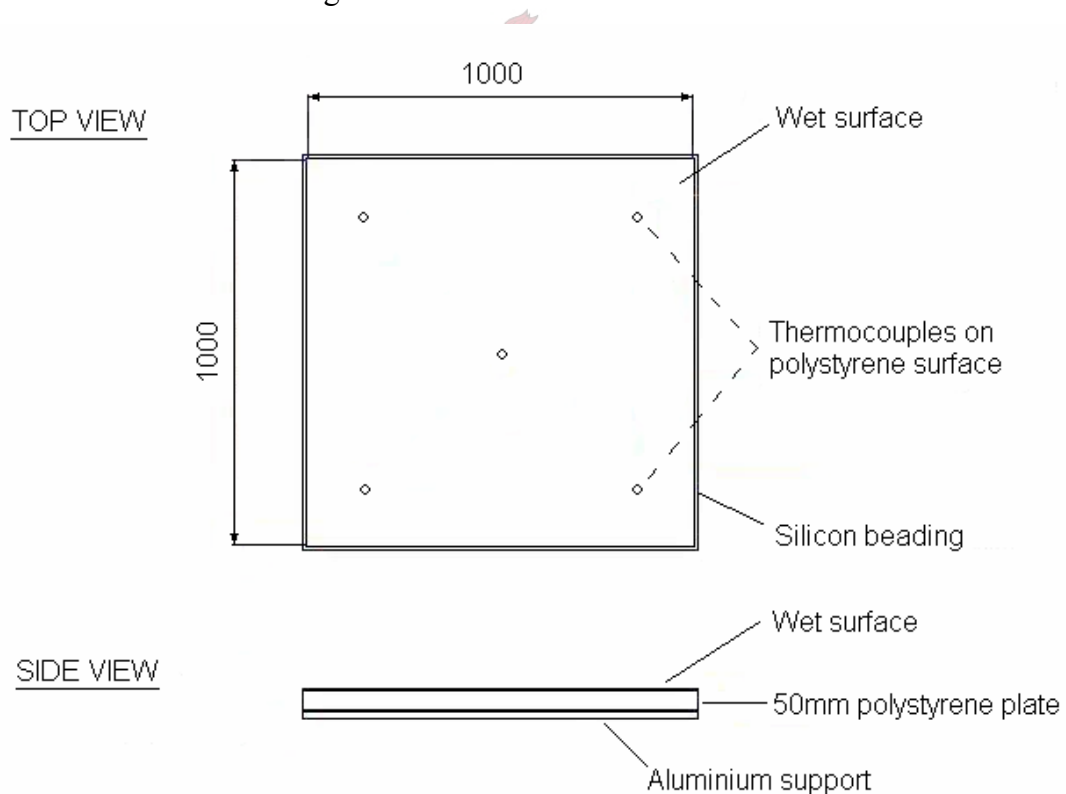


Figure 2.5: Front and top views of evaporation pan.

It consisted of a 50 mm thick horizontal polystyrene plate having an effective upper surface area of approximately  $0.97 \text{ m}^2$ , which was painted with a waterproof matt black paint. A 3mm high bead of silicon sealant was run along the perimeter of the pan, with

the purpose of containing a 1- 2 mm deep layer of water. Five type-T thermocouples were embedded in the surface of the plate with the purpose of measuring the water temperature. Four of the five were positioned in the corners of the pan, 150mm from adjacent sides, while the fifth was placed in the centre.

The wind speed, ambient air- and dew-point temperatures were measured with the aid of a weather station at a height of 1 m above the ground. A Kipp and Zonen pyranometer was used measure the total incident solar radiation on the surface, while diffuse solar radiation readings were measured by shielding the pyranometer from direct sunlight for a period long enough for stable measurements to be taken. All tests were conducted on clear sunny days.

### 2.3.3 Results and discussion

The evaporation rate from the water surface was measured by adding consecutive quantities of water (500 ml) to the evaporation pan at a temperature similar to that of the remaining water, and recording the period of time taken for each to evaporate. With the average temperature of the water known during the particular period, the mass flowrate or evaporation rate could be determined. This evaporation rate will be denoted by  $m_{exp}$ .

The author presents the following equation for the prediction of the approximate evaporation rate for cases where the water surface temperature is measurably higher than that of the ambient air. The derivation of equation (2.7) is given in Appendix B.1, equation (B.31).

$$m_{vom} = 7.61 \times 10^{-4} \left( \left( g \mu^2 (\rho_{avi} - \rho_{avo}) c_p / (k \rho_{av}^2) \right)^{1/3} + 0.0104 v_w \right) \cdot (p_{vo} - p_{vi}) / T_m \quad (2.7)$$

In the above expression  $\rho_{avi}$  represents the density of the moist air at the humidity and temperature of the ambient air, while  $\rho_{avo}$  is the density of saturated air at the temperature of the water. The symbol  $\rho_{av}$  is the average between the two aforementioned densities, while  $(p_{vo} - p_{vi})$  is the difference in vapour pressure between the water and air respectively. The symbol  $m_{vom}$  represents the mean mass flowrate of

the vapour at the saturated condition. All thermophysical properties are calculated at the mean temperature  $T_m$  between the ambient air  $T_a$  and water temperature  $T_w$ . Note that this expression is only applicable when the water temperature  $T_w$  exceeds the ambient air temperature  $T_a$ .

The use of the expression below is recommended when the ambient air temperature  $T_a$  exceeds the water surface temperature  $T_w$  or when density differences are very small (see equation B.34).

$$m_{vom} = \left( \frac{3.87}{\rho \cdot c_p} + \frac{0.0022 v_w}{Pr^{2/3}} \right) \cdot \left( \frac{c_p \cdot \rho \cdot D}{k} \right)^{2/3} \cdot \frac{(p_{vo} - p_{vi})}{R_v T_m} \quad (2.8)$$

Equation (2.8) is found to be in good agreement with equations recommended by *Tang et al.* (2004) for the evaporation of water from both open water- and wetted surfaces.

*Monteith and Unsworth* (1990) provide a relationship that is used extensively in the evapotranspiration field. The predicted evaporation rate is given by equation (2.9).

$$m_{mon} = \left( \frac{\Delta \cdot \alpha_w \cdot I_h + (p_{vsi} - p_{vi}) \cdot h_w}{\Delta + \gamma^*} \right) \cdot \left( \frac{A}{i_{fg}} \right) \quad (2.9)$$

Such an expression deals with an analysis that is quite different to that of a water surface exposed to the natural environment. However, if the results provided by equation (2.7) are of a similar magnitude to those predicted by an accepted relationship, such as that by *Monteith and Unsworth* (1990), this would further suggest that the expression developed (equation 2.7) may well be of reasonable accuracy.

The derivation of this expression is tedious and unlikely to be of any benefit to the current study, for further information on this equation the reader is referred to *Westdyk and Kröger* (2003).

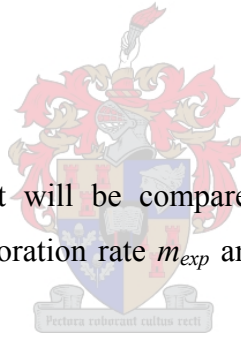
The adjusted psychrometric constant in equation (2.9) is represented by  $\gamma^*$  which is determined by

$$\gamma^* = Le^{\frac{2}{3}} \cdot \gamma = \left( \frac{k}{D \cdot \mu \cdot c_p} \right)^{\frac{2}{3}} \cdot \left( \frac{c_{pma} \cdot P_{atm}}{0.622 \cdot i_{fg}(T_{wb})} \right) \quad (2.10)$$

where  $Le$  is the Lewis number, defined as  $k/(D \cdot \mu \cdot c_p)$ . The symbol  $c_{pma}$  is the specific heat capacity of the moist air and  $i_{fg}(T_{wb})$  is the latent heat of vaporization of water, evaluated at the wet-bulb temperature  $T_{wb}$ . The  $\Delta$  symbol is the average slope of the saturation pressure line between the ambient wet-bulb temperature  $T_{wb}$  and water surface temperature  $T_w$  and is given by equation (2.11). The difference in vapour pressure between the air and the saturation pressure at the same dry-bulb temperature is represented by  $(p_{vsi} - p_{vi})$ . The water surface area is given by the symbol  $A$ , while  $i_{fg}$  is the latent heat of vaporisation. The temperature  $T$  is the average between the surface  $T_s$  and wet-bulb temperatures  $T_{wb}$ .

$$\Delta = \frac{i_{fg} \cdot p_{sat}(T)}{T^2 \cdot R_v} \quad (2.11)$$

The rates of evaporation that will be compared in the following section are the experimentally measured evaporation rate  $m_{exp}$  and the given by equations (2.4), (2.7) and (2.9).



Since the driving force behind the evaporation process is the difference in vapour pressure, which is a function of ambient air- and water temperature, care needs to be taken with respect to the measurement of these two values.

Ambient air temperature readings were taken at a height of 1 m above the ground with the aid of the weather station and with auxiliary thermocouples used to measure the temperature gradient in the air above the water surface. Only a slight deviation was found between the two sets of data; the auxiliary thermocouples were preferred since they were the same type of thermocouple used in the measuring of the water surface temperature.

An analysis was performed on equation (2.7) to determine the sensitivity of the expression to an increase or decrease in measured water temperature by 1°C. It was

found that equation (2.7) is very sensitive to change early in the morning and towards evening, while a difference in the predicted evaporation rate of approximately 10% was found during the day. These findings suggest that extreme care should be taken when measuring the water surface temperature  $T_w$ .

With the above taken into account, the heat fluxes associated with a thin film of water on a black surface exposed to the natural environment were analysed theoretically. The results of this analysis can be summarised by equation (2.12), the details of which can be found in Appendix B (equation B.37).

$$T_{w\text{ surface}} = T_{w\text{ measured}} - I_h \cdot z \quad (2.12)$$

where  $z$  is the depth of the water film, measured in meters.

Evaporative testing was performed from 17.164 h on April the 13<sup>th</sup> for a period of 24 hours, during which no cloud cover was present. The solar irradiation and wind speed present during this time are shown in figure 2.6.

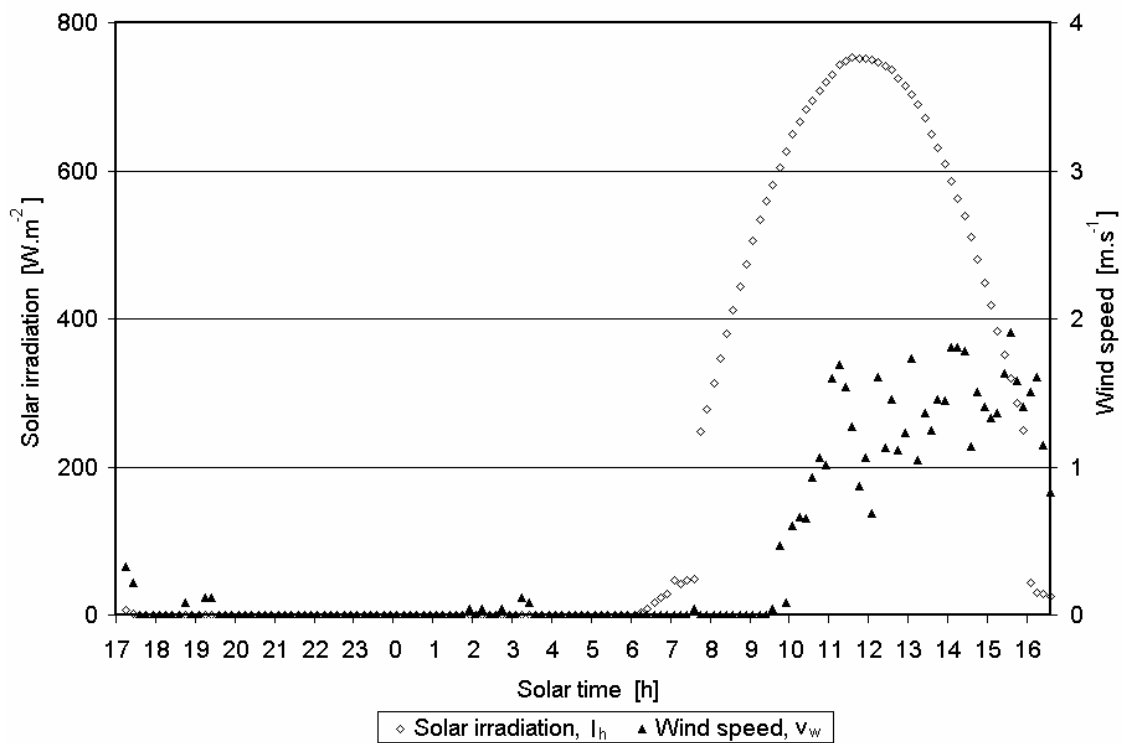


Figure 2.6: Solar irradiation and wind speed readings on 13/14 April 2005.

Figure 2.7 shows a comparative plot between the water-, ambient air-, dew-point temperatures. Note that  $T_w$  is the surface water temperature, as corrected according to equation (2.12). The figure indicates that the water surface temperature only exceeds the ambient air temperature between 8.09 h and 14.75 h; thus equation (2.7) is only applicable during this period. It is also interesting to note that as soon as solar irradiation readings diminish, the water surface temperature drops below the dew-point temperature and thus condensation can be expected to occur.

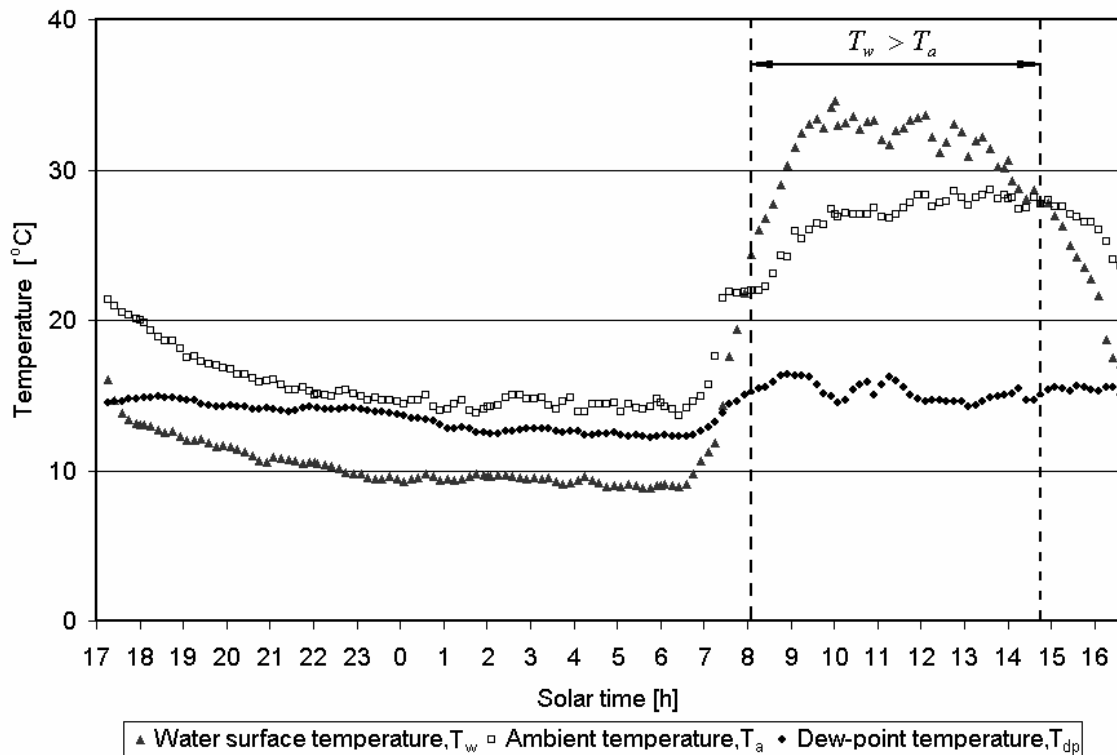


Figure 2.7: Measured water-, ambient air and dew point temperatures.

Table 2.1 compares the quantity of water evaporated between 8.319 h and 14.752 h, with the amount of water that is expected to evaporate during this period according to equations (2.4), (2.7) and (2.9). The error margin is calculated with respect to the experimentally measured quantity.

It is clearly shows that the best results obtained throughout the course of the day are attained with the use of equation (2.7).

Table 2.1: Comparison between cumulative evaporation rates.

	Equation	Measured [kg]	Error [%]
$m_{exp}$		3.979	
$m_{en}$	(2.4)	4.270	7.29
$m_{vom}$	(2.7)	4.066	2.19
$m_{mon}$	(2.9)	4.739	19.10

The above evaporation rates are compared graphically in figure 2.8 and 2.9. Figure 2.8 displays results between approximately 8.00 h and 15.00 h, while figure 2.9 shows the predicted evaporation rates over a period of 24 hours. Note that in figure 2.8 the experimentally measured values  $m_{exp}$  are assumed to be constant during each particular period of analysis. Observation of figure 2.9 shows that when the water temperature  $T_w$  drops below the dew-point temperature  $T_{dp}$ , equations (2.4) and (2.8) predict condensation on the water surface, as expected.

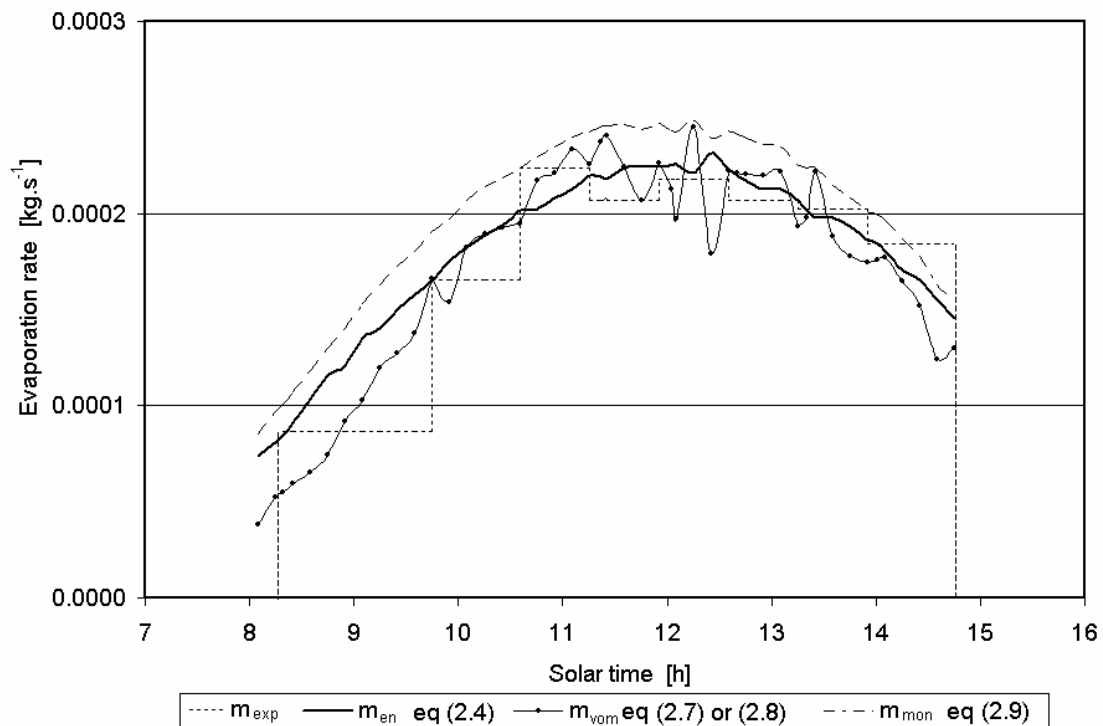


Figure 2.8: Comparative evaporation rates during daytime operation.

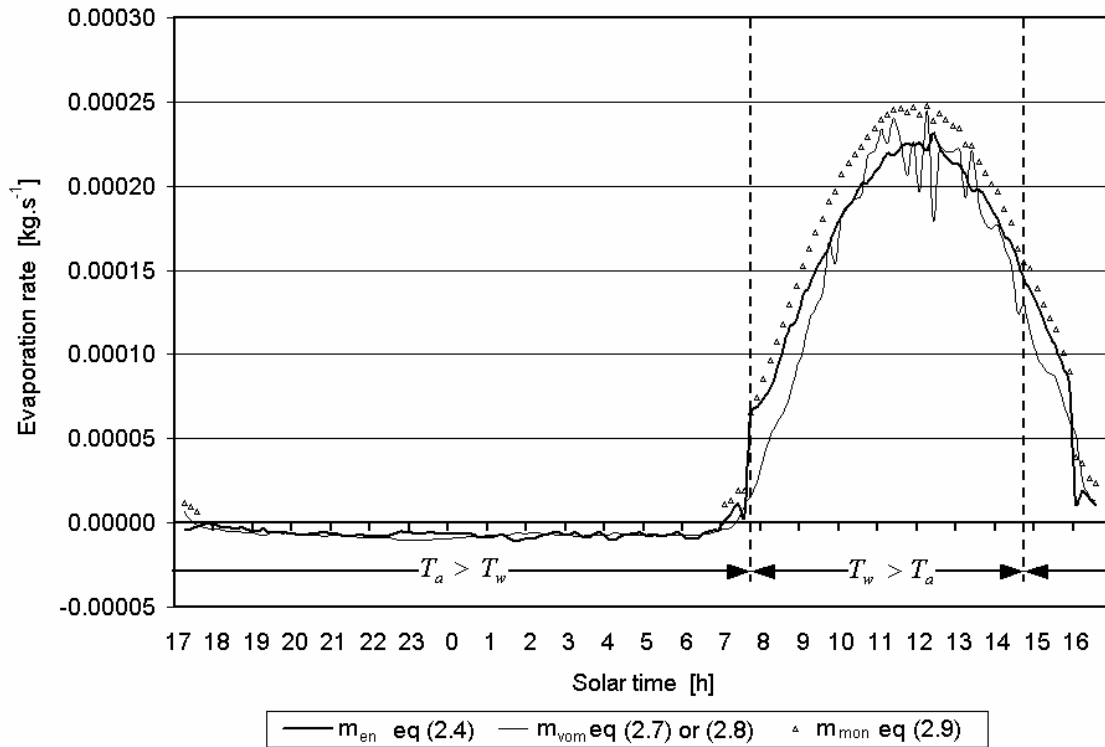


Figure 2.9: Predicted evaporation rates compared over period of 24 hours.

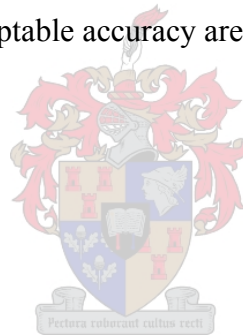
## 2.4 Conclusion

The results regarding the convective heat transfer coefficient in figure 2.2 shows that the trend of the experimental results is similar to that predicted by equation (2.1). The results obtained are considered acceptable and equations (2.1) and (2.2) will be used where applicable.

The results of the evaporation tests were far more interesting than those considered above. In the introduction to section 2.3 it was stated that this was the first time that an expression predicting evaporation rates was supported by good experimental results. A summary of the predicted evaporation rates with respect to the experimentally measured rate of evaporation was given in table 2.1. The results show that equation (2.7) predicts the rate of evaporation the most accurately of the given expressions, with an error margin of just more than 2%.

It is found that all of the evaporation rates over-predict the experimentally measured value early in the morning, and under-predict towards afternoon. This however has the net result of cancelling each other out, to provide better than expected cumulative results. It is expected that the lack of wind on this particular morning (see figure 2.6) lead to an increase of moist air directly above the experimental apparatus. This resulted in an increased vapour pressure of the air above the water, and thus less of a potential for evaporation. The excessive evaporation found to occur in the afternoon could possibly be attributed to an increase in the radiation reflected from the buildings surrounding the apparatus, and thus an increase in the energy absorbed by the water surface.

If the testing on the 13<sup>th</sup>/14<sup>th</sup> April is considered, it is interesting to note that portion of the total heat flux for which convection is responsible is less than 10%. This suggests that even if the convective heat transfer coefficient used is not very accurate, evaporative results within acceptable accuracy are still possible.



## CHAPTER 3

# Thermal behaviour and energy storage of water

- 3.1 Storage of solar energy in water
  - 3.2 Open body of water exposed to the natural environment
  - 3.3 Solar collector with plastic covered water tank
  - 3.4 Solar collector with condensation
  - 3.5 Conclusion
- 

### 3.1 Storage of solar energy in water

It has been shown by many researchers (see *Duffie and Beckman* (1991)) that although thermal energy can be stored in numerous forms, water is the medium that is used most extensively, and is often both inexpensive and readily available. *Holman* (1986) states that solar radiation is absorbed very rapidly in the top layer of a water body, followed by an approximately exponential decay with depth in the water. This relationship is given by equation (B.35)

Thus according to *Kreider et al.* (1989), water has the ability to both act as a collector of solar energy and serve as an excellent storage medium. This characteristic is exploited with the use of solar ponds; which are classified either as salt gradient ponds or freshwater solar ponds. In salt gradient solar ponds the use of salt leads to an increase in water density and thus suppressed convection, while freshwater solar ponds utilise transparent membranes to achieve the same goal.

Neither of the above systems are applicable to an aquaculture system, since not all species are tolerant of salt water, especially at high concentrations and the use of a membrane would retain gasses that would otherwise need to be expelled from the body of water. An algal build-up on the membrane would also lead to decreased levels of

both available oxygen and transmitted sunlight. However, the thermal behaviour of such a system without any evaporative losses could provide important insight into possible greenhouse improvements at a later stage, and since a rapid increase in water temperature is attained with the latter of the two, it will be considered in more detail in section 3.3.

*Sartori (1996)* compares the thermal behaviour of a solar still and a solar evaporator. A solar evaporator is simply a volume of water that is exposed to environmental conditions, while a solar still makes use of a cover. This is a very interesting study, since a comparison between the two is essentially a performance evaluation of the use of a greenhouse to heat water, which is aligned with the objective of this study.

## 3.2 Open body of water exposed to the natural environment

As mentioned above, the thermal behaviour of a body of water that is exposed to the natural environment is of interest since it essentially represents an aquaculture pond system, which experiences high thermal losses. In such an experimental setup these losses can be improved upon with the use of a cover, or a greenhouse in practise, and thus provides a basis for comparison. It is a simple system upon which improvements can be made. Such a system could be considered an extension of the evaporation concept considered in section 2.3, the only difference between the two systems is that since the depth of the water film is substantially more in this case, the thermal inertia of the water body needs to be taken into account.

### 3.2.1 Analysis

Figure 3.1 shows a horizontal water surface of unit area, contained within a tank of depth,  $t_w$  that has a well-insulated base and sides, and is exposed to the environment during the day.

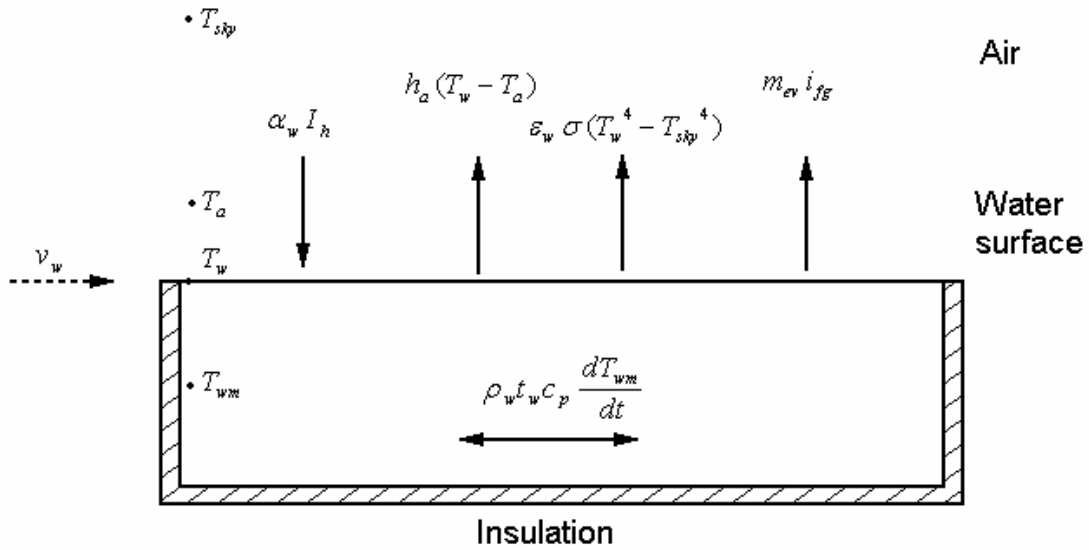


Figure 3.1: Drawing of water tank with associated heat fluxes.

If an energy balance is applied to the volume of water in the figure, the heat fluxes can be summed as follows:

$$\alpha_w I_h - \varepsilon_w \sigma (T_w^4 - T_{sky}^4) - h_a (T_w - T_a) - m_{ev} i_{fg} - \rho_w t_w c_p \frac{dT_{wm}}{dt} = 0 \quad (3.1)$$

The terms in the above equation represent the absorbed solar radiation, the radiative-, convective- and evaporative heat fluxes, and the quantity of heat responsible for the change in stored energy of the water tank respectively. All but the last term have been described in detail in Chapter 2.

The last term consists of the water density  $\rho_w$ , tank depth  $t_w$ , water specific heat capacity  $c_{pw}$  and the rate of change in mean water temperature  $dT_{wm}/dt$ . Note that since convection and radiation are surface phenomena the water surface temperature  $T_w$  has been used in those terms, while the stored energy term is concerned with a change in the mean water temperature  $T_{wm}$ .

If the ambient conditions and water temperatures are known, equation (3.1) can be rewritten and the evaporation rate  $m_{ev}$  from the body of water can be determined.

### 3.2.2 Experimental setup and procedure

An apparatus that could be classified as a solar evaporator was constructed and utilised for experimental testing. Figure 3.2 shows the apparatus used, while a photograph of the system can be found in Appendix C (figure C.1).

The water tank is filled to the surface and the water is heated by solar radiation, resulting in radiative and convective gains or losses, changes in temperature of the water body and evaporative losses, which are monitored regularly. Temperatures are measured at specific heights with the use of the thermocouple spindle, from which the water temperature distribution can be determined.

The base of the water tank is black, so the assumption is made that all solar radiation not reflected at the surface is absorbed by the water body. The sides of the water tank are covered in aluminium foil to prevent heat absorption by the side walls, while the water surface is maintained as close as practically possible to the top of the tank in an effort to minimize detrimental edge effects.

A “thermocouple spindle” was made to measure the temperature of the water at various depths. It was comprised of a thin PVC frame that held seven type T thermocouples that rotated slowly in a horizontal plane through the water at the appropriate depths required to determine a sufficiently accurate temperature profile in the water tank. Measurements were taken at 190, 180, 170, 100, 30, 20 and 10 mm from the base, as well as at the base of the water tank. A drawing of the thermocouple frame is given in Appendix C (figure C.2).

The wind speed and ambient- and dew-point temperatures were measured with the aid of a weather station at a height of 1 m above the ground. A Kipp and Zonen pyranometer was used measure the total incident solar radiation present at the water surface. Diffuse solar radiation was measured by shielding the pyranometer from direct sunlight for a period long enough for stable readings to be taken.

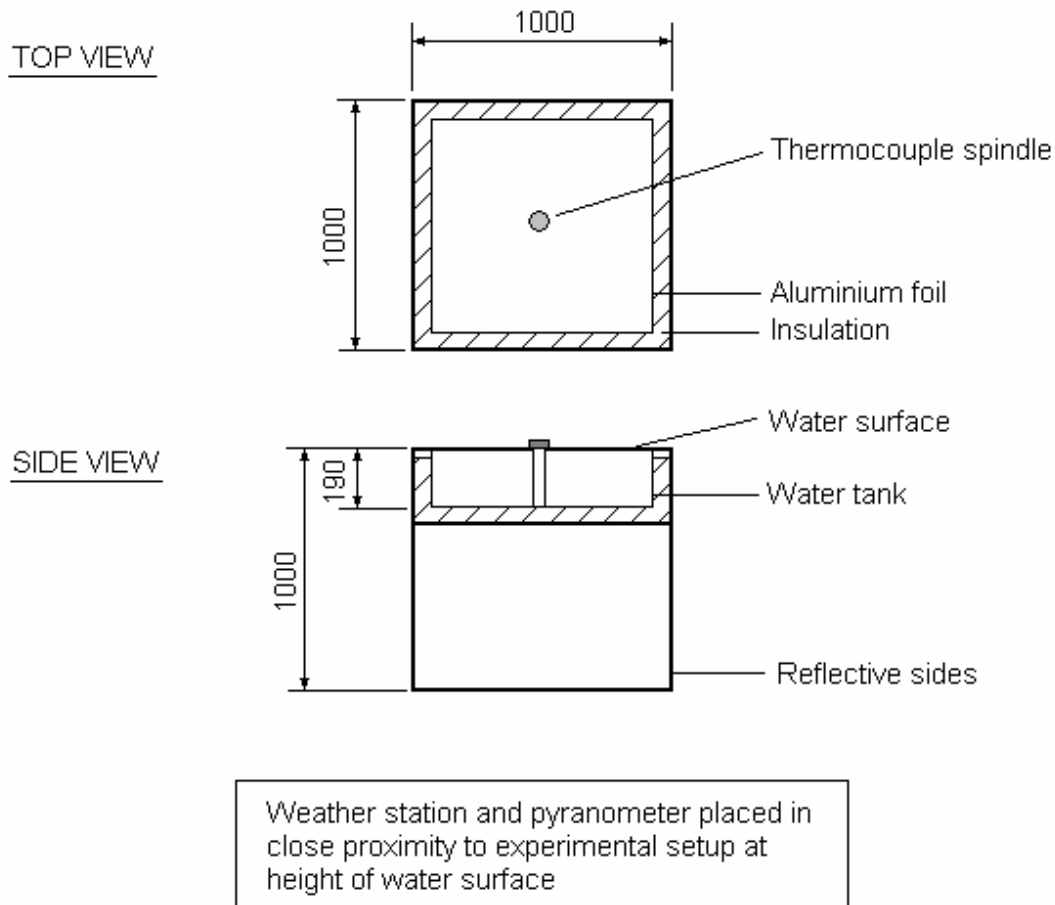


Figure 3.2: Front and top views of experimental setup.



### 3.2.3 Results and discussion

Data was recorded from late afternoon on the 28<sup>th</sup> April 2005 for a period of 24 hours. This data consisted of temperatures at depths throughout the water body, solar radiation readings and various ambient conditions. Figures 3.3 displays the total solar irradiation and wind speed readings, while the ambient air, water and dew-point temperatures are shown in figure 3.4. All given values are averaged over a period of ten minutes.

Figure 3.3 shows that although not particularly windy, wind was still present throughout the entire period. This would generally suggest that significant evaporation should have occurred, however due to the nature of the experimental setup the temperature of the water surface is far less than that encountered in section 2.3.

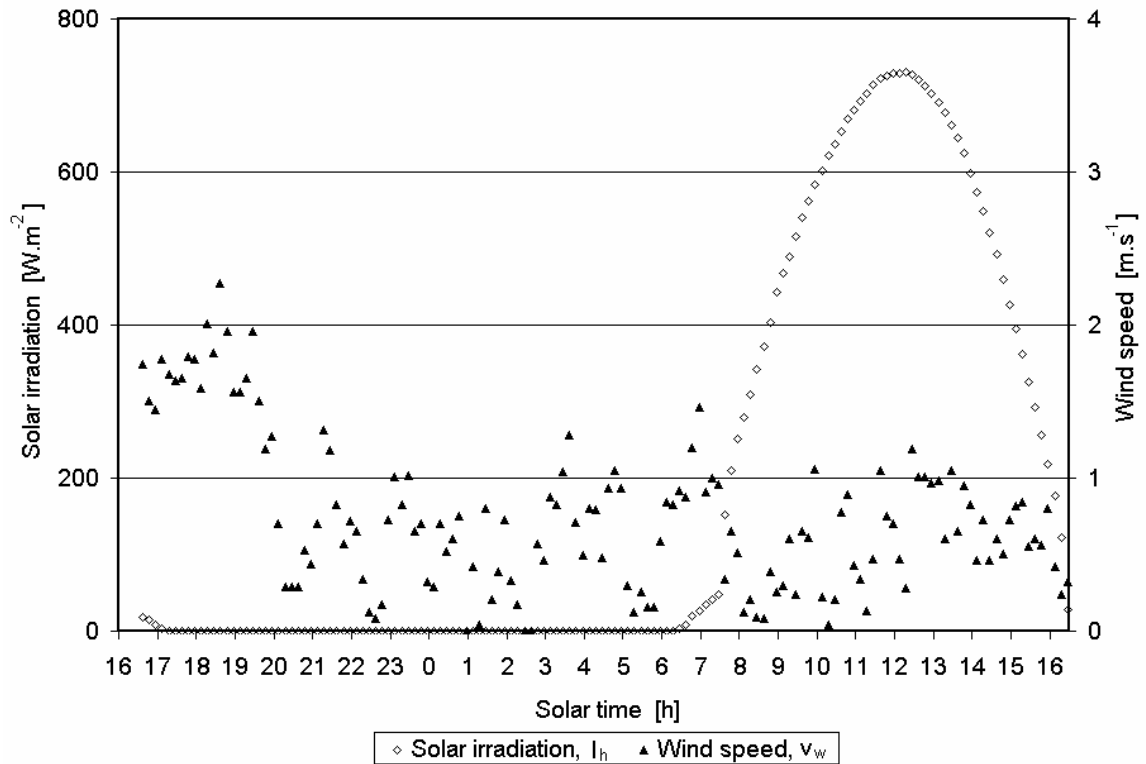


Figure 3.3: Solar irradiation and wind speed readings.

Observation of figure 3.4 shows that the value of the water surface temperature never drops below that of the dew-point temperature, and thus evaporation is continuously taking place.

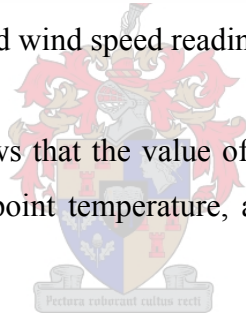


Figure 3.5 displays the water temperature profile found to occur during the period of analysis, it shows substantial cooling of the upper layer of water whenever solar radiation is absent. In general however, the change in temperature remains approximately constant from 20 mm below the surface until about 40 mm from the base. From the figure it is evident that the base is always at a greater temperature than that midway up when solar radiation is present.

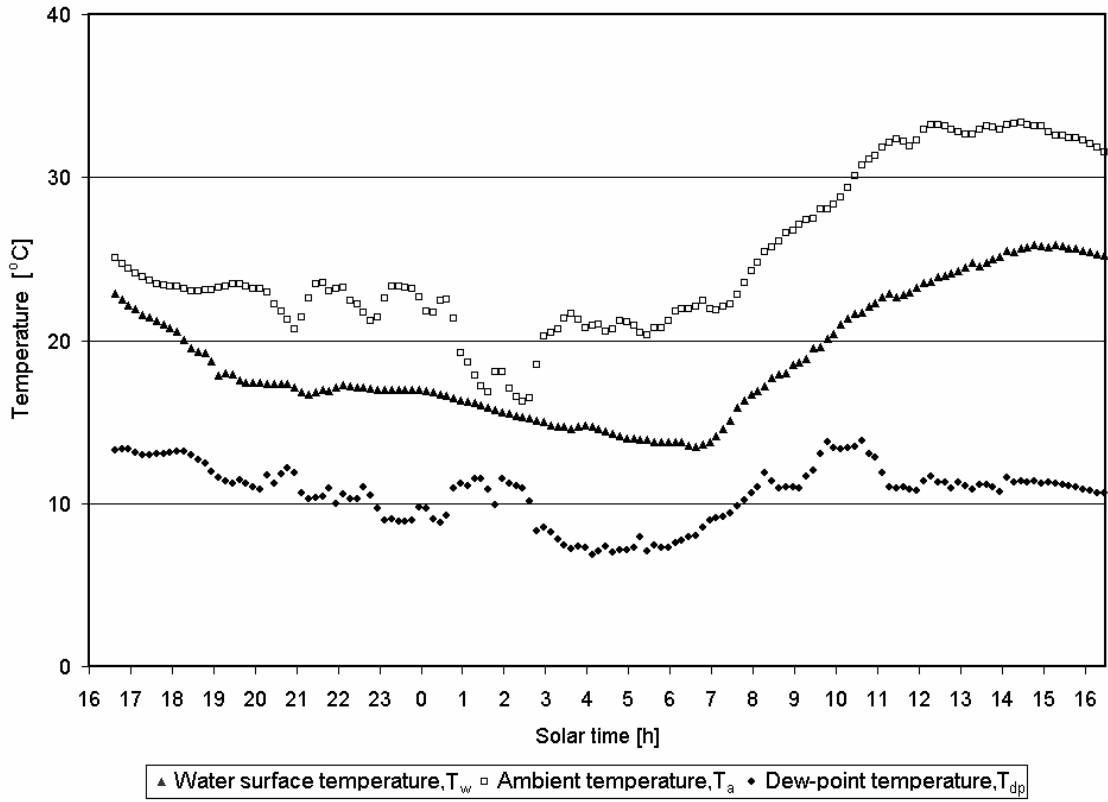


Figure 3.4: Ambient air-, water surface- and dew-point temperatures.

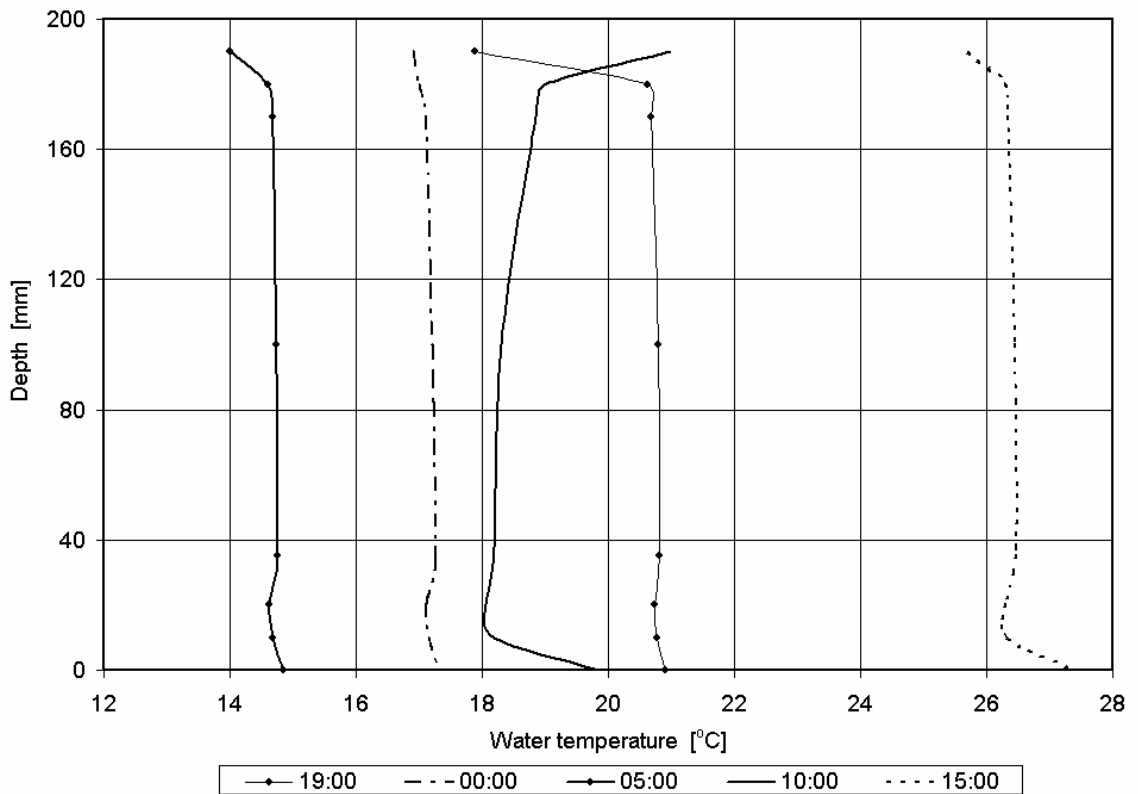


Figure 3.5: Water temperature distribution.

The use of some of the equations for evaporation rates employed in section 2.3 are reused in this analysis. The measured evaporation rate, as determined before is designated by  $m_{exp}$ .

Rewriting equation (3.1) in terms of the evaporation rate gives

$$m_{en} = \left( \alpha_w I_h - \varepsilon_w \sigma (T_w^4 - T_{sky}^4) - h_a (T_w - T_a) - m_{ev} i_{fg} - \rho_w t_w c_p \frac{dT_{wm}}{dt} \right) / i_{fg} \quad (3.2)$$

This is the evaporation rate as determined with the use of an energy balance,  $m_{en}$  and is used for comparison in conjunction with the evaporation rates as predicted by equations (2.8) and (2.9) in figure 3.6 below.

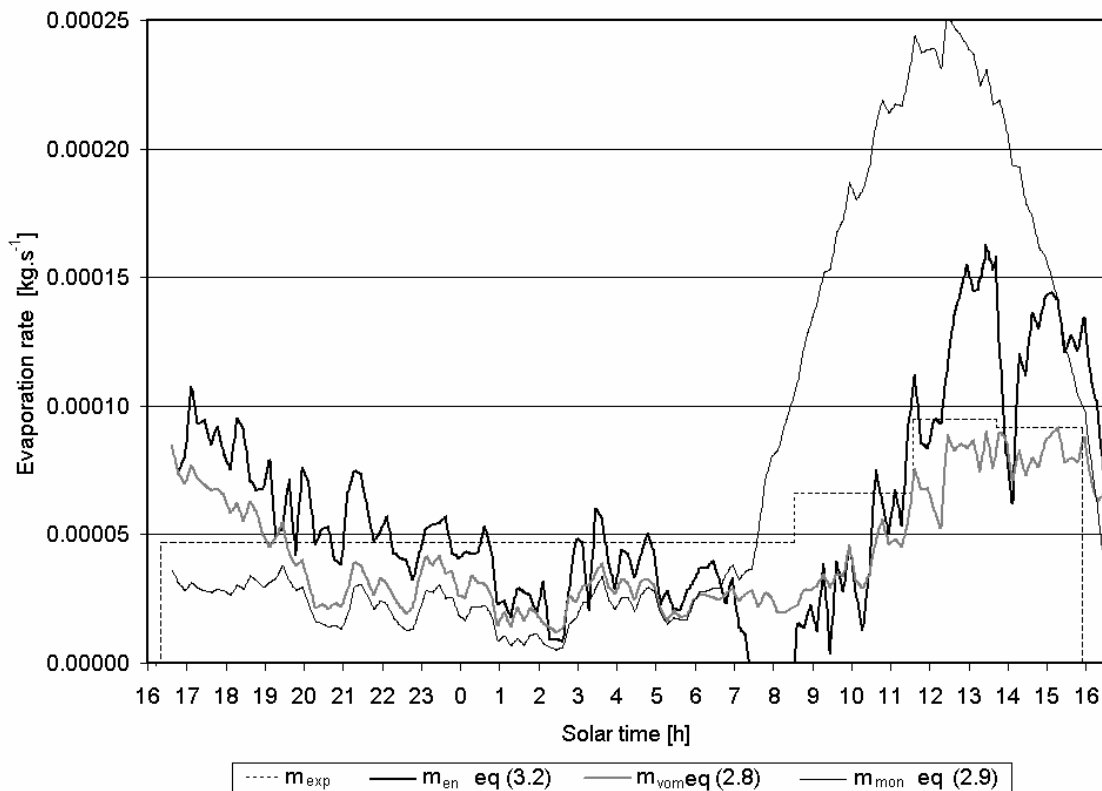


Figure 3.6: Comparative evaporation rates.

### 3.3 Solar collector with plastic covered water tank

As mentioned in section 3.1, freshwater solar ponds utilise transparent membranes in an attempt to hinder convective losses and eliminate evaporative losses from a body of water.

An experimental setup was utilised that consisted of a body of water that was covered by a thin plastic film and contained within an insulated tank with a glass cover. The glass cover and water temperatures were measured while the system was exposed to ambient conditions during the day and night. The system was then modelled theoretically, and the predicted results compared to those measured; *Lombaard (2002)* conducted similar tests with satisfying results on similar apparatus. This use of thermal insulation across the upper surface of the glass cover is also investigated.

#### 3.3.1 Analysis

Figure 3.7 shows a schematic drawing of the solar collector with plastic-covered water tank. By applying the conservation of energy law to the glass cover and the water tank, equations (3.3) and (3.4) are obtained respectively (see Appendix C).

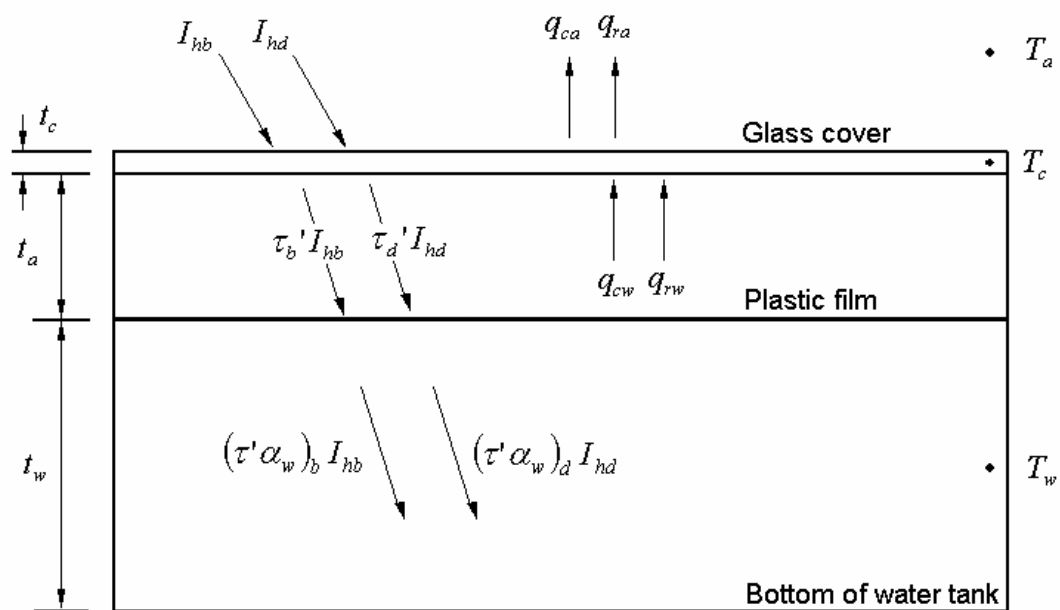


Figure 3.7: Schematic drawing of solar collector with plastic-covered water tank.

$$\begin{aligned}
 & \frac{(1-\rho_{bc})(1-\tau_{abc})}{1-\rho_{bc}\tau_{abc}} \cdot I_{hb} + \frac{(1-\rho_{dc})(1-\tau_{adc})}{1-\rho_{dc}\tau_{adc}} \cdot I_{hd} + \sigma \left( \frac{1}{\varepsilon_c} + \frac{1}{\varepsilon_f} - 1 \right)^{-1} (T_w^4 - T_c^4) \\
 & + \left[ 1 + 1.44 \left[ 1 - \frac{1708}{Gr_{cw} Pr_{cw}} \right] + \left[ \left( \frac{Gr_{cw} Pr_{cw}}{5830} \right)^{1/3} - 1 \right] \right] \frac{k_{cw}}{t_a} (T_w - T_c) \\
 & = \frac{\left[ 0.2106 + 0.0026 v_w \left[ \frac{\rho T_m}{\mu g (T_c - T_a)} \right]^{1/3} \right]}{\left[ \frac{\mu T_m}{g (T_c - T_a) c_p k^2 \rho^2} \right]^{1/3}} \cdot (T_c - T_a) + \varepsilon_c \sigma (T_c^4 - (0.727 + 0.006 T_{dp}) T_a^4)
 \end{aligned} \tag{3.3}$$

$$\begin{aligned}
 & \left[ \frac{(1-\rho_{bc})^2 \tau_{abc}}{(1-\rho_{bc}^2 \tau_{abc}^2)} \right] \left[ 1 - \frac{\rho_{baf} + (1-2\rho_{baf})\rho_{bfw} \tau_{abf}^2}{1-\rho_{baf}\rho_{bfw} \tau_{abf}^2} \right] \left[ 1 - \rho_{dc} \frac{\rho_{baf} + (1-2\rho_{baf})\rho_{bfw} \tau_{abf}^2}{1-\rho_{baf}\rho_{bfw} \tau_{abf}^2} \right]^{-1} \\
 & \cdot (1-\rho_{bw}) I_{hb} + \left[ \frac{(1-\rho_{dc})^2 \tau_{adc}}{(1-\rho_{dc}^2 \tau_{adc}^2)} \right] \left[ 1 - \frac{\rho_{daf} + (1-2\rho_{daf})\rho_{dfw} \tau_{adf}^2}{1-\rho_{daf}\rho_{dfw} \tau_{adf}^2} \right] \\
 & \cdot \left[ 1 - \rho_{dc} \frac{\rho_{daf} + (1-2\rho_{daf})\rho_{dfw} \tau_{adf}^2}{1-\rho_{daf}\rho_{dfw} \tau_{adf}^2} \right]^{-1} (1-\rho_{dw}) I_{hd} \\
 & = \left[ 1 + 1.44 \left[ 1 - \frac{1708}{Gr_{cw} Pr_{cw}} \right] + \left[ \left( \frac{Gr_{cw} Pr_{cw}}{5830} \right)^{1/3} - 1 \right] \right] \frac{k_{cw}}{t_a} (T_w - T_c) \\
 & + \sigma \left( \frac{1}{\varepsilon_c} + \frac{1}{\varepsilon_f} - 1 \right)^{-1} (T_w^4 - T_c^4) + \rho_w t_w c_{pw} \frac{dT_w}{dt}
 \end{aligned} \tag{3.4}$$

### 3.3.2 Experimental apparatus and procedure

The solar collector of concern consists of a 1 m x 1 m x 0.195 m black fibreglass water tank. A clear 0.2 mm thick Luminal Anti-Fog plastic covers the surface of the water with the purpose of suppressing evaporation. A 1 m x 1 m x 4 mm glass sheet covers the solar collector and is separated from the plastic film by a 0.1 m air space.

The water tank is insulated by 50 mm thick polystyrene, such that negligible conduction losses occur. The inner sides of the water tank are covered in highly reflective

aluminum foil to minimize any heat transfer between opposing sides, the water and the enclosed air gap. The solar collector was supported on a square pedestal with reflective sides that housed much of the data logging equipment. The apparatus is displayed figure 3.8.

The thermocouple frame mentioned in section 3.2 was employed to measure the water temperature at various depths, with the only difference being that the tank was only filled to a height of 170 mm from the base. Two thermocouples were placed beneath the base of the fiberglass water tank and three on the glass lid of the solar collector. Those on the glass lid were covered by highly reflective foil to minimize unwanted radiative contributions.

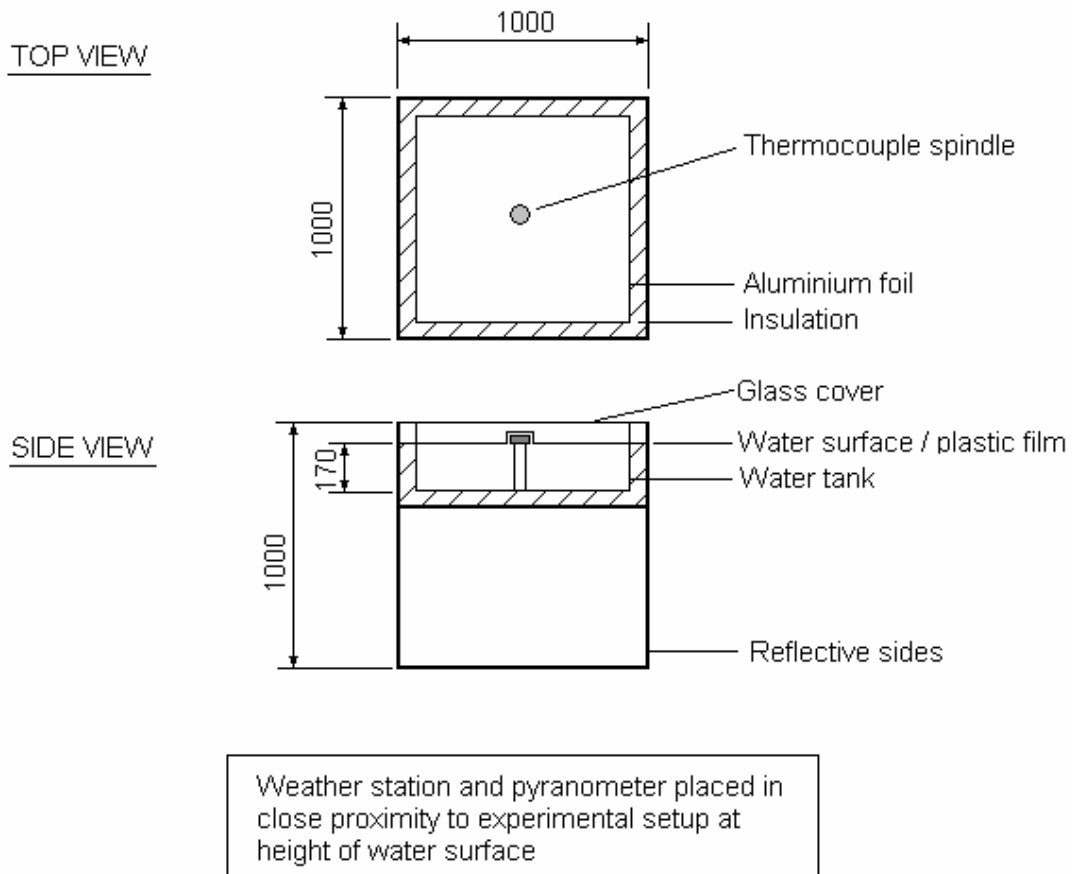


Figure 3.8: Experimental apparatus.

The total incident solar radiation was measured with aid of a Kipp and Zonen pyranometer. Diffuse radiation values were determined by casting a shadow over the instrument until such time that it stabilized. The beam radiation component was then

simply the difference between the measured total and diffuse radiation values. The weather station mentioned in figure 3.8 was used to measure the ambient temperature, wind speed and dew point temperature at one-minute intervals. A photograph of the solar collector is shown in Figure C.3.

### 3.3.3 Results and discussion

Tests were conducted on a continuous basis during extended periods of clear weather. The purpose of the tests was to predict the glass cover- and mean water temperatures with the theoretical models developed and to compare these temperatures with those measured through experimentation. The apparatus was given sufficient time to acclimatize with the environment and data taken on the 12<sup>th</sup> of January 2005 was considered suitable for analysis.

Observation of figure 3.9 shows that the wind speed was approximately constant throughout the period of analysis until the latter portion of the afternoon, at which point it was found to increase. The continuous solar radiation profile shows that no clouds were present during the period in which experimental readings were being taken.

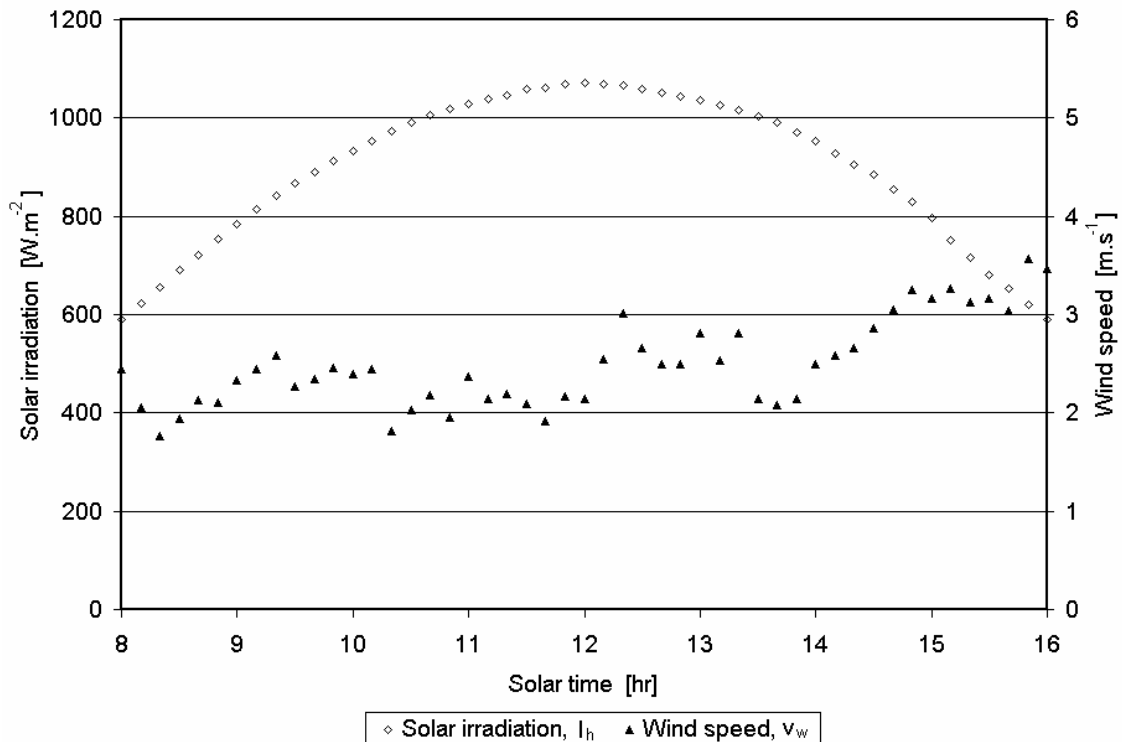


Figure 3.9: Total solar irradiation and wind speed readings.

Figure 3.10 shows the water temperature profile in the solar collector. The profile is seen to be approximately exponential, while relative cooling at the water surface (170 mm) becomes evident as the day progresses and the ambient temperature starts to decrease.

Figure 3.11 displays the measured and predicted glass cover- and mean water temperatures. The predicted temperatures are determined by solving equations (3.3) and (3.4) simultaneously, a mediocre agreement is found to exist between these values and those measured.

It was stated earlier that the decision was made not to include the change in stored energy of the glass cover in the current analysis. This choice was made since this particular inclusion was not expected to have any significant effect on the results; *Lombaard* (2002) attained acceptable results on an identical apparatus without the inclusion of this term.

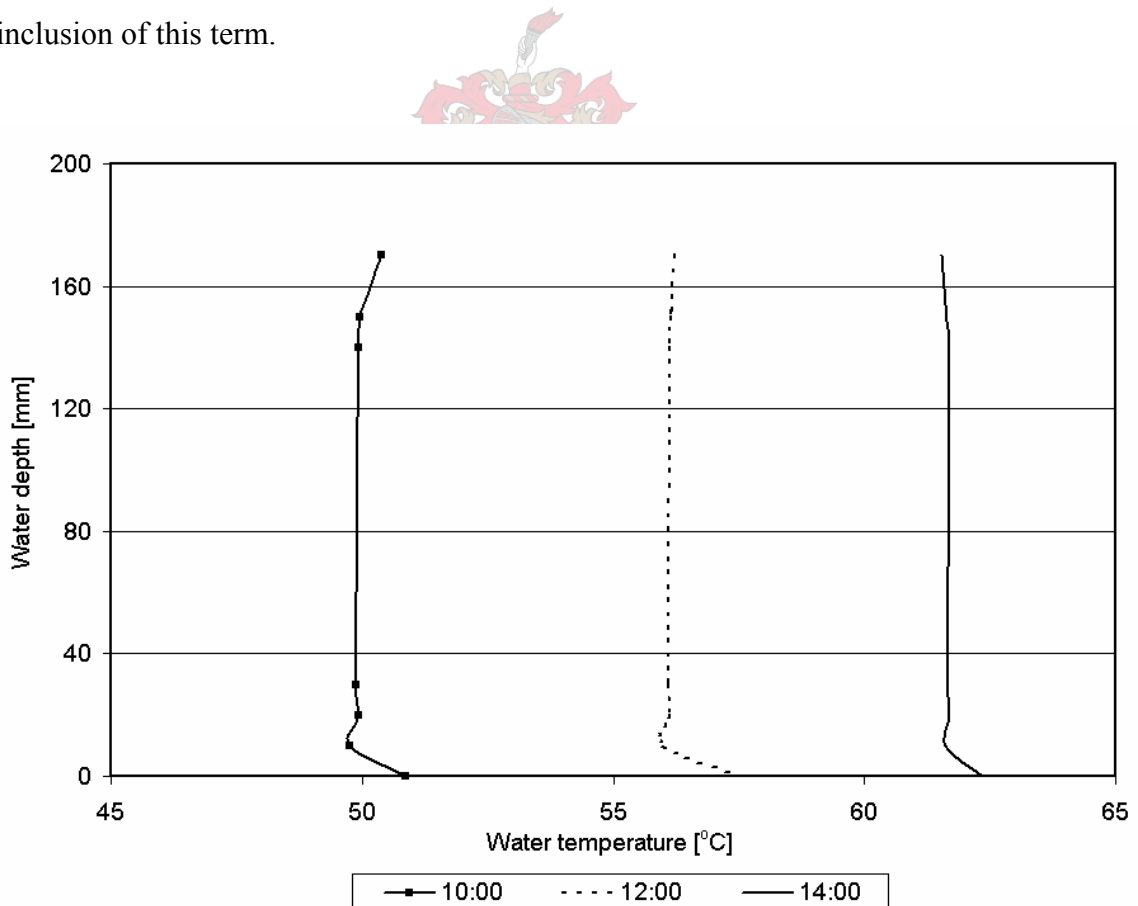


Figure 3.10: Water temperature profile.

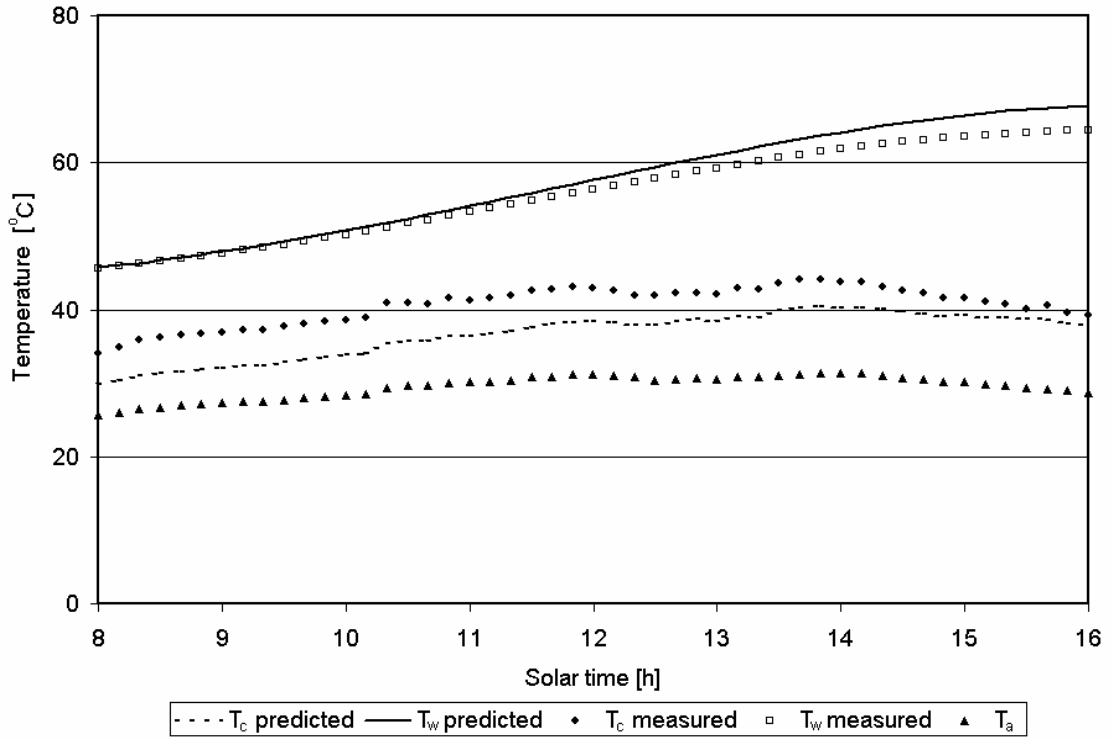


Figure 3.11: Ambient air temperature and predicted- and measured glass cover and mean water temperatures.

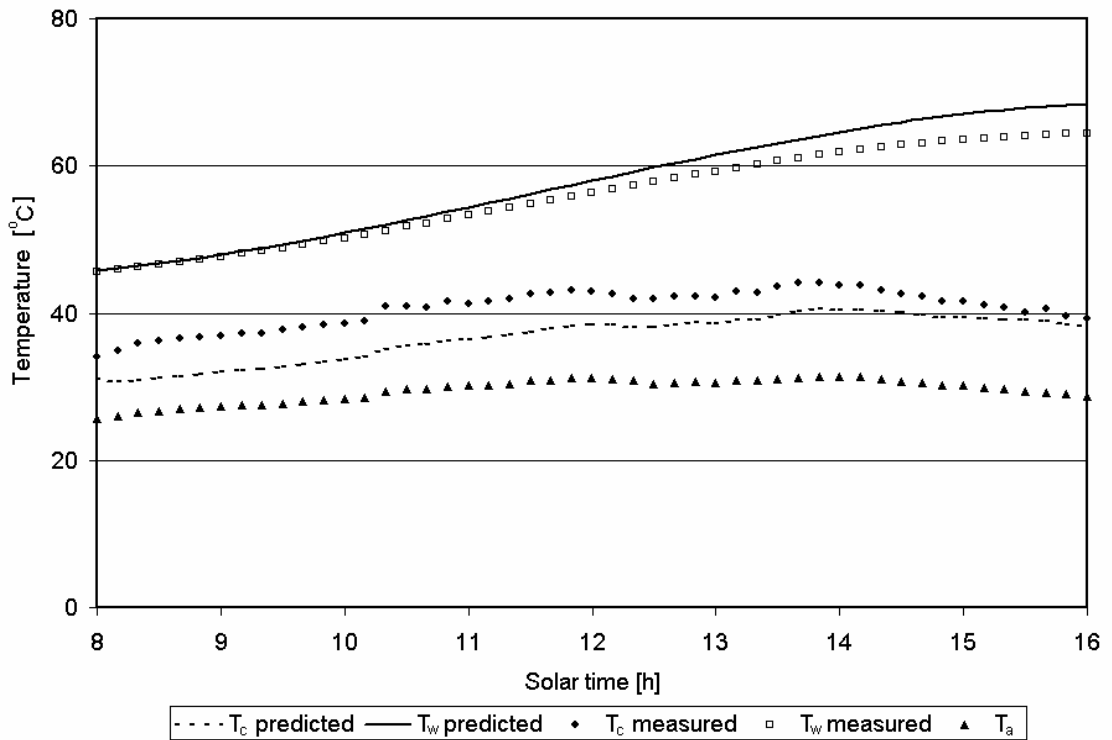


Figure 3.12: Results from same analysis as above, including effect of glass cover stored energy.

The results attained after having taken the stored energy term of the glass into account is displayed in figure 3.12; as expected the two figures differ very little from one another.

Displayed below are the results obtained with the use of equations (3.3) and (3.4) during night-time operation. The sky temperature in equation (3.3) needs to be represented by equation (2.6) for night-time operation.

Similarly, the results obtained with placing thermal insulation across the upper surface of the glass cover correspond reasonably well with one another. The thermal insulation used is sold under the name Sisalation, and is comprised of a thin layer (1 mm thick) of laminated aluminium. It was placed over the upper surface of the solar collector and sealed such that it was airtight. This form of insulation offers little resistance to conductive losses, but with a very low emissivity ( $\epsilon \approx 0.1$ ) it substantially reduces radiative losses from the particular system.

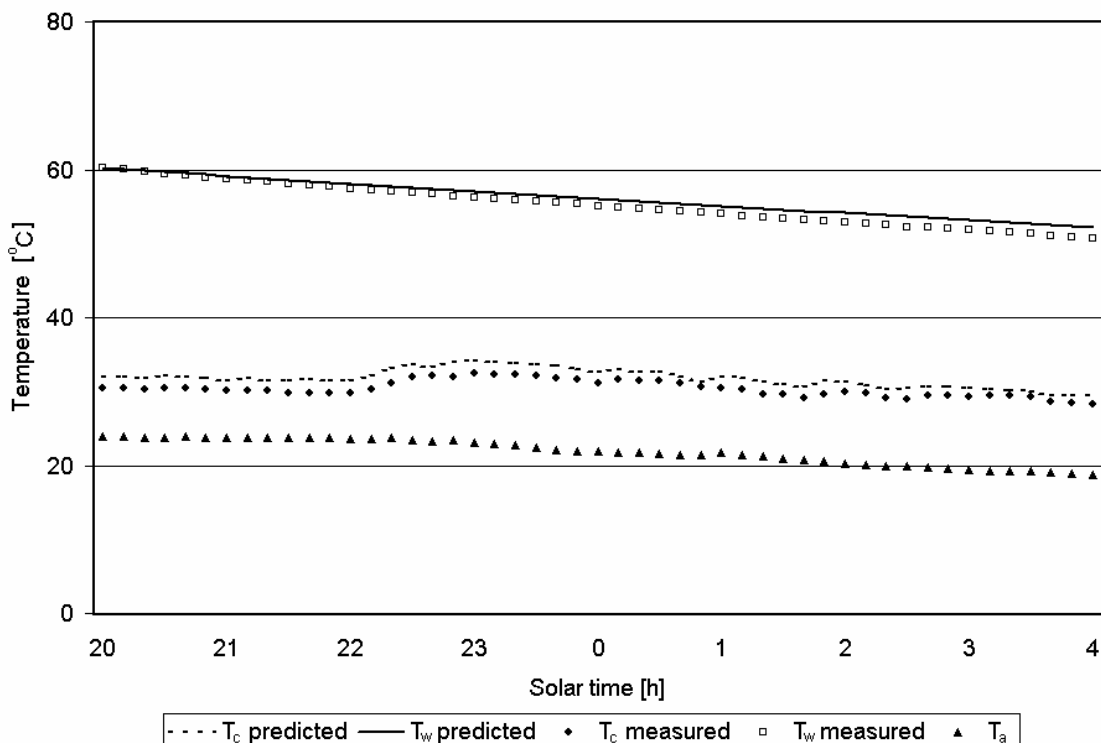


Figure 3.13: Ambient air temperature and predicted- and measured glass cover and mean water temperatures during the night.

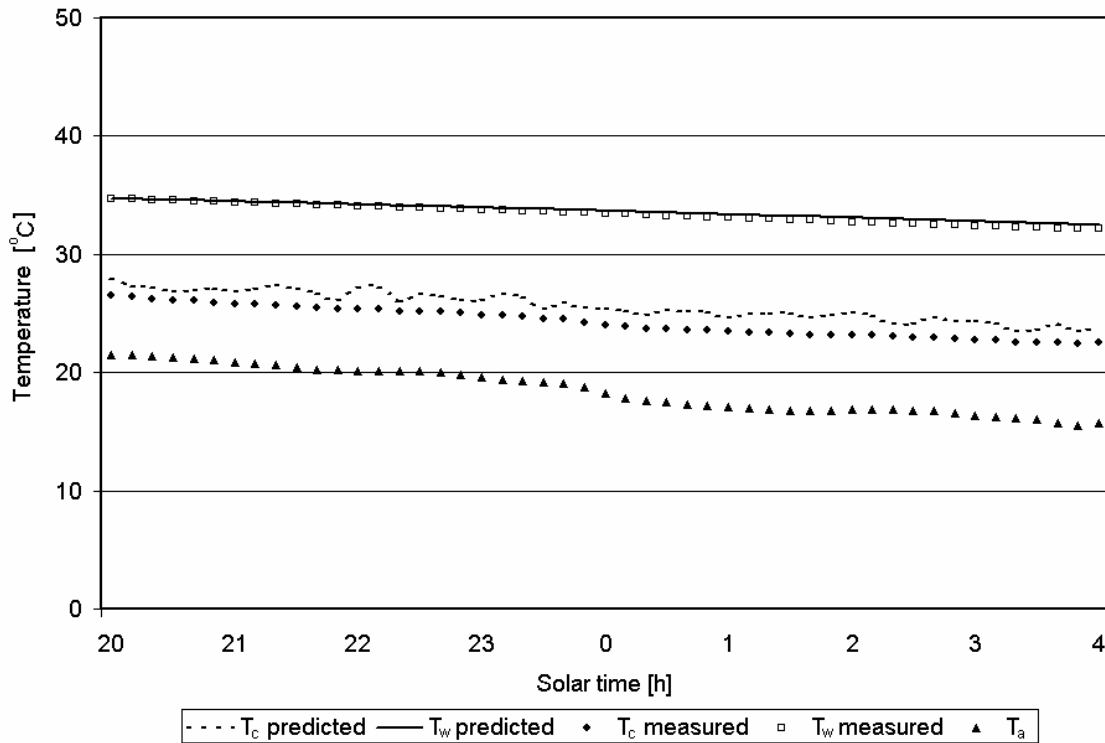


Figure 3.14: Ambient air temperature and predicted- and measured glass cover and mean water temperatures with Sisalation usage.

If the emissivity of the upper glass surface in equation (3.3) is set to that of the Sisalation, solving equations (3.3) and (3.4) simultaneously gives the results shown in figure 3.14 above. As with the modelling of the night-time operation, relatively good results were obtained.

### 3.4 Solar collector with condensation

If the same experimental setup as that in section 3.3 is considered, the thermal behaviour of the system is changed to a large degree by the removal of the plastic film covering the water surface.

Initially evaporation occurs from the water surface into the air until the air is fully saturated. Following this, condensation starts to occur on the lower surface of the glass plate and on the inner sides of the enclosure. As time progresses the condensed droplets within the enclosure increase in size, until such time that the gravitational force on the

droplets exceeds the surface tension and other microscopic forces retaining the droplets on the surface; this results in a condition referred to as runoff. This process then repeats itself. While this phenomenon occurs on the vertical sides of the enclosure, droplets on the horizontal surface reach sizes that far exceed those elsewhere in the system.

A literature study (see Chapter 1) revealed that horizontal roofs are very rarely used in greenhouses since pitched roofs assist in natural ventilation within the system, coincidentally this would also avoid the above problem within a saturated system. This may suggest why the author was unable to find any publications regarding condensation on horizontal glass plates. Technical papers found often dealt either with polyethylene, PVC or glass structures, however correlations associated with the influence of condensation on light transmission and reflection are only concerned with droplets with a maximum diameter of 1.5 – 2 mm on an inclined or vertical surface. This presented a problem since initially the droplets were very small, but once stabilised, the droplets reached diameters of approximately 10 – 12 mm (see figures 3.15 and 3.16).



Figure 3.15: Condensation of fine droplets.



Figure 3.16: Size of droplets attained once system became stabilised.

Another problem encountered with modelling the above system is explained below. When the system appears to have stabilised and the rate of evaporation equals the rate of condensation, then the influence of evaporation and condensation can be ignored, and the system can be modelled in a similar manner to that in section 3.3. However, when an increase or decrease in the glass cover temperature occurs, further evaporation or condensation will occur within the enclosure. This must be taken into account if the system is to be accurately modelled, but adds complexities to an already uncertain model.

With this in mind, it was attempted to model the system with constant glass/condensation solar properties, and under the assumption that no evaporation/condensation occurs within the system. Adapting the governing equations developed in section 3.3, the following glass/condensation properties were found to predict glass- and water temperatures that tracked the measured temperatures most accurately:  $\rho' = 0.1$ ,  $\tau' = 0.55$ ,  $\alpha' = 0.35$ .

It is interesting to view the temperature distribution in the water tank when compared to that found with the use of a plastic film on the water surface. Since the absorptivity of the cover is greater than before, the cover temperature exceeds the mean water temperature, which results in heating of the upper water layer and a greater variation in temperature (see figure 3.17).

Figure 3.18 displays the measured and predicted results obtained for the current system during daytime operation. The predicted results are obtained by solving equations (3.5) and (3.6) simultaneously. Note that the mean water temperature has been used in the calculations that follow.

$$0.35 \cdot (I_{hb} + I_{hd}) + \sigma \left( \frac{1}{\varepsilon_w} + \frac{1}{\varepsilon_w} - 1 \right)^{-1} (T_w^4 - T_c^4) + h_e \frac{k_{cw}}{t_a} (T_w - T_c) \quad (3.5)$$

$$= \frac{\left[ 0.2106 + 0.0026 v_w \left[ \frac{\rho T_m}{\mu g (T_c - T_a)} \right]^{1/3} \right]}{\left[ \frac{\mu T_m}{g (T_c - T_a) c_p k^2 \rho^2} \right]^{1/3}} \cdot (T_c - T_a) + \varepsilon_c \sigma (T_c^4 - (0.727 + 0.006 T_{dp}) T_a^4)$$

$$0.55 \cdot (I_{hb} + I_{hd}) = h_e \frac{k_{cw}}{t_a} (T_w - T_c) + \sigma \left( \frac{1}{\varepsilon_w} + \frac{1}{\varepsilon_w} - 1 \right)^{-1} (T_w^4 - T_c^4) + \rho_w t_w c_{pw} \frac{dT_w}{dt} \quad (3.6)$$

Note that the emissivities within the enclosure are replaced with those of water, while the convective heat transfer coefficient within the system is represented by  $h_e$ . If the water temperature is greater than the cover temperature then the correlation offered by *Holland et al.* (1975) in equation (C.9) is applicable, while if the cover temperature exceeds the water temperature, *Holman* (1986) recommends the use of equation (3.7).

$$h_e = 0.58 \cdot (Gr_{cw} \cdot Pr_{cw})^{0.2} \cdot \frac{k_{cw}}{t_a} \quad (3.7)$$

The results are also displayed for the system during night-time operation, and night-time operation with the use of Sisalation in figures 3.19 and 3.20 respectively. Note that

the sky temperature in equation (3.5) needs to be represented by equation (2.6) and not (2.5) as during daytime operation.

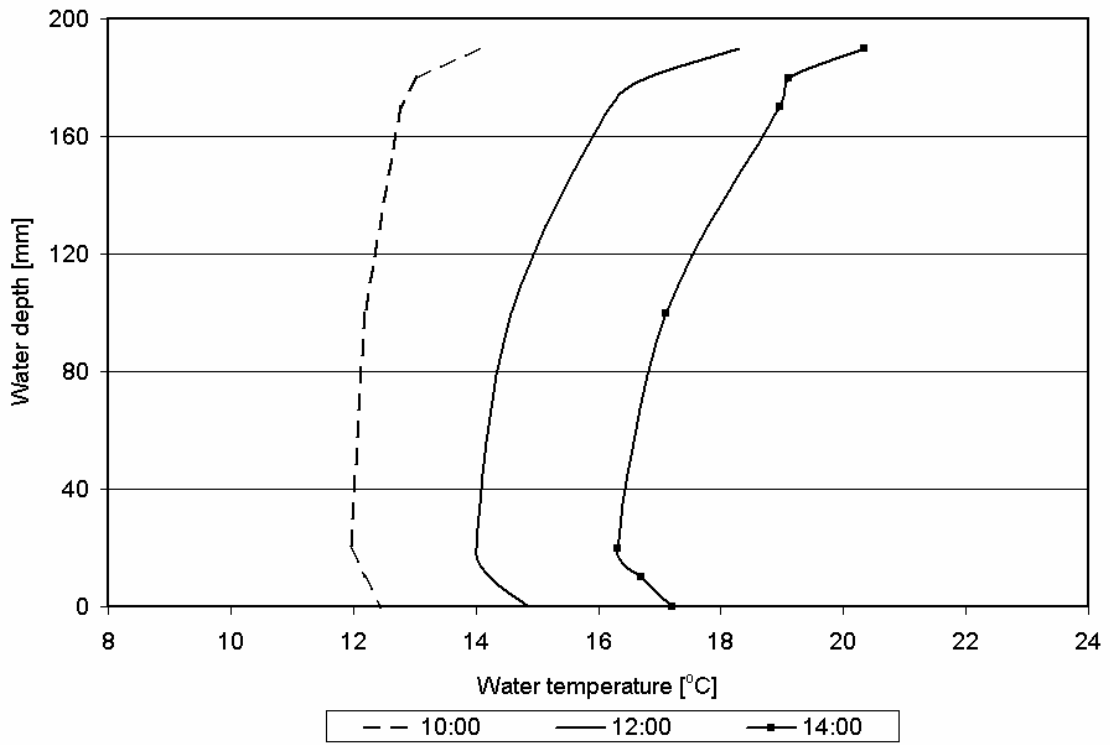


Figure 3.17: Water temperature distribution.

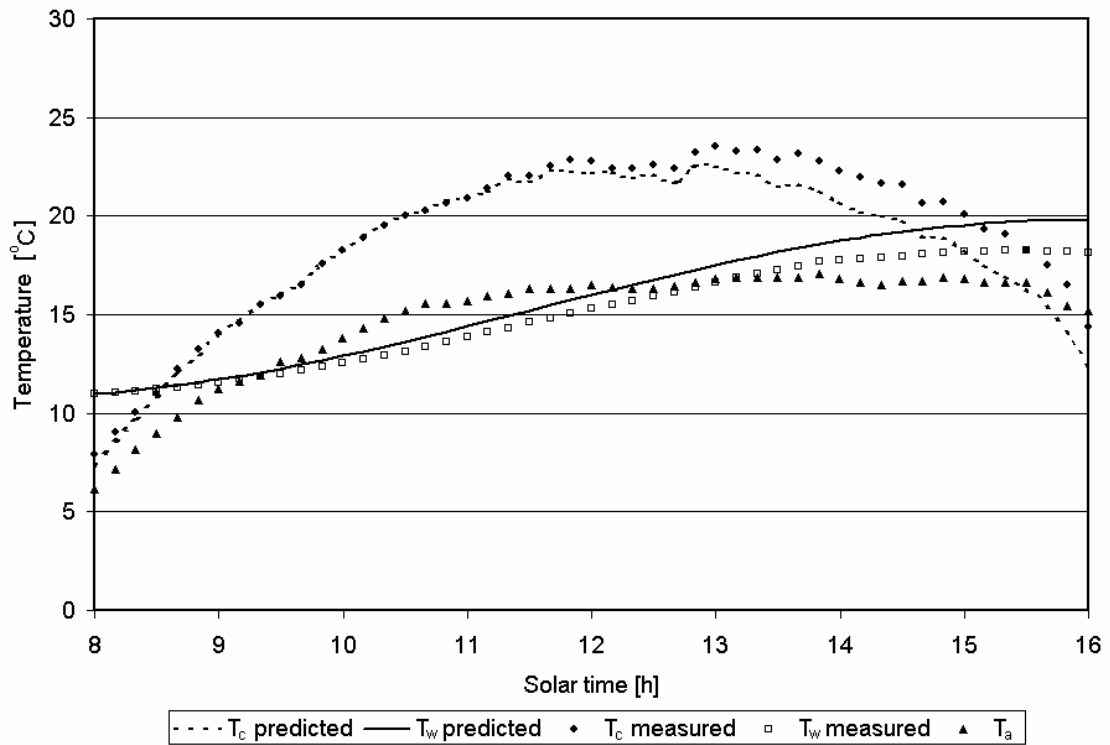


Figure 3.18: Measured- and predicted glass and mean water temperatures.

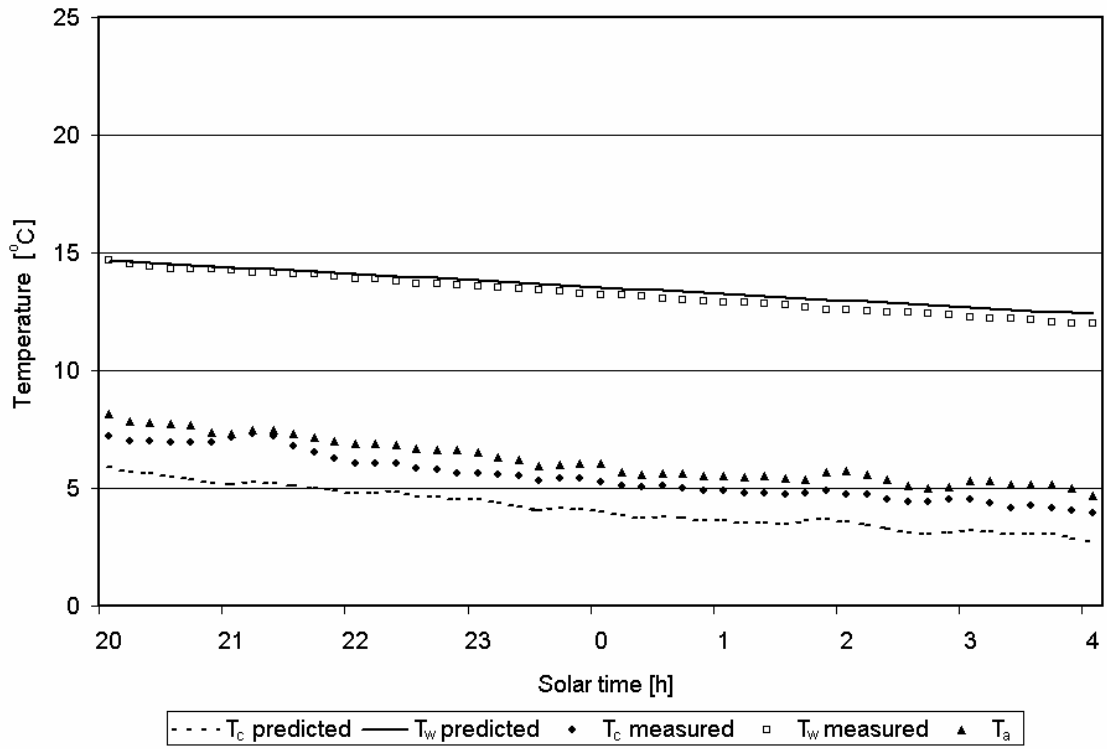


Figure 3.19: Results attained for night-time operation.

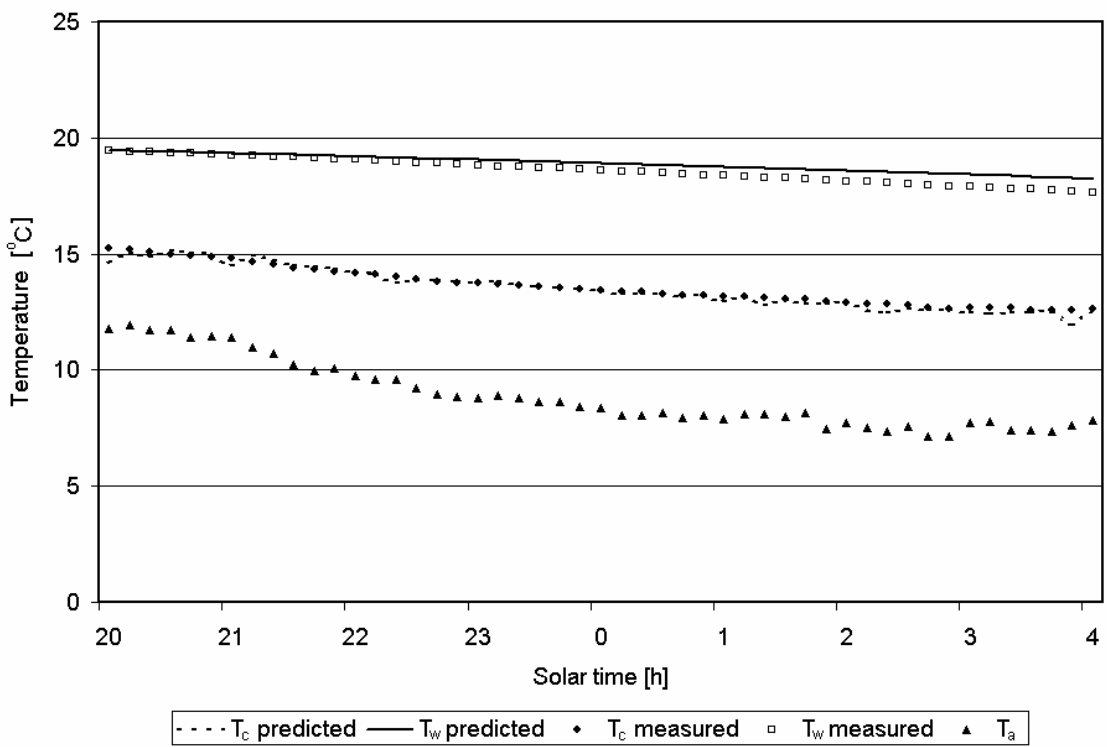


Figure 3.20: Measured- predicted temperatures with Sisalation usage.

### 3.5 Conclusion

The results of section 3.2 are summarised in figure 3.6. It shows a reasonable correlation between the measured evaporation rates from the water tank  $m_{exp}$ , and those predicted by equation (2.8). The use of an energy balance with equation (3.2) shows very erratic results, which if averaged out over a longer period of time, may too provide reasonable results. This erratic nature may be attributed to the term in equation (3.2) associated with the change in internal energy of the volume of water. This change is a function of the change in average temperature of the water and is highly sensitive to small changes in this value.

Equation (2.9) provides a very poor prediction of the evaporation rate. During the day it overestimates the mass flow from the water surface by a very large margin, but provided a reasonable estimate when applied to the wetted surface in Chapter 2. This expression is used extensively in evapotranspiration calculations that involve the evaporation of moisture from leaves or other botanical surfaces. Clearly applications such as this are quite different to the current analysis since they do not consider a change in internal energy of the system, this may explain the inaccuracy obtained in figure 3.6. A full numerical example is available in Appendix C.



The solar collector with plastic-covered water tank was considered in section 3.3, the following can be concluded from the associated experimental work.

The use of a transparent membrane on the surface of a body of water to suppress evaporation is very effective and mean water temperatures of approximately 35 °C greater than the ambient air temperature were attained. Figure 3.11 compares the measured- and predicted glass cover and mean water temperatures, with a maximum temperature difference between the measured and predicted values of approximately 5- and 3 °C respectively. This error is found with both an initial temperature difference and a cumulative error.

The fact that the predicted water temperature was too high and the cover temperature suggests that the heat transferred between the water surface and cover is less than

expected. This is unlikely however, since *Lombaard* (2002) followed the same procedure with better results, even though he only compared the measured and predicted temperatures over a period of an hour.

As shown by figure 3.10, very little difference exists between the mean- and surface water temperatures; and the comparison between figure 3.11 and 3.12 show that neglecting the stored energy in the glass cover was an acceptable approximation. The apparatus was well sealed and infiltration of ambient air into the enclosure was not permitted, thus the reason for the difference in measured- and predicted temperatures is still unknown.

Good results were obtained on the same apparatus during night-time operation, with and without the use of Sisalation. Figures 3.13 and 3.14 indicate a maximum difference of approximately 2 °C for the glass cover temperature and less for the mean water temperature.

Section 3.4 was included since a saturated system is of great interest to the current study, most points of interest have however already been considered. Theoretical modelling of the daytime operation was simply included as an approximation, while the night-time models are of more importance.

The results obtained were relatively good, with figures 3.18, 3.19 and 3.20 showing better correlations than those in section 3.3.

## CHAPTER 4

# Greenhouse modelling

- 4.1 Modelling objectives
  - 4.2 Fundamental system
  - 4.3 Night-time insulation usage
  - 4.4 Day- and night-time insulation usage
  - 4.5 Conclusion
- 

### 4.1 Modelling objectives

In this chapter a basic greenhouse model is developed, with the intention of quantifying the heat fluxes to and from the system when exposed to ambient conditions. The horizontal roof and walls are of glass construction, while a concrete slab serves as a floor; since glass has a high transmissivity, this implies that the quantity of solar energy incident on the system is very high, but also that the losses incurred are extensive. Once complete, this model will determine the temperatures that can be attained within such a greenhouse. A sketch of the greenhouse is shown in figure 4.1.

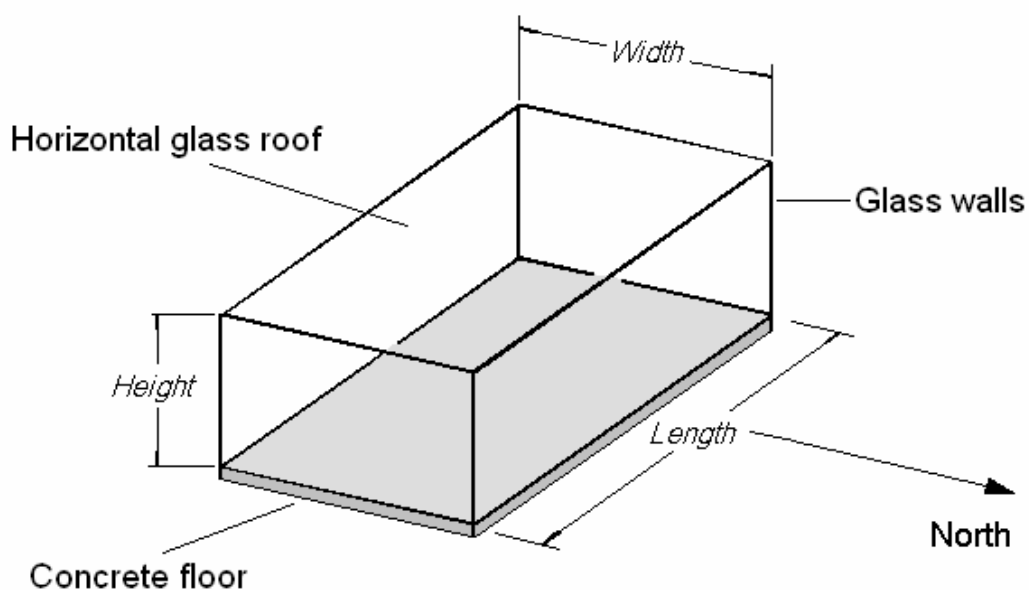


Figure 4.1: Sketch of fundamental greenhouse.

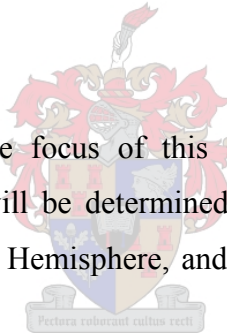
This model will also be used to determine the influence of insulation usage on certain surfaces of the greenhouse, to determine the maximum temperatures that are theoretically possible during winter operation.

## 4.2 Fundamental system

The basic model was of rectangular construction, with a 100 mm concrete floor, and a 4 mm standard glass flat roof and walls. Dry air conditions were assumed to exist within the structure.

The weather profile used in the model is from Sishen, South Africa (23.00° E, 27.67° S). Ambient air temperature, humidity, total- and diffuse solar radiation and wind speed-readings are given on an hourly basis for this particular location. Skies are assumed to be clear and the wind is assumed to blow across the roof and three of the four walls.

Since the winter period is the focus of this study, the thermal behaviour of the greenhouse on June the 21<sup>st</sup> will be determined. This date is selected since it is the winter solstice in the Southern Hemisphere, and the day on which the available solar radiation is at it's least.



### 4.2.1 Analysis

The given system is analysed in the following manner: the structure is divided into seven parts, namely the roof, the floor, the four walls and the enclosed air within the greenhouse. An energy balance is applied to each of these components while exposed to the selected ambient conditions, with the result that each of these temperatures are predicted for any time and day throughout the year. Note that the floor, roof, walls and enclosed air are each assumed to have a constant temperature throughout, and conduction between adjacent surfaces is assumed negligible.

The first step is to determine the nature of the solar radiation on all of the greenhouse surfaces.

A measure of the position of the sun in the sky is known as the zenith angle  $\theta_z$ , and the calculation thereof is critical to the current analysis. The angle formed between the sun and the normal to a particular surface is known as the incidence angle,  $\theta$ . As stated in Appendix A, the incidence- and zenith angles can be calculated according *Duffie and Beckman* (1991) with the aid of equations (A.1) and (A.2) for any randomly orientated surface.

Note that at any time of the day it is only possible for two of the four vertical walls to experience direct sunlight, and thus two of the surfaces will have incidence angles greater than  $90^\circ$ .

The geometric factor  $R_b$  is a ratio between the intensity of the solar radiation on a particular surface and that on a horizontal surface; it is defined by equation (A.9) and is has to be considered if non-horizontal surfaces are to be analysed.

Determining the portion of sunlight that is transmitted, absorbed and reflected from each of the greenhouse surfaces is crucial. From Appendix D, equations (D.9) and (D.13) express the reflectivity and transmissivity for any non-opaque surface; and can then be used in conjunction equations (D.4), (D.5) and (D.6) to calculate the effective reflectivity, -transmissivity and -absorptivity of the particular surface.

The above relations hold for a wall of the greenhouse which is in direct sunlight, however if one or more of the walls does not receive direct solar radiation then the situation becomes somewhat more complex. It becomes necessary to determine through which particular wall the light has been transmitted before striking the wall of interest, and the associated area for which that portion of light is responsible. The reader is referred to Appendix E for the appropriate equations.

The areas in Appendix E are calculated with use of the horizontal- and vertical components of the incident sunlight, which have yet to be defined. Determining these values requires that it be known in which quadrant the sun is present. Figure 4.2 below shows a theoretical plot of the sun's path on January the 1<sup>st</sup> and July the 1<sup>st</sup>.

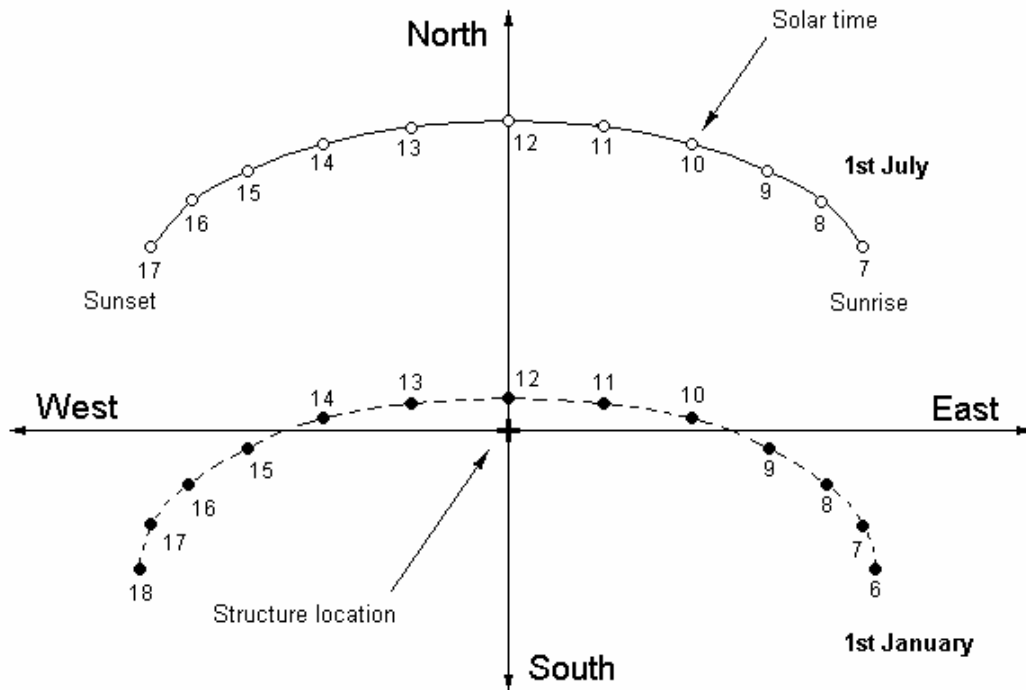


Figure 4.2: Path of the sun from above on the 1<sup>st</sup> of January and the 1<sup>st</sup> of July.

The horizontal component of the incident sunlight is simply calculated by taking the difference between the solar- and surface azimuth angles

$$\theta_{horiz} = \gamma - \gamma'_s \quad (4.1)$$

The vertical component is represented by the expression below.

$$\theta_{vert} = \tan^{-1} \left( \frac{\tan \alpha_s}{\cos \theta_{horiz}} \right) \quad (4.2)$$

With the above taken into consideration, if a glass window is not in direct sunlight it can be determined through which window the transmitted light that strikes the particular window has passed and the area for which that portion of light is responsible.

Now that the solar calculations have been taken into account, energy conservation equations can be developed for the respective greenhouse surfaces.

## 4.2.1.1 Flat glass roof

Consider the heat fluxes associated with the roof of the greenhouse.

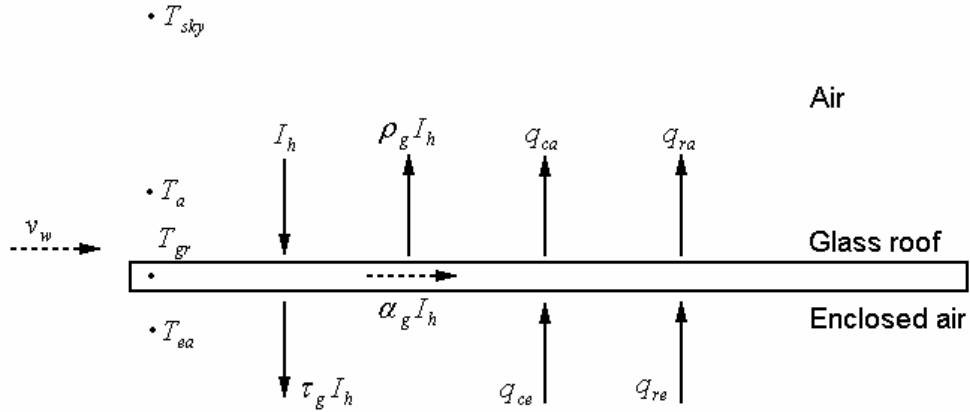


Figure 4.3: Energy balance on the roof of the greenhouse.

If a control volume is drawn around the roof, the energy entering and leaving the control volume can be summed as shown below.

$$I_h + q_{ce} + q_{ra} = \rho_g \cdot I_h + \tau_g \cdot I_h + q_{ca} + q_{ra}$$

$$(I_{hb} + I_{hd}) \cdot (1 - \tau_g - \rho_g) + q_{ce} + q_{ra} - q_{ca} - q_{ra} = 0$$

$$I_{hb} \cdot \alpha_{bg} + I_{hd} \cdot \alpha_{dg} + q_{ce} + q_{ra} - q_{ca} - q_{ra} = 0 \quad (4.3)$$

The subscripts *ce* and *re* represent the convective and radiative heat transfer within the greenhouse, while *ca* and *ra* represent the convective and radiative heat transfer to the environment.

Note that with respect to figure 4.3 the convective heat fluxes can be expressed as:

$$q_{ce} = h_e \cdot (T_{ea} - T_{gr}) \quad (4.4)$$

$$q_{ca} = h_a \cdot (T_{gr} - T_a) \quad (4.5)$$

The internal convective heat transfer coefficient for a horizontal surface is found according to *Holman* (1986) in equation (4.6) below:

$$h_e = \frac{k}{L} \cdot Nu \quad (4.6)$$

where  $Nu$  is the Nusselt number with a value defined by one of the following applicable relations.

$$Nu = 0.13 (Gr Pr)^{1/3} \quad \text{cooled surface facing downward, } Gr Pr < 2.10^8$$

$$Nu = 0.16 (Gr Pr)^{1/3} \quad \text{cooled surface facing downward, } 2.10^8 < Gr Pr < 10^{11}$$

$$Nu = 0.58 (Gr Pr)^{1/5} \quad \text{heated surface facing downward}$$

The convective heat transfer coefficient on the upper surface is determined according to *Burger and Kröger* (2004) as shown in equations (2.1) and (2.2).

The radiative heat transfer within the greenhouse is likely to become quite a complex analysis, the benefits of which are doubtful. While the difference in temperature between the floor and the other surfaces within the greenhouse may be substantial, the temperature of the glass surfaces are expected to be similar and thus the only radiative transfer considered within the enclosure is that between the concrete floor and the glass surfaces.

The radiative heat flux heat flux reaching the roof from the concrete floor is then

$$q_{ra} = \frac{\sigma \cdot (T_f^4 - T_{gr}^4)}{A_{gr} \cdot R_{rf}} \quad (4.7)$$

Where the resistance to transfer  $R_{rf}$  is:

$$R_{rf} = \left( \frac{1 - \varepsilon_r}{\varepsilon_r \cdot A_r} + \frac{1}{A_r \cdot F_{rf}} + \frac{1 - \varepsilon_f}{\varepsilon_f \cdot A_f} \right). \quad (4.8)$$

The radiative heat flux leaving the upper surface of the roof is emitted to a sky temperature  $T_{sky}$  defined by equations (2.5) and (2.6), and where

$$q_{ra} = \varepsilon_g \cdot \sigma \cdot (T_{gr}^4 - T_{sky}^4) \quad (4.9)$$

Then if equation (4.3) is considered, it can be rewritten as:

$$I_{hb} \cdot \frac{(1 - \rho_b) \cdot (1 - \tau_{ab})}{1 - \rho_b \cdot \tau_{ab}} + I_{hd} \cdot \frac{(1 - \rho_d) \cdot (1 - \tau_{ad})}{1 - \rho_d \cdot \tau_{ad}} + h_e \cdot (T_{ea} - T_{gr}) + \frac{\sigma \cdot (T_f^4 - T_{gr}^4)}{A_r \cdot R_{rf}} - h_a \cdot (T_{gr} - T_a) - \varepsilon_g \cdot \sigma \cdot (T_{gr}^4 - T_{sky}^4) = 0 \quad (4.10)$$

#### 4.2.1.2 Vertical glass walls

In a similar manner to which the glass roof was analysed, consider the vertical glass walls. Assume for the sake of notation that the window in the analysis faces north.

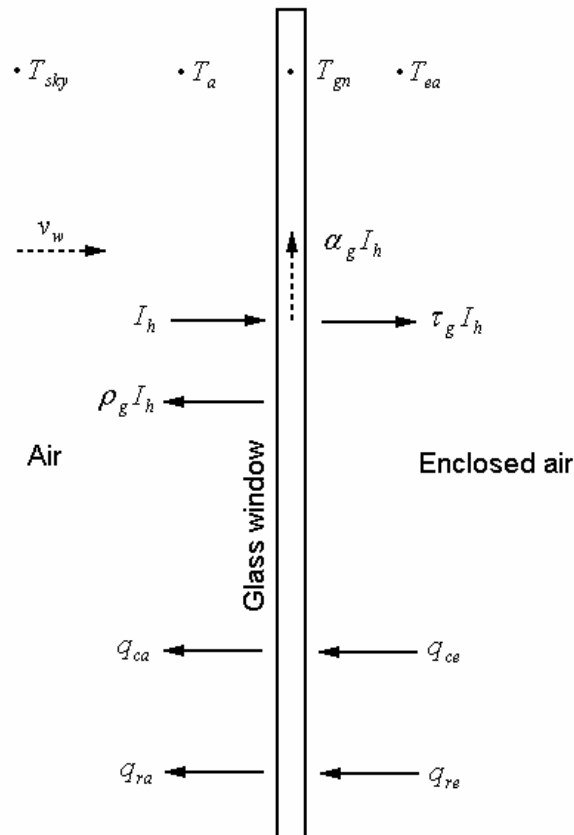


Figure 4.4: Heat fluxes imposed on vertical glass window.

Equation (4.3) is applicable to this window as well; the only difference in this case is the change in convective heat transfer coefficients.

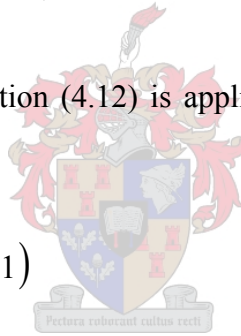
Empirical correlations for combined forced- and free convection are not readily available for vertical plates due to the numerous complexities present, which are not found on horizontal plates. Thus in an attempt to solve this problem, it was decided that heat transfer coefficients for both free- and forced convection would be determined and the larger of the two would be retained for use in the model.

For free convection *Churchill and Chu* (1975) supply the following relation:

$$Nu = 0.825 + \frac{0.387 Ra^{1/6}}{\left(1 + (0.492/Pr)^{9/16}\right)^{8/27}} \quad (4.11)$$

While for flat plate flow equation (4.12) is applicable for both laminar and turbulent conditions, *Holman* (1986):

$$Nu = Pr^{1/3} \cdot (0.037 \cdot Re^{0.8} - 871) \quad (4.12)$$



Note that the applicable characteristic length is only half the length of the window across which the wind blows, since it is the average heat transfer coefficient across the surface that is desired.

Therefore the conservation of energy equation applicable to the vertical walls is very similar to equation (4.10) for the horizontal surface.

$$I_{hb} \cdot \frac{(1 - \rho_b) \cdot (1 - \tau_{ab})}{1 - \rho_b \cdot \tau_{ab}} + I_{hd} \cdot \frac{(1 - \rho_d) \cdot (1 - \tau_{ad})}{1 - \rho_d \cdot \tau_{ad}} + h_e \cdot (T_{ea} - T_{gn}) + \frac{\sigma \cdot (T_f^4 - T_{gn}^4)}{A_n \cdot R_{nf}} - h_a \cdot (T_{gn} - T_a) - \varepsilon_g \cdot \sigma \cdot (T_{gn}^4 - T_{sky}^4) = 0 \quad (4.13)$$

## 4.2.1.3 Concrete floor

The analysis of the concrete floor differs from that of the vertical and horizontal glass sheets, in that the concrete slab is opaque, the thermal inertia is taken into consideration and while exposed to the enclosed air on one surface, it is assumed to be fully insulated on the other.

The conservation of energy equation then reads as follows:

$$I_h = (1 - \alpha_c) \cdot I_h + q_{ce} + q_{re} + m \cdot c_p \cdot \frac{dT_f}{dt} \quad (4.14)$$

If equations (2.1) or (2.2) are used to determine the natural convective heat transfer coefficient for the upper surface, then it remains only for the radiative heat transfer between the floor and the glass surfaces to be taken into account as shown in equation (4.7) and (4.8).

Rewriting equation (4.14) as follows:

$$0 = (1 - \alpha_c) \cdot I_h - h_e \cdot (T_f - T_{ea}) - \frac{\sigma \cdot (T_f^4 - T_{gr}^4)}{A_f \cdot R_{fr}} - \frac{\sigma \cdot (T_f^4 - T_{gn}^4)}{A_f \cdot R_{fn}} - \frac{\sigma \cdot (T_f^4 - T_{gw}^4)}{A_f \cdot R_{fw}} - \frac{\sigma \cdot (T_f^4 - T_{ge}^4)}{A_f \cdot R_{fe}} - \frac{\sigma \cdot (T_f^4 - T_{gs}^4)}{A_f \cdot R_{fs}} - \frac{m}{A_f} \cdot c_p \cdot \frac{(T_f - T_{f \text{ initial}})}{dt} \quad (4.15)$$

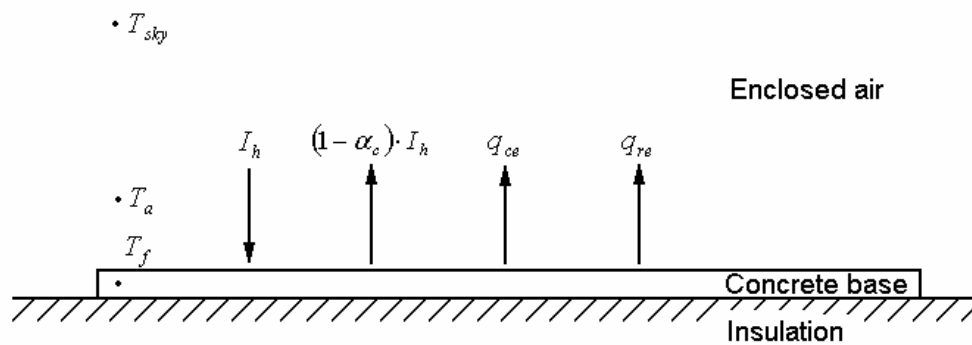


Figure 4.5: Heat fluxes associated with concrete floor.

#### 4.2.1.4 Enclosed air

Since the temperature of the enclosed air,  $T_{ea}$  is highly unlikely to reach very high temperatures, and since short-wave radiation has no influence on air, the radiation exchange within the enclosure and direct solar radiation have no influence on the enclosed body of air.

This means that the air will only experience convective heat gains / losses from the greenhouse surfaces and a change in internal energy as shown below.

$$\begin{aligned}
 & h_e \cdot A_f \cdot (T_f - T_{ea}) + h_e \cdot A_r \cdot (T_{gr} - T_{ea}) + h_e \cdot A_n \cdot (T_{gn} - T_{ea}) + h_e \cdot A_s \cdot (T_{gs} - T_{ea}) \\
 & h_e \cdot A_w \cdot (T_{gw} - T_{ea}) + h_e \cdot A_e \cdot (T_{ge} - T_{ea}) + m \cdot c_{pa} \cdot \frac{(T_{ea} - T_{ea\ initial})}{dt} = 0 \quad (4.16)
 \end{aligned}$$

Note that the internal convective heat transfer coefficients  $h_e$  in the above expression, are those applicable to each of the appropriate surfaces.

It is now possible for equations (4.10), (4.13), (4.15) and (4.16) to be solved simultaneously with the aid of the Gauss-Seidel method to determine the predicted temperatures. This is possible if an estimate of the initial floor- and enclosed air temperatures is made, the above-mentioned equations can be solved to determine the applicable temperatures at each time step.

#### 4.2.2 Simulation results

The simulation was run on June the 21<sup>st</sup> for a glass greenhouse with a 100 mm concrete floor, and for the same greenhouse with a 100 mm layer of concrete ( $\rho_c = 2300 \text{ kg.m}^{-3}$ ,  $c_{pc} = 880 \text{ J.kg}^{-1}.\text{K}^{-1}$ ,  $\alpha_c = 0.61$ ,  $\epsilon_c = 0.9$ ) replaced by a layer of water of the same thickness. The greenhouse was given arbitrary dimensions of 15 m in length, 5 m in width and a height of 2.8 m. The building faces directly north, with the 15 m length running from east to west. Figures 4.6 and 4.7 show the solar irradiation, and relative humidity- and wind speed readings expected on June the 21<sup>st</sup>. Take note that the sun rises and sets at 07:00 and 17:00 respectively. The wind speed measured at a height of

10 m above the ground, ranges approximately between 2.8 and 3.9 m.s<sup>-1</sup>, while the least humid time of the day can be seen to be at about 15:00.

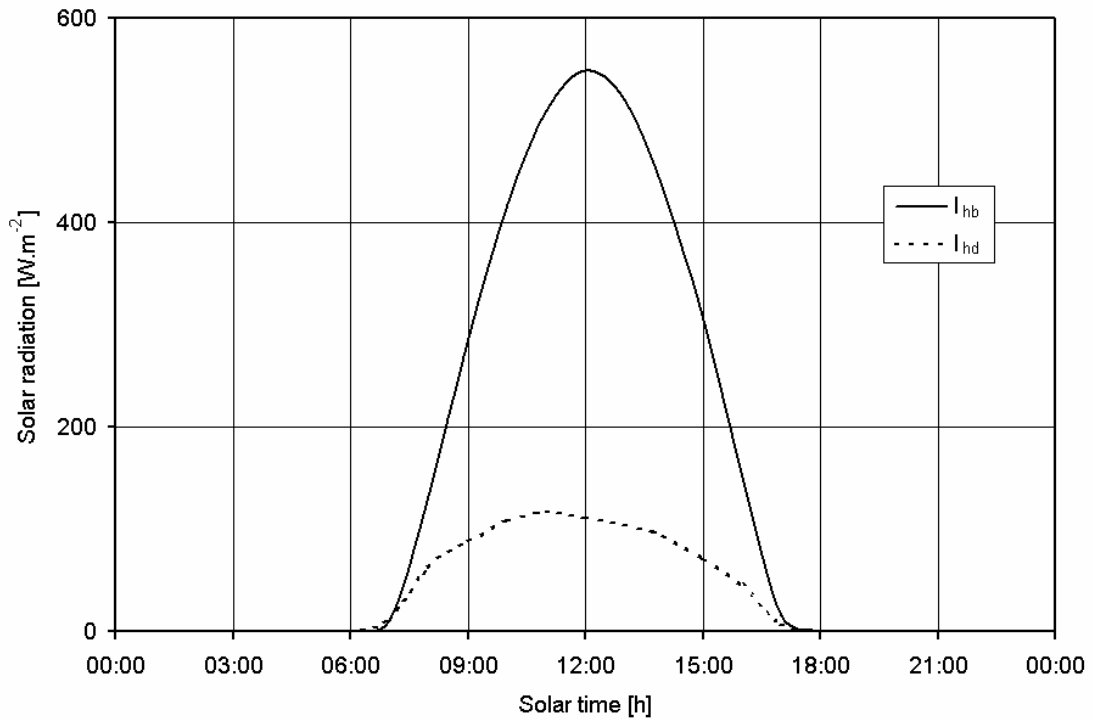


Figure 4.6: Beam- and diffuse solar irradiation profiles.

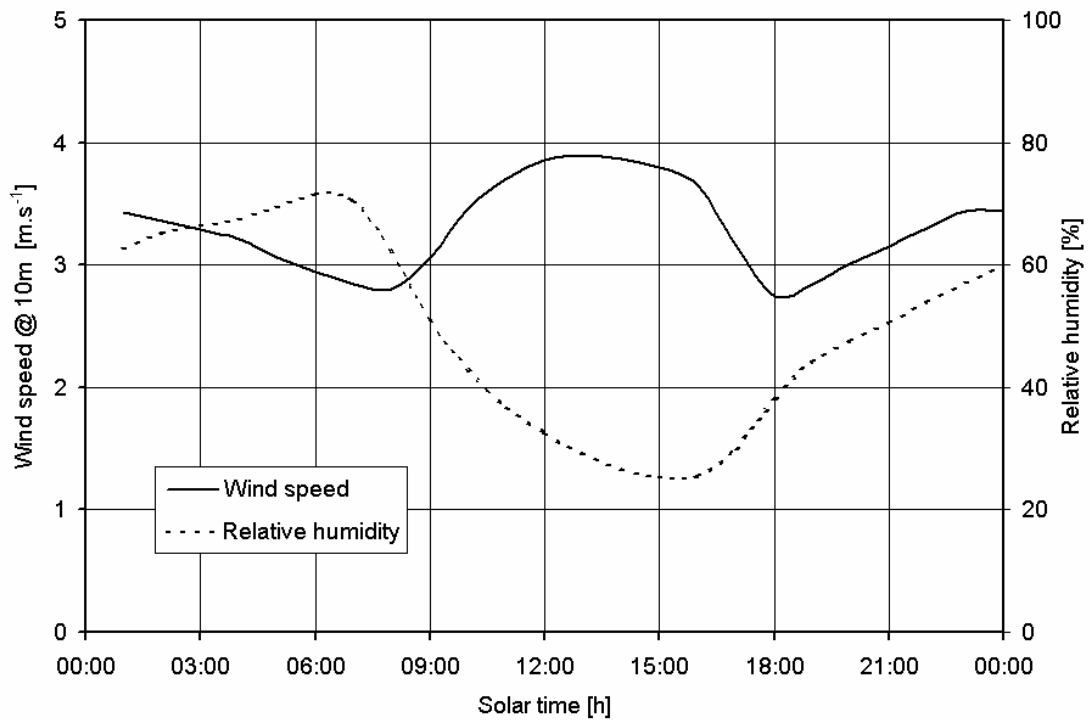


Figure 4.7: Relative humidity- and wind speed readings.

The floor-, enclosed air and mean glass temperatures predicted by the model for a 100 mm concrete floor are displayed in figure 4.8, the figure includes the ambient air temperature.

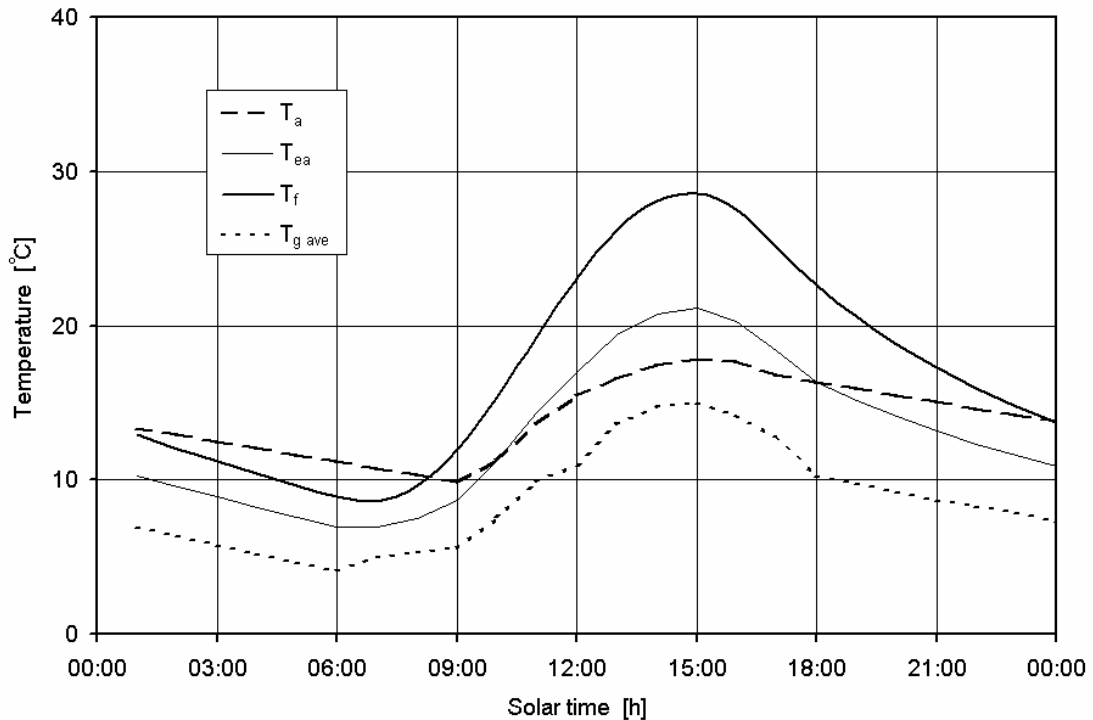


Figure 4.8: Predicted temperatures within greenhouse with concrete floor.



Figure 4.8 shows that the mean glass temperature  $T_{g\ ave}$  reaches temperatures in the region of 5°C while the ambient air temperature  $T_a$  is always well above this value. Similarly, the enclosed air temperature  $T_{ea}$  only exceeds the ambient air temperature between 10:00 and 18:00 and thus the purpose of the greenhouse is almost defeated, since for the greater part of the day the air outside is warmer than that inside. The concrete floor can be seen to reach a temperature of approximately 28°C.

If a water layer of equal thickness replaces the concrete slab, then the temperatures displayed in figure 4.9 are predicted. As with the concrete floor, the water layer is assumed to be fully insulated on the lower surface, also the air within the structure is assumed to be 100% saturated. The thermophysical properties of saturated air can be determined according to *Kröger* (1998).

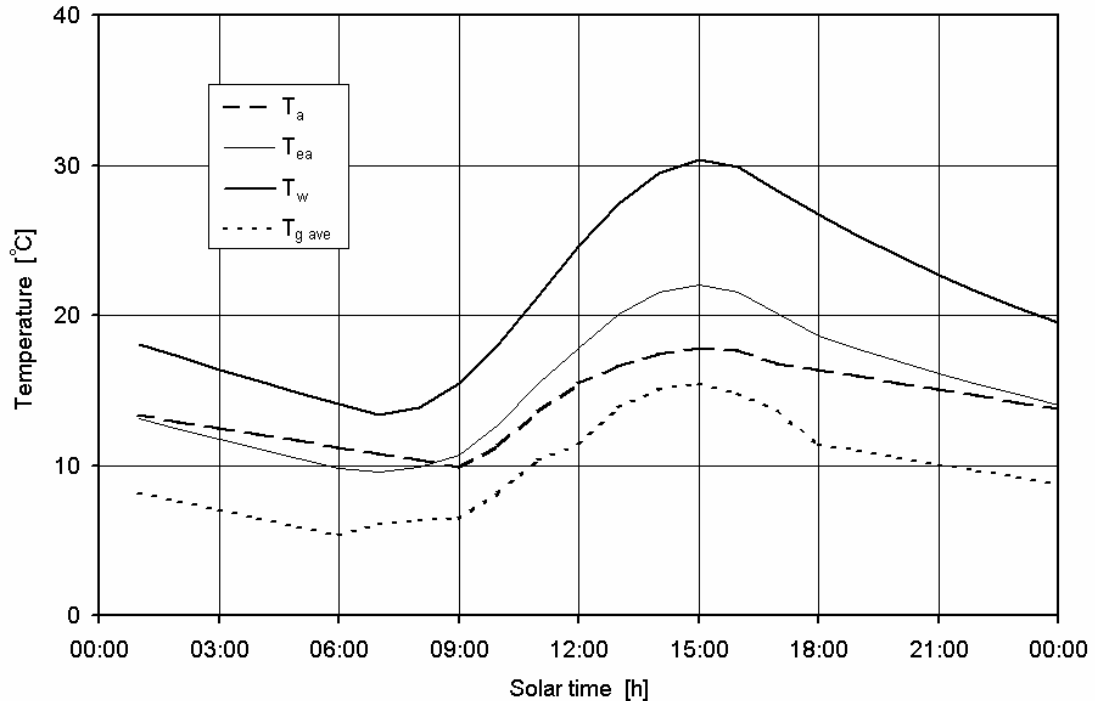


Figure 4.9: Predicted temperatures in greenhouse with 100 mm water floor.

The figure displays a similar mean glass temperature to that in figure 4.8; the enclosed air- and water temperatures are however slightly higher than those achieved with the concrete floor. The rate of change in temperature of these values is less than in figure 4.8; this is attributed to the fact that the product of the density and specific heat capacity of water is greater than for concrete, and thus more energy is required to change the temperature of a set quantity of water than concrete.

### 4.3 Night-time insulation usage

This section incorporates the use of insulation into the model developed in section 4.2. It was decided that the insulation used would be placed on all the outer surfaces of the structure at sunset and removed at sunrise. Many types of thermal insulation are commercially available, and focus on reducing either convective or radiative losses; the assumption is made that the insulation used in the model is 100% effective and permits no convective or radiative losses from the outer surfaces of the structure.

Figure 4.10 shows the predicted temperatures associated with the concrete floored greenhouse with full insulation during the night.

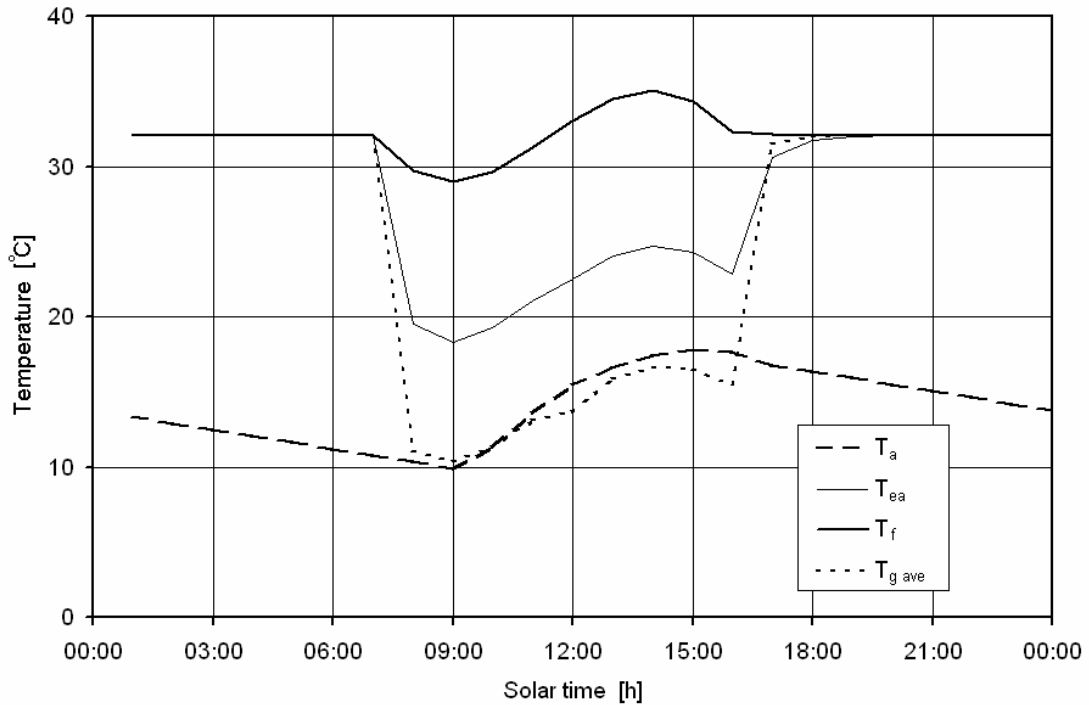


Figure 4.10: Predicted temperatures in greenhouse with concrete floor and thermal insulation usage at night.



Figure 4.10 shows that when insulation is used, the enclosed temperatures tend towards just more than 32°C, which is substantially higher than that achieved without the use of insulation as depicted by figure 4.8. It also shows that the temperatures achieved by the concrete floor and enclosed air are greater than without the use of insulation. A sharp drop in the predicted temperatures is visible when the insulation is removed at daybreak, this is particularly prevalent if the mean glass temperature is considered which falls to temperatures only slightly higher than those achieved without insulation usage. Conversely, a sharp increase is found to occur with the addition of insulation at sunset.

Predicted results for the greenhouse with 100 mm water floor and night-time insulation usage are displayed graphically in figure 4.11.

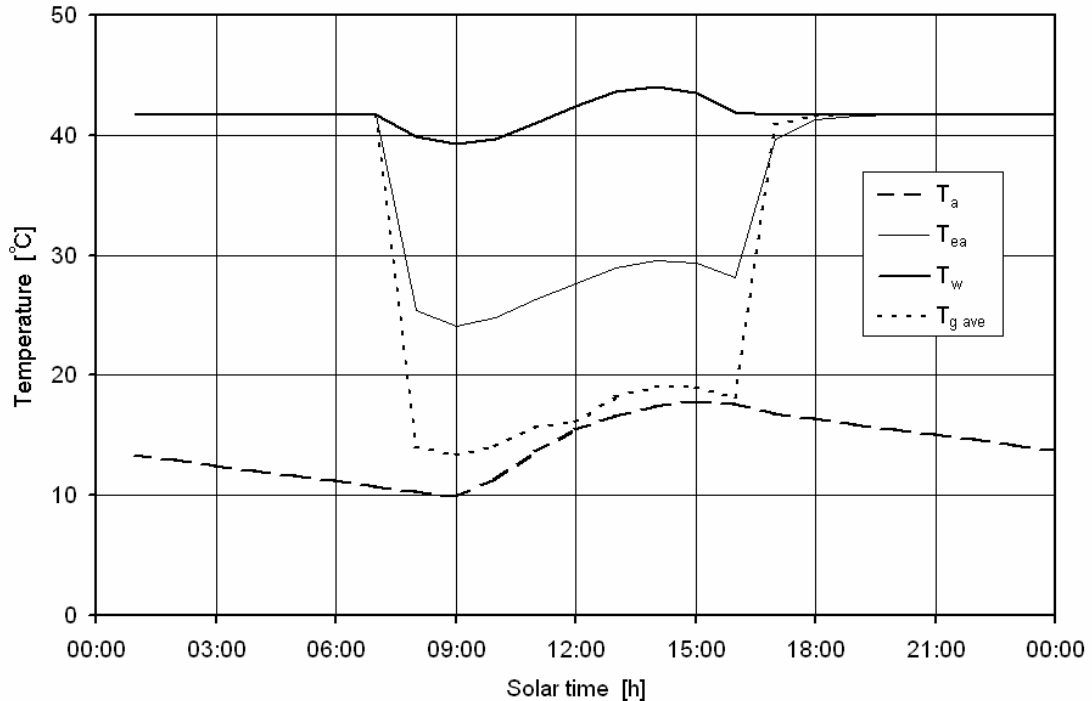


Figure 4.11: Predicted temperatures in greenhouse with water floor and thermal insulation usage at night.

The figure indicates that the system temperatures tend towards approximately 42°C when insulation is used. An increase in the mean daytime temperature of approximately 20 and 10°C was experienced by the floor (water) and enclosed air respectively, compared to when insulation was present.

The mean glass temperature is also found to increase slightly by replacing the concrete floor with a water layer.

#### 4.4 Day- and night-time insulation

This section extends the analysis considered in the latter part of section 4.3. A glass greenhouse with a 100 mm water layer floor is fully insulated during the night; since the day of interest is June the 21<sup>st</sup>, when the sun is only in the first and second quadrants (see figure 4.2), the southern wall is permanently insulated since it receives no direct sunlight. The decision was also made to retain the insulation on the western wall until midday, at which point the insulation was added to the eastern wall and retained until

dawn the following day. These changes would ensure that no sunlight would pass through the entire system without influencing the heat gain of the greenhouse. The predicted temperatures of the greenhouse are shown in figure 4.12.

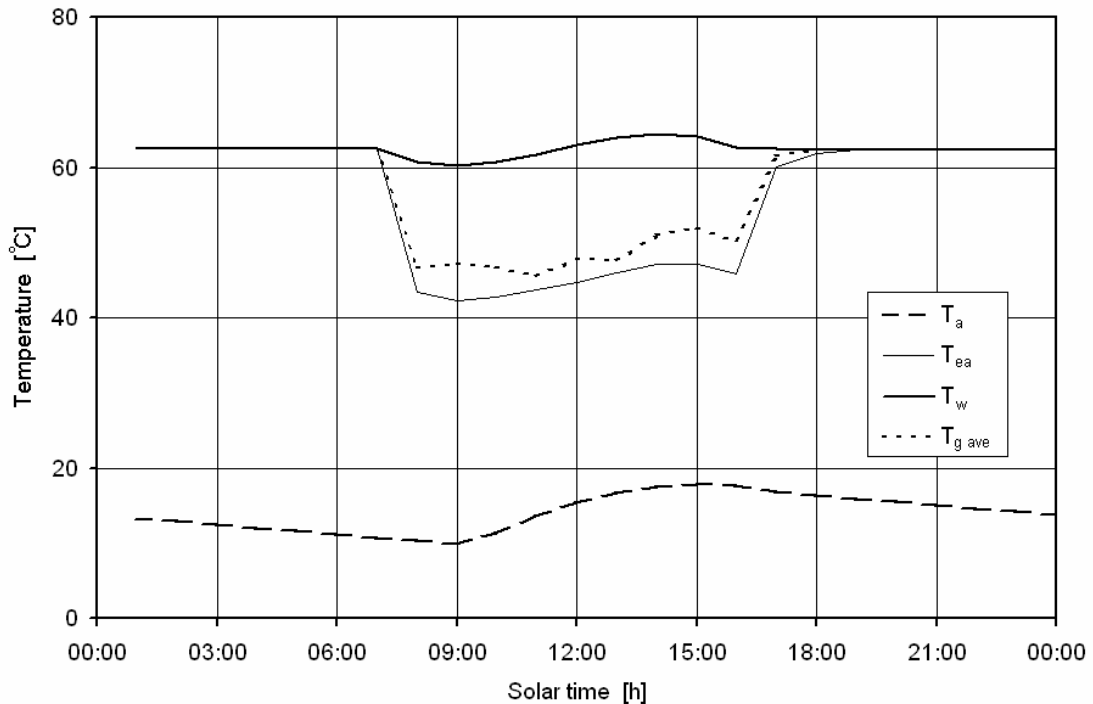


Figure 4.12: Predicted greenhouse temperatures.



The figure shows that the system temperatures now tend to 63°C, approximately 21°C more than without the daytime insulation. Since some of the walls are now non-opaque the solar absorptivity is now far higher and the eastern-, western and southern walls now reach very high temperatures, while the glass roof and northern wall don't exceed 27°C. The solar absorptivity of the insulated surfaces is taken as 0.6, which is an average value similar to that of brick or concrete.

#### 4.5 Conclusion

This chapter modelled the thermal behaviour of a flat roofed glass greenhouse which was very poor at retaining energy; this occurred to the extent that the air within the greenhouse became cooler than the ambient air at times, see figure 4.8. At first glance this may suggest the presence of an error, but if it is considered that all the glass

surfaces have a high emissivity ( $\varepsilon_g = 0.9$ ) and absorb very little of the incident solar energy, low temperatures are probable during winter weather conditions.

An all glass structure has very poor heat retention, since the absorptivity of glass is so low the solar energy that doesn't strike the floor, which has a higher solar absorptivity, essentially "passes through the system unnoticed" and is wasted. Thus, the performance of such a system can be increased either by increasing the heat retained in the floor, reducing the solar energy passing through the system or minimising any night-time losses experienced.

Sections 4.2 and 4.3 clearly show that a volume of water is more efficient in receiving and providing energy than an equal volume of concrete. This potential for receiving energy is due to the greater solar absorptivity of water than concrete, and is based on the assumption that all solar radiation not reflected at the water surface is absorbed (compare the  $\alpha$ -value of 0.61 for concrete to figure 2.4 for water). As mentioned above, the ability of a material to store energy is dependant on the density / specific heat capacity product, which in this case is greater for water than for concrete.

Figures 4.10 and 4.11 show that substantial gains can be made by insulating a glass greenhouse during the night, while figure 4.12 shows that significant gains can be made using insulation both during the day and night. Using darker insulation and thus increasing the solar absorptance of the walls could increase this gain in energy further. The systems described are idealised and the results are approximate; the model does however give an indication of the potential gains possible with insulation usage.

## CHAPTER 5

# Aspects of greenhouse design

- 5.1 System considerations
  - 5.2 Proposed improved design
  - 5.3 Aspects of optimal design analysis
  - 5.4 Welgevallen system analysis
- 

### 5.1 System considerations

Chapter 4 dealt with theoretical modelling of a glass greenhouse, and illustrated how the temperatures within such a system can be elevated substantially if the associated thermal behaviour is well understood.

In this chapter an optimal design is proposed for the housing of species such as tilapia that require elevated temperatures. This does not build upon another design, but is that system which in the opinion of the author will receive the greatest quantity of solar radiation and simultaneously experience minimal losses.

Thereafter, the tilapia system at the Welgevallen Research Centre is analysed, and recommendations presented as to how the system can be improved upon without major structural changes, with the result that the temperature of the water is increased to a sufficient level.

### 5.2 Proposed optimal design

The primary objective of this study is to increase the temperature of a body of water contained within a greenhouse during the cold winter season; the greenhouse configuration that has been calculated to most efficiently achieve this objective is shown in figure 5.1.

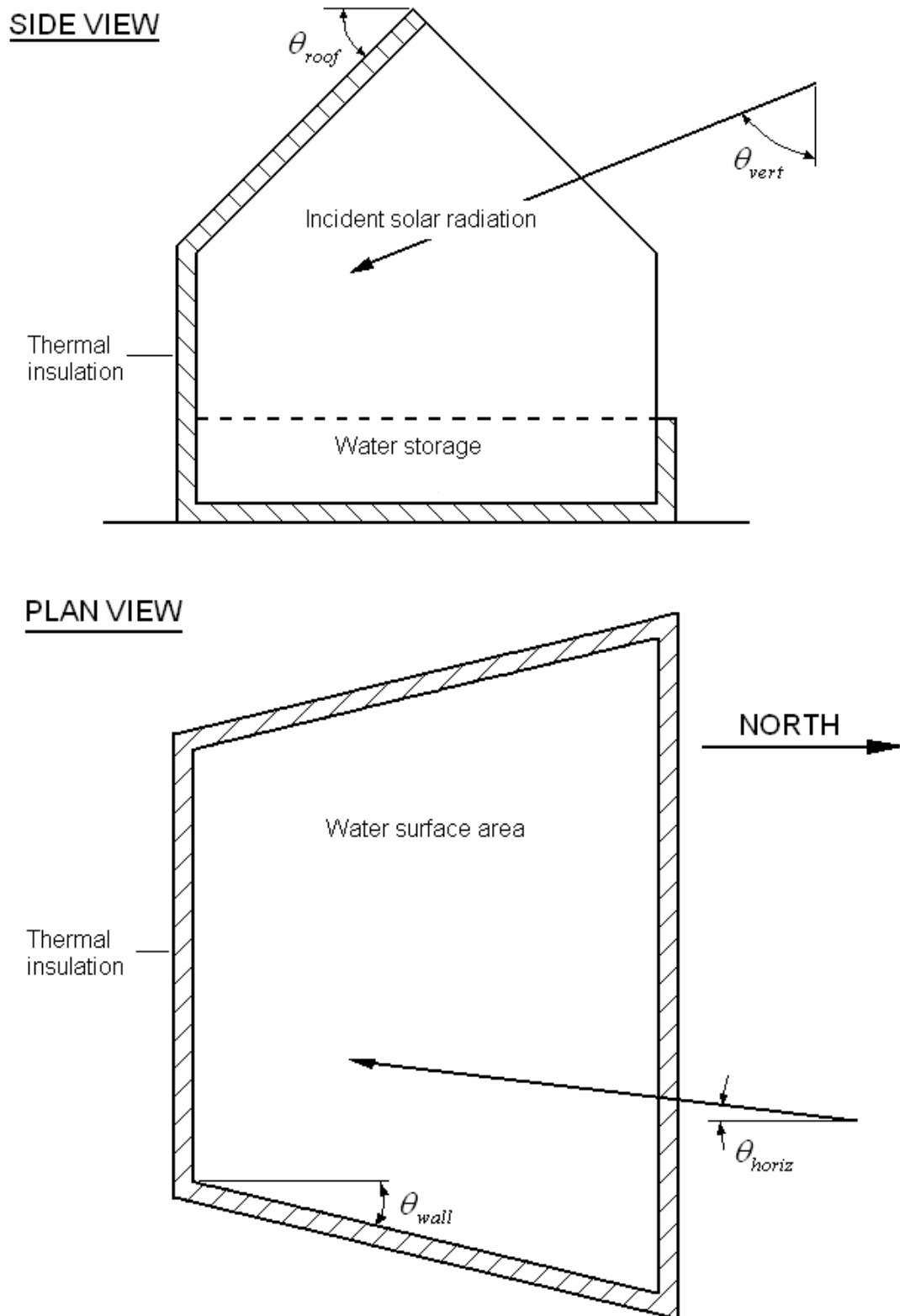


Figure 5.1: Side and plan views of the proposed greenhouse structure.

The side view in the figure shows a cross-sectional view of the greenhouse from the east. The south wall, floor, rear roof section and lower north wall are opaque and fully

insulated, while the upper north wall and front roof section are of glass or plastic construction, with a high transmissivity. Other than these two transparent surfaces, all surfaces within the enclosure have a high solar absorptivity. Water is assumed to cover the entire surface area of the floor and is filled up to a set height, this is fully insulated and losses only occur from the upper surface. Note that the roof is pitched; this prevents the build-up of condensation on the roof panels and assists with natural ventilation during summer months.

The plan view of the structure shows a quadrilateral with north and south walls parallel to each other, while the eastern and western walls are slanted in opposing directions by an angle  $\theta_{wall}$ . The walls are angled such that the net energy into the greenhouse is greater than the loss to the environment. It is also required that the inner surfaces of the eastern and western walls have a high solar absorptance.

The available solar radiation is expected to be the lowest on the 21<sup>st</sup> of June, the winter solstice in the southern hemisphere. South Africa lies approximately between the latitudes of 23° and 34°S and according to equation (A.3), at midday on the 21<sup>st</sup> of June 2005 the zenith angle at the respective latitudes is 46.44° and 57.44°. This indicates that if  $\theta_{roof}$  is set to approximately 45° at northern latitudes and approximately 30° further south, then no sunlight will be wasted on the external surface of the rear roof section, regardless of where the structure is positioned in the country.

Equation (A.3) can be solved for a zenith angle of 90° to determine the time of sunrise and sunset at a particular location. On June the 21<sup>st</sup> at 23° and 34°S, sunrise occurs at 06.71 and 07.13, while sunset happens at 17.29 and 16.87 respectively (all times are measured in solar time). Thus, it could be assumed that on average sunrise and sunset occurs at 07:00 and 17:00 on this particular day, as was indicated by the Sishen solar profile at 27.67°S (see figure 4.6).

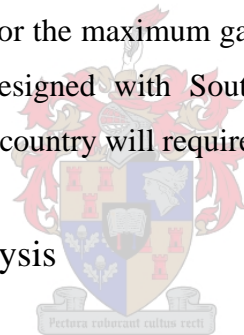
Observation of figures 4.9, 4.10 and 4.11 show a distinct decrease in the predicted temperatures after the removal of the thermal insulation at dawn. These temperatures then increase as the day progresses, they reach a maximum value and then decrease slightly, after which the insulation is replaced on the system for the night. This form of operation is clearly sub-optimal.

The figures indicate that the gain in energy of the system exceeds the losses incurred at approximately 09:00, two hours after sunrise. Similarly, the predicted temperatures reach their peak at roughly 15:00, two hours before sunset. Thus, it is recommended that for the current greenhouse the entire system should be fully insulated until two hours after sunrise, at which point the insulation on the front roof section and north wall should be removed, and should be replaced two hours before sunset.

At 09:00 and 15:00, the horizontal component of the sunlight incident on the system is calculated with equation (4.1) to be  $46.31^\circ$  and  $43.13^\circ$  at  $23^\circ$  and  $34^\circ\text{S}$  respectively. Then if the wall angle  $\theta_{wall}$  is set to appropriately  $45^\circ$ , the thermal insulation will be removed once  $\theta_{horiz}$  equals  $\theta_{wall}$  in the morning and replaced again when that occurs in the afternoon.

Thus for any location within the given latitudes, the appropriate roof  $\theta_{roof}$  and wall angle  $\theta_{wall}$  can be determined for the maximum gain in solar energy. Take note that this particular layout has been designed with South Africa as the proposed location. Applying the above in another country will require alterations to the given design.

### 5.3 Optimal design analysis



When the northern wall and front roof section of the system in figure 5.1 are covered with thermal insulation, the system is fully insulated and ideally no energy can either enter or leave the greenhouse. Once removed however, it is necessary to determine whether or not a net loss or gain is experienced by the system when exposed to low solar radiation, and cold but clear weather. If the result is such that the greenhouse experiences an increase in energy, then the primary objective of this study has been attained. If the greenhouse is able to maintain the temperature of the enclosed water at the upper limit of the temperature range when skies are clear, then if the system is sealed during periods of cloudy cold weather, the storage potential of the water is such that enough energy should be retained to keep the water temperature above the lower limit until the clear weather returns.

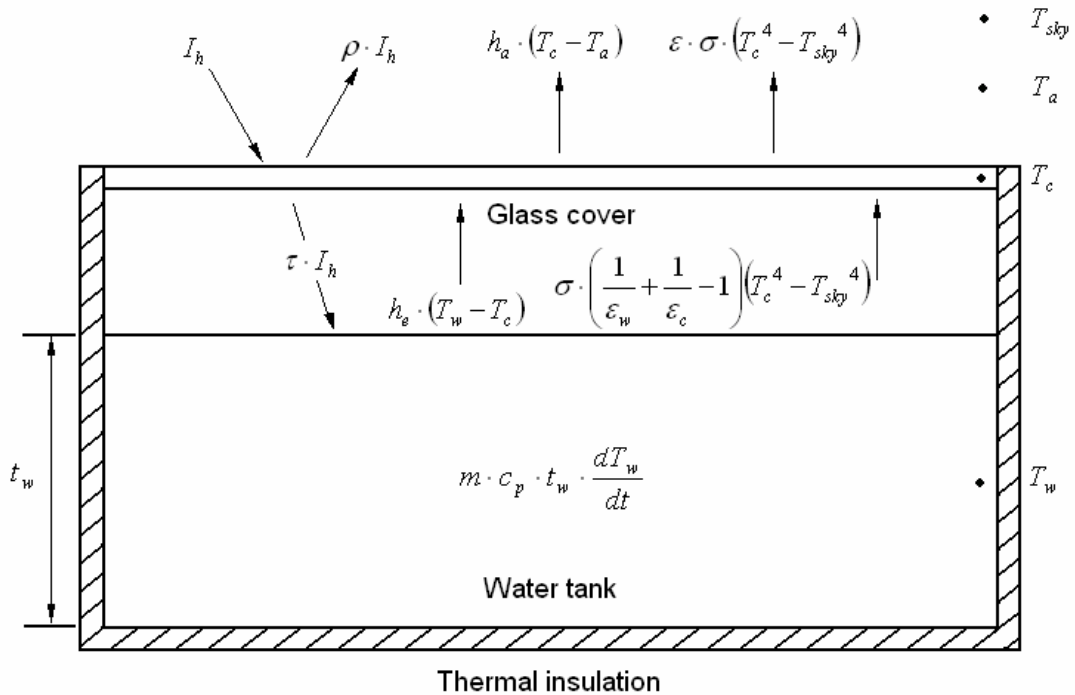


Figure 5.2: Simplified greenhouse model.

Observation of the system reveals that it bears a striking resemblance to that of a solar collector. Modelling of the exact system presents numerous complications, and thus it is highly simplified in the following model in an attempt to evaluate the storage potential of the proposed greenhouse. The model above is essentially identical to the plastic-covered water tank considered in section 3.3. The system is displayed in figure 5.2.

The ambient temperature, dew-point temperature and solar radiation readings applicable to June the 21<sup>st</sup> in Sishen will be used in conjunction with the above model. The initial temperature of the water will be set to the upper temperature limit applicable to tilapia, namely 35°C, while the depth of the water  $t_w$  will be taken as 500mm. Since the model is highly simplified the convective heat transfer coefficients,  $h_a$  and  $h_e$  will be taken as 10 W.m<sup>-2</sup>.K<sup>-1</sup>. The absorptivity and transmissivity of the glass cover are taken as 0.05 and 0.85 respectively.

The governing equations for the glass cover and water tank are given by equations (5.1) and (5.2):

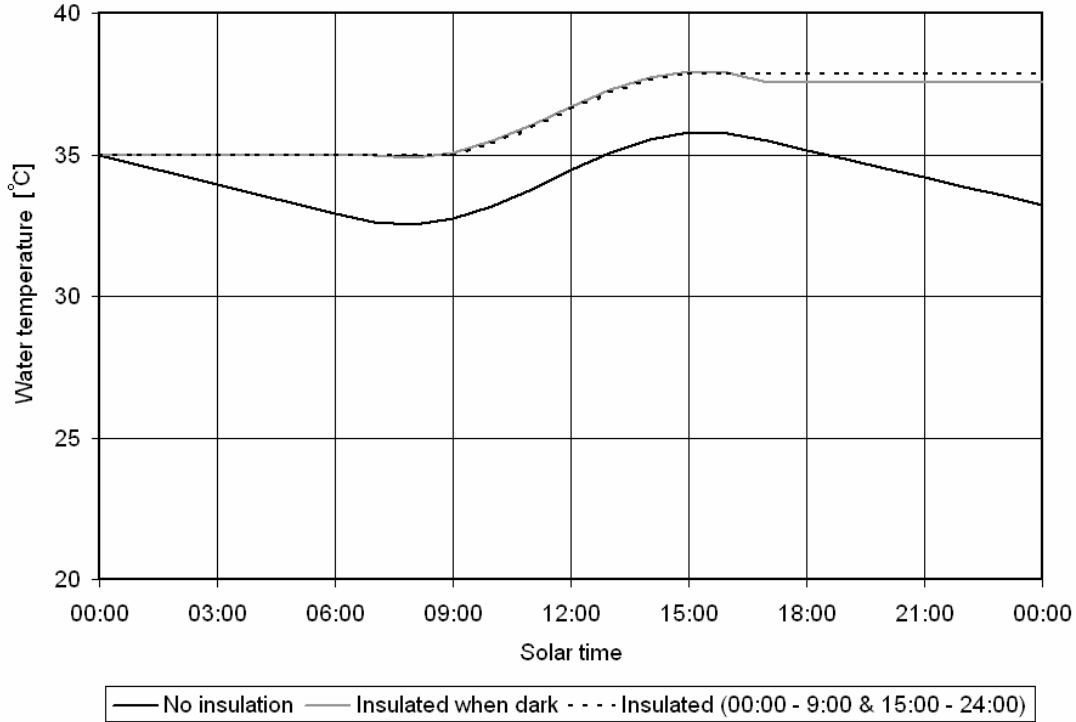


Figure 5.3: Mean water tank temperature on June 21<sup>st</sup>.

$$\alpha_c \cdot I_h + h_e(T_w - T_c) + \sigma \left( \frac{1}{\varepsilon_w} + \frac{1}{\varepsilon_c} - 1 \right) (T_w^4 - T_c^4) = h_a(T_c - T_a) + \varepsilon_c \cdot \sigma (T_c^4 - T_{sky}^4) \quad (5.1)$$

$$\tau_c \cdot I_h = h_e(T_w - T_c) + \sigma \left( \frac{1}{\varepsilon_w} + \frac{1}{\varepsilon_c} - 1 \right) (T_w^4 - T_c^4) + \rho_w \cdot t_w \cdot c_p \frac{(T_w - T_{winitial})}{3600} \quad (5.2)$$

Solving equations (5.1) and (5.2) simultaneously produces the results displayed in figures 5.3 and 5.4.

The above figure displays the comparative water temperatures attained without insulation, insulation usage while dark and the use of insulation from 00:00 to 09:00 and from 15:00 to 24:00 as recommended. The mean water temperature is found to decrease without insulation usage, indicating a net loss from the system, while the proposed usage can be found to achieve the best results. The influence of removing the insulation 2 hours after sunrise and adding it 2 hours before sunset, as suggested in section 5.2 is evident if the two sets of insulated results are compared. The glass cover temperatures in the above analysis are displayed in figure 5.4.

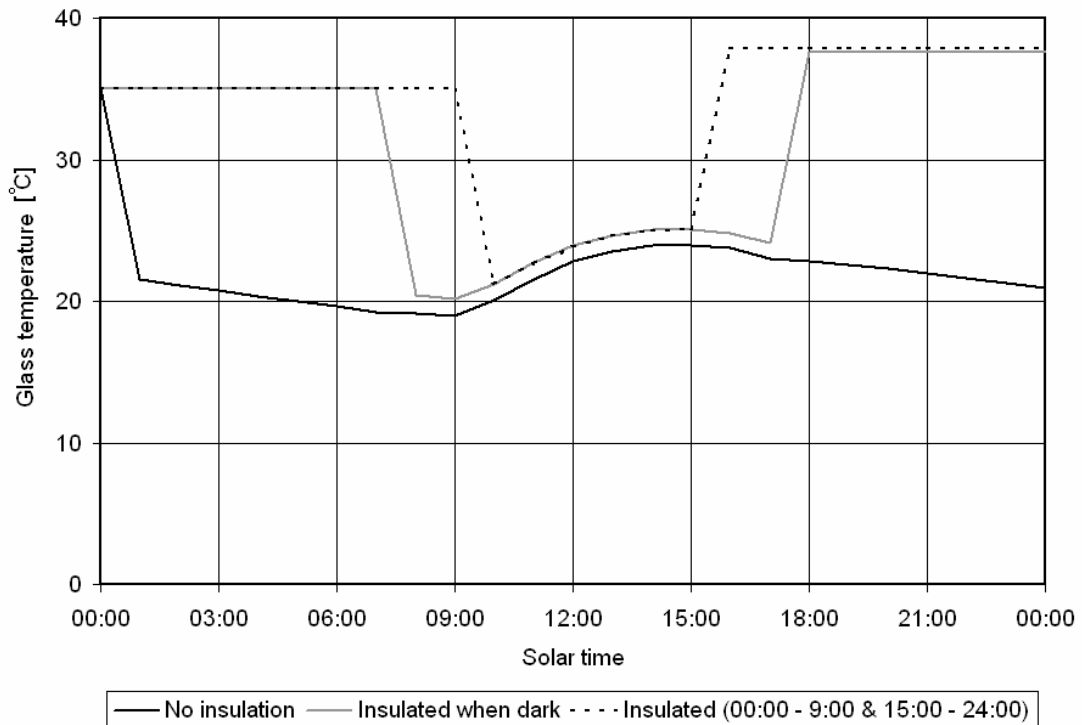
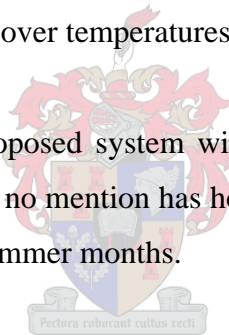


Figure 5.4: Comparative glass cover temperatures.

It has been shown that the proposed system will definitely attain the required water temperature during mid-winter, no mention has however been made about the operation of the system during warmer summer months.



In section 4.2 a glass greenhouse with a 100 mm concrete floor was considered and the predicted temperatures displayed in figure 4.7 for operation on June the 21<sup>st</sup>. The temperatures were generally lower than the range acceptable to tilapia, and thus improvements on the system needed to be considered. Figure 5.5 shows the predicted results for the same system modelled on December the 21<sup>st</sup>, the summer solstice.

The figure shows a vast improvement to that considered during winter months, and even though large losses are incurred high temperatures are still possible during the day. Such a system is obviously useless from an aquaculture perspective, since any species housed in such a system would perish quickly if temperatures of this magnitude were produced. Thus, it needs to be ensured that the above cannot happen to the proposed system.

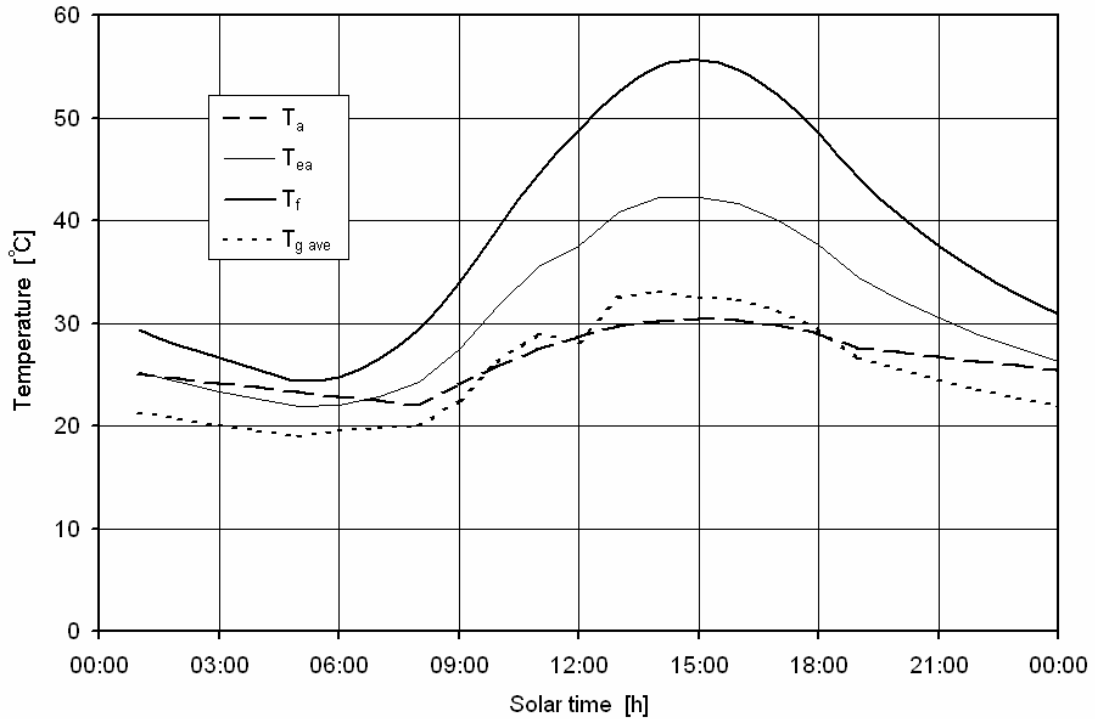


Figure 5.5: Predicted glass greenhouse temperatures on December 21.

The two most important concepts to consider when keeping a structure cool are shading and ventilation. During summer it is suggested that the entire roof and eastern and western walls be fully insulated, and that insulation not be used on the transparent north window during the night. Thus, the only way in which sunlight can enter the system is through the north window. However figure 4.2 indicates that the zenith angle is very small during summer months and therefore the quantity of solar radiation passing through the northern window is expected to be very little. Furthermore, the use of an overhang could be considered on the front section of the roof to provide shading of the northern window if necessary.

If it is found that the system still becomes too warm, ventilation could be considered. Since the proposed structure has a pitched roof, air could be extracted just below the apex of the roof through the eastern and western walls. Due to the fact that warm air is less dense than cooler air, ventilation will occur naturally if openings are provided in the lower half of the walls. If this is still not satisfactory, forced ventilation could be employed through the use of fans.

#### 5.4 Welgevallen system analysis

It was stated in Chapter 1 that one of the goals of this study was to increase the water temperature in the aquaculture system housing tilapia at the Welgevallen Research Centre. It was required that guidelines be provided on how the heat gain of the system could be improved by making non-structural alterations to the existing greenhouse. A side view of the structure is given in figure 5.6 as viewed from the west; the structure faces slightly west of north.

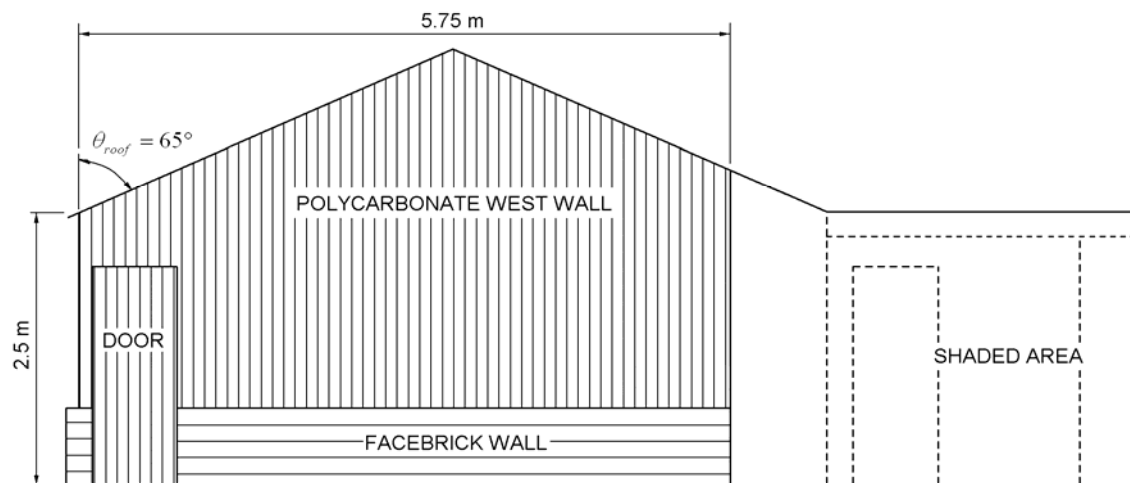


Figure 5.6: Side view of greenhouse structure.

The walls, door and roof of the structure are primarily constructed from corrugated polycarbonate (*Modek Greca*, clear 1 mm) with a steel frame. The northern wall has 7 polycarbonate windows that stretch the full length of the wall, whereas the roof has a relatively flat pitch, elevated at  $65^\circ$  to the vertical. The lower section of the northern and western walls is facebrick, while a slab of concrete serves as the floor. The southern wall of the enclosure is cement, while the area further south (further right in the figure) is shaded by an overhang that shelters a walkway.

A plan view of the greenhouse is shown in figure 5.7, it displays 14 PVC tanks that house the tilapia, 12 of which are in direct sunlight. Four large cylindrical biofilters are positioned opposite the entrance, while behind the biofilters; a polycarbonate wall separates the current structure from a cooler adjacent greenhouse.

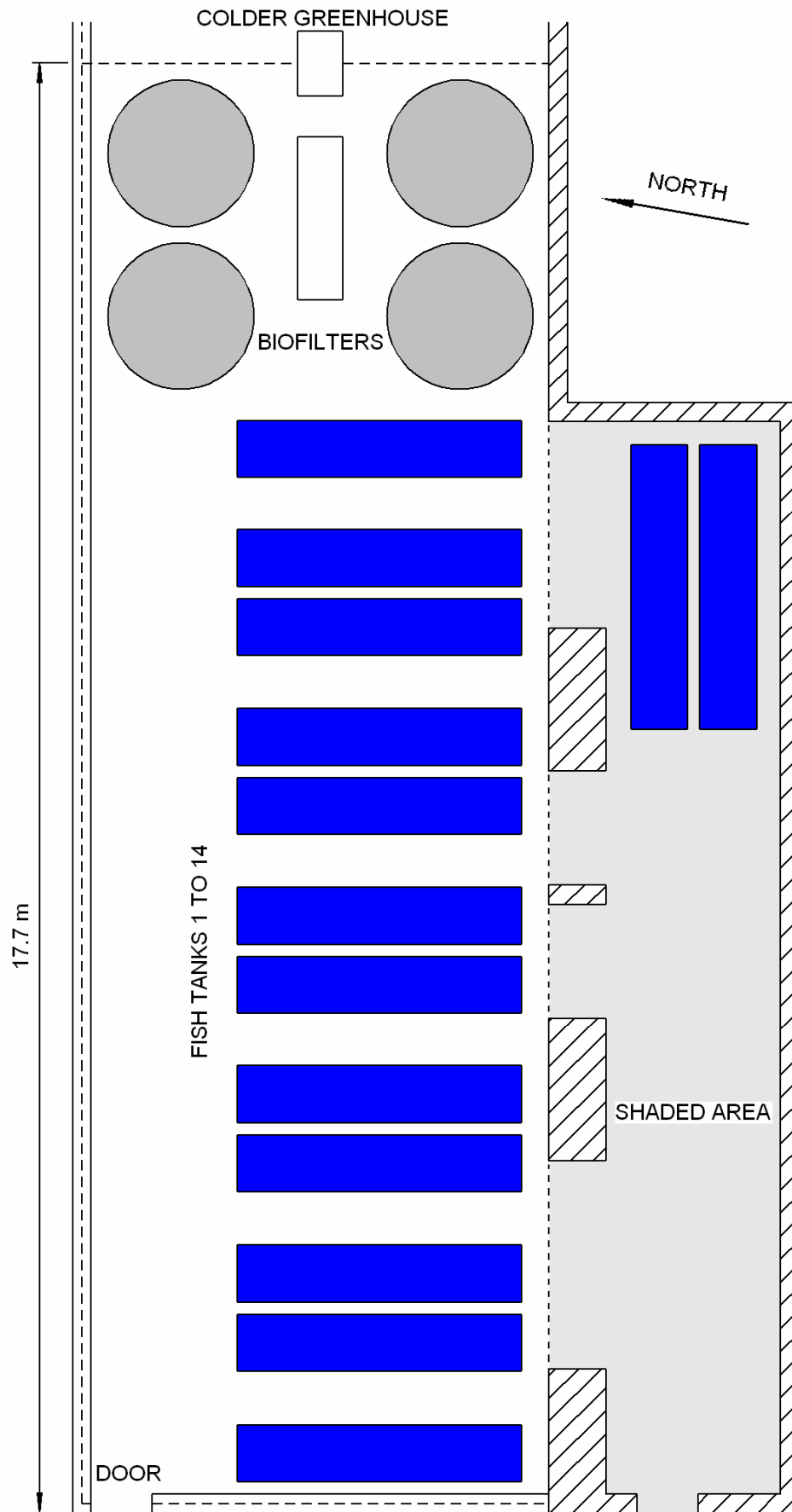


Figure 5.7: Plan view of Welgevallen greenhouse layout.

The following observations were made with regard to the energy flows to and from the system:

Since the polycarbonate sheeting is corrugated (see figure 5.8), it rarely fits flush against the steel structure supporting the greenhouse. Attempts have been made to minimise the infiltration of unconditioned outside air entering the system by injecting a foam sealant into many of the cavities and joints.

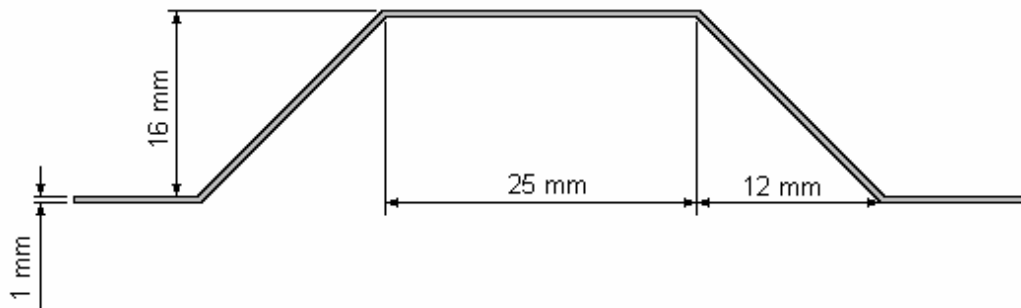


Figure 5.8: Profile of corrugated polycarbonate.

The greenhouse is approximately north facing, and thus has the potential to receive large quantities of solar radiation. The roof is slightly pitched, with both halves of the roof transmitting sunlight. The polycarbonate panels are hazy in appearance, due to the accumulation of dirt and as a result of ageing. The presence of condensation within the system is negligible.

The eastern section of the greenhouse is separated from an adjacent cooler greenhouse by the same polycarbonate sheeting used in the walls and roof. This wall is likely to be a source of substantial heat loss. An air-conditioning unit is mounted on this wall and simultaneously cools the adjacent greenhouse, while heating the current system.

The tanks are blue in colour and are of PVC construction; they are supported by galvanised steel stands and thus do not experience conductive losses through the base into the floor. Black nets cover the upper surface of all the tanks, and thus the absorbed solar radiation should be sufficient. The water is cycled from the tanks, passing through a belt filter (solids removal) and biofilters before returning to the source. A marginal

quantity of water is lost through the operation of the belt filter, and thus the water cycle is essentially a closed system.

The southern wall is painted white and can reach a thickness of 0.75 m in places. This wall has four archways that lead into a room that is fully shaded at all times; it contains two tanks and a control panel at the entrance. This room, although open, is far cooler than anywhere else in the greenhouse and definitely a source of heat loss from the main enclosure.

There is very little that can add to the heat load within the system, three large lights hang from the roof to provide artificial lighting when required. A pump drives the water cycle, while the belt filter motor and two small fans are also found within the enclosure. The influence of these components is expected to be negligible.

The nearest surrounding structures to the greenhouse are sufficiently far away, such that the influence of shading should be negligible during times of the day when the quantity of available solar radiation is of significance.

Application of the following recommendations will assist in increasing the enclosed water temperature:



The entry of outside air into the greenhouse is detrimental to the current objective. Thus, it should be made absolutely sure that the entire building is airtight. All doors should have airtight seals, or airlocks as used in the tunnel systems at the same location. The air and pump used for providing aeration to the aquaculture system should be located within the greenhouse structure.

The polycarbonate panels allow solar radiation to enter the system, but also have a high emissivity leading to large radiative losses, they offer marginal conductive resistance to heat leaving the system and the corrugations may well lead to turbulent forced convective losses from the outer surface. It is recommended that the panels be maintained as clean as practically possible to permit maximum transmission of solar radiation.

The gain in useful solar energy through the eastern and western walls is unlikely to be substantial during winter months, while the loss of energy through the eastern wall to the cooler greenhouse is unacceptable. Both walls should be fully insulated at all times, thus eliminating any light transmission and radiative and convective losses from the system. Although not ideal because the pitch of the roof is a bit low, the southern portion of the roof could also be fully insulated since the losses incurred may well exceed the gain in solar radiation.

It was stated above that the shaded southern room adjoining the greenhouse is expected to be a large source of heat loss. This can be solved in one of two manners: If the two shaded tanks are ignored, insulating the whole south wall could seal off the entire shaded portion of the greenhouse and thus eliminate the heat loss. Otherwise the outer surfaces of the shaded room could be insulated, this would retain heat within the system and the large separating walls could provide significant energy storage. In both cases, while often not aesthetically pleasing, darkening the walls would result in increased solar absorptance.

As recommended in Chapter 4, full thermal insulation should be added to the exposed northern wall and front roof section approximately two hours before sunset and retained until two hours after sunrise. This proposal may however pose a labour issue since covering both panels could become quite labour intensive, thus the use of radiative insulation such as Sisalation (see Chapter 3) might need to be considered. Substantial gains can still be achieved with Sisalation and may prove a better option since it is easier to handle, and lends itself to mechanised application. The environmental integrity of the insulation needs to be considered in conjunction with the capital- and installation cost involved, as well as the above-mentioned factors, to determine which form of insulation is best suited to the specific application.

## CHAPTER 6

# Conclusion

- 6.1 Research findings
  - 6.2 Greenhouse conclusions
  - 6.3 Further investigation
- 

### 6.1 Research findings

The first tests performed were those to determine the convective heat transfer coefficient between a horizontal surface and the natural environment. The literature reveals a wide range of correlations attempting to predict the convective heat transfer coefficient, with varying results. The process was analysed theoretically by *Kröger* (2002) and later refined with experimental work by *Burger and Kröger* (2004). The results obtained through testing in the present study were sufficiently accurate when compared to those predicted by *Burger and Kröger* (2004).

Experiments were conducted to determine the evaporation rate from a water surface exposed to the natural environment. As with the convective heat transfer coefficient, many empirical correlations are available for predicting the rate of evaporation from a water surface, with a large variation found to occur in the rates predicted. The results obtained in this study were very pleasing and the author was fortunate to obtain a difference of less than three percent (see table 2.1) between the quantity of water actually evaporated throughout the day and the amount predicted by the relevant expression (equation 2.7). This is the first time that experimental results have been found to correlate well with a theoretically determined evaporation rate. Note that this correlation requires that the water surface temperature exceed the ambient air temperature.

A body of water within an insulated tank was then considered, with the upper surface exposed to the environment. This experiment was conducted since the apparatus

mimicked the fundamentals of a solar pond, the results of which are of interest to this study. The ambient air temperature exceeded the measured water surface temperature throughout the duration of the experiment and thus the correlation applicable to the evaporation pan (equation 2.11) was unfortunately not of application. The results obtained by alternate expressions were not as good, but displayed reasonable trends. *Monteith and Unsworth* (1990) published an equation for evaporation rate prediction, primarily for horticultural applications. Good results were obtained with the use of this expression in earlier experiments, but was found to be clearly limited to applications without a stored energy component, since unsatisfactory results were obtained in the current experiment.

Experimental work was done to confirm the results obtained by *Lombaard* (2002) regarding the coefficient of extinction for glass, as used in the solar collector. The findings matched those obtained previously precisely, with a value of  $13 \text{ m}^{-1}$ .

The performance of a solar collector with a plastic covered water tank was investigated in section 3.3. The apparatus serves as both an excellent storage medium and collector of solar energy, with high water temperatures being attained during the day. The daytime operation of the system was modelled, as well as the operation of the system during the night, when the solar collector releases the energy stored during the day. The influence of thermal insulation on the reduction of night-time losses from the system was also investigated.

The temperatures predicted by the model representing daytime operation did not agree particularly well with those measured experimentally. This particular model was the source of much frustration and was really thoroughly investigated, with the source of the error still eluding the author. Predicted night-time temperatures, with and without the use of thermal insulation did however correlate much better with those measured.

Experiments were later performed on the same solar collector incorporating water storage without the use of the plastic film. The behaviour of the system was found to change entirely. Due to evaporation at the water surface, the horizontal glass cover soon became burdened with heavy condensation. Condensation of this nature is rarely found in practical applications and thus the influence of such condensation on sunlight is not

well documented. Fixed solar properties of the glass/condensation were assumed with surprisingly good results. The lack of plastic film on the water / air interface provided a water temperature profile that was substantially warmer at the surface during daytime operation. This is attributed to the greater solar absorptance of the glass/condensate, which indirectly heats the upper portion of the water tank.

Modelling the same system during night-time operation with and without insulation usage provided very good results, with a better correlation between predicted- and measured temperatures found than with the use of a plastic film.

## 6.2 Greenhouse conclusions

In Chapter 4 a fundamental greenhouse model was developed, it was of glass construction with an insulated 100 mm concrete floor. This served as a reference, since it was exposed to large quantities of solar radiation and thus could possibly absorb large quantities of solar energy, but was simultaneously very basic in design and experienced large night-time losses.

When compared to an identical structure with a 100 mm deep water layer as a floor, the model was found to predict warmer temperatures within the system, while the rate of change of the temperatures was also found to be less. The former characteristic is attributed to the fact that water has a greater solar absorptivity than concrete, while the latter occurs because the specific heat capacity of water is greater than that of concrete.

The influence of thermal insulation was investigated during the night. With the absence of sunlight, the entire structure was encapsulated in insulation, ideally permitting no radiative or convective losses from the outer surfaces of the structure. Similar results were found as before, with the system containing water stabilising at a higher temperature during the night than that with a concrete floor. It was observed in both scenarios that the floor- and enclosed air temperatures were found to decrease once the insulation was removed at daybreak, and started to increase only after a period of about two hours. A similar occurrence was observed before sunset. This was clearly indicative of sub-optimal insulation usage and required further consideration.

Lastly, insulation was used permanently on the south wall and on the west wall until midday, and on the east wall from midday onwards; as before complete insulation was used during the night. This simulation was run only on the greenhouse containing water and as expected, a further increase in temperature was achieved. It was found that increasing the inner solar absorptance of the walls could increase this even further.

An optimal greenhouse design was presented in section 5.2 that in the opinion of the author acts as an excellent solar collector while simultaneously minimising the loss of energy incurred during the night. This section proposes concepts to those interested in building structures of this nature on how to optimise the solar input to the system, without attaining unreasonable temperatures during warmer summer months.

It was further proven with the aid of a very simple model that the conceptual system would indeed experience a net gain in energy, even on the day of the year with the least available solar radiation, provided that clear skies were present. Thus, if the water within the system is kept at the upper temperature limit (35°C), the proposed system would be able to maintain an acceptable water temperature during extended periods of rain or cloud.

Section 5.3 analyses the greenhouse covered aquaculture system at Welgevallen Research Centre in Stellenbosch. The layout is described briefly and all possible flows of energy, entering or leaving the system are analysed. Recommendations were then presented as to how the potential problems could be solved with little structural changes. The author believes that if the given suggestions are applied to this particular system, that there should be no reason why the necessary temperatures are not attained.

The supplied recommendations are conceptual in nature and thus the practical implications thereof may still need to be considered. It is important to note that environmental conditions such as sunlight and rain rapidly degrade certain materials, and may make certain types of insulation redundant.

### 6.3 Further investigation

As mentioned, the optimised greenhouse design developed in Chapter 5 presented educated guidelines for those involved in the construction of such buildings to benefit from. Extending this study with an exact theoretical analysis of this system could prove to be very interesting; firstly in winter to see what temperatures can in fact be attained, and during summer to determine if the precautionary measures put in place prevent the system from overheating. An analysis of the most applicable form of thermal insulation to be used in the current system would also prove to be very useful.

Since many aquaculture species are also faced with the problem that the ambient conditions regularly exceed their upper temperature limit; a study of a similar nature focussed on cooling the enclosed water cycle, coupled with the current study, would comprehensively cover this topic.

Lastly, current trends in intensive aquaculture have been focussed on the development of hybrid systems. Such facilities incorporate previously closed system aquaculture farms with horticultural applications. In the opinion of the author linking two or more systems, each with a different focus but the same temperature requirements, such as aquaculture and hydroponics, should be the direction in which further studies in this field are directed.

# References

---

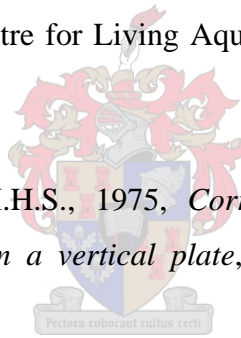
Berdahl, P. and Fromberg, R., 1982, *The thermal radiance of clear skies*, Solar Energy, 32(5), 299-314.

Burger, M. and Kröger, D.G, 2004, *Experimental convection heat transfer coefficient between a horizontal surface and the natural environment*, (submitted for publication.)

Cathcart, T.P. and Wheaton, F.W., 1987, *Modeling temperature distribution in freshwater ponds*, Aquacultural Engineering 6, 237-257.

Chervinski, J., 1982, *Environmental physiology of tilapias*, In: R.S.V. Pullen and R.H. McConnel (eds.), *The biology and culture of tilapias*, ICLARM Conference Proceedings, International Centre for Living Aquatic Resources Management, Manila, 119-128.

Churchill, S.W. and Chu, H.H.S., 1975, *Correlating equations for laminar and turbulent free convection from a vertical plate*, Int. J. Heat. Mass transfer, vol.18, p.1323.



Critten, D.L. and Bailey, B.J., 2002, *A review of greenhouse engineering developments in the 1990's*, Agric. For. Meteorol. 112, 1-22.

Cuenco, M.L., 1989, *Aquaculture systems modeling: An introduction with emphasis on warmwater aquaculture*, International Centre for Living Aquatic Resources Management, Manila, Philippines.

Dalton, J., *Experimental essays on the constitution of mixed gases on the force of steam or vapour from water and other liquids at different temperatures both in a Torricellian vacuum and in air; on evaporation and on the expansion of gases by heat*, Mem. Manchester Liter. and Phil. Soc. 5 – 11, 1802, pp. 535 – 602.

Duffie, J.A. and Beckman, W.A., 1991, *Solar engineering of thermal processes*, 2<sup>nd</sup> edition, John Wiley and sons.

Hepher, B. and Prugrinin, Y., 1982, *Tilapia culture in ponds under controlled conditions*, In: R.S.V. Pullen and R.H. McConnel (eds.), *The biology and culture of tilapias*, ICLARM Conference Proceedings, International Centre for Living Aquatic Resources Management, Manila, 185-203.

Hollands, K.G.T., Raithby, G.D. and Konicek, L., 1975, *Correlation equations for free convection heat transfer in horizontal layers of air and water*, *International Journal of Heat and Mass Transfer*, vol. 18, p.879.

Holman, J.P., 1986, *Heat transfer*, McGrawHill Book Company, New York.

Jalabert, B. and Zohar, Y., 1982, *Reproductive physiology in cichlid fishes with particular reference to tilapia and sarotherodon*, In: R.S.V. Pullen and R.H. Lowe-McConnel (eds.), *The biology and culture of tilapias*, Proceedings of the International Conference on the Biology and Culture of Tilapias, International Centre for Living Aquatic Resources Management, Manila, 129-140.



Klemetson, S.L. and Rogers, G.L., 1985, *Aquaculture pond temperature modeling*, *Aquacultural Engineering* 4, 191-208.

Kreider, J.F., Hoogendoorn, C.J. and Kreith, F., 1989, *Solar design: Components, systems and economics*, Hemisphere publishing, New York.

Kröger, D.G., 2004, *Air-cooled heat exchangers and cooling towers*, Penwell Corp, Tulsa.

Kröger, D.G., 2002, *Convection heat transfer coefficient between a horizontal surface and the natural environment*, *South African Institution of Mechanical Engineering Research and Development*, 18(3), pp.49-53.

- Lombaard, F., 2002, *Performance of a solar air heater incorporating thermal storage*, Master of Science in Mechanical Engineering thesis, University of Stellenbosch.
- Losordo, T.M. and Piedrahita, R.H., 1991, *Modelling temperature variation and thermal stratification in shallow aquaculture ponds*, *Ecol. Modell.* 54, 189-226.
- Mair, G.C. and Abella, T.A., 1997, *Technoguide on the production of genetically male tilapia (GMT)*, Freshwater Aquaculture Centre, Central Luzon State University, 77 pp.
- Mair, G.C., Abucay, J.S., Skibinski, D.O.F., Abella, T.A. and Beardmore, J.A., 1997, *Genetic manipulation of sex ratio for the large-scale production of all male tilapia (Oreochromis Niloticus)*, *Canadian Journal of Fisheries and Aquatic Sciences*, 54, 396-404.
- Merker, G.P., *Konvektive Wärmeübertragung*, Springer-Verlag, Berlin, 1987.
- Mills, A.F., 1992, *Heat transfer*, Irwin Incorporated, Illinois.
- Modest, M.F., 1993, *Radiative heat transfer*, McGraw-Hill Inc., New York.
- Monteith, J.L. and Unsworth, M.H., 1990, *Principles of environmental physics*, 2<sup>nd</sup> Edition, Edward Arnold, A division of Hodder & Stoughton, London.
- Nijskens, J., Deltour, J., Coutisse, S. and Nisen, A., 1984, *Heat transfer through covering materials of greenhouses*. *Agric. For. Meteorol.* 33, 193-214.
- Philapaert, J.C. and Ruvet, J.C., 1982, *Ecology and distribution of tilapias*, In: R.S.V. Pullen and R.H. McConnel (eds.), *The biology and culture of tilapias*, ICLARM Conference Proceedings, International Centre for Living Aquatic Resources Management, Manila, 15-59.
- Pieters, J.G., 1995, *Influence of condensation on the heat balance and the light transmission of a greenhouse*, Ph.D. Dissertation, Gent University, Belgium.

Pieters, J.G. and Deltour, J.M., 1997, *Performances of greenhouses with the presence of condensation on cladding materials*, J. Agric. Eng. Res. 68, 125-137.

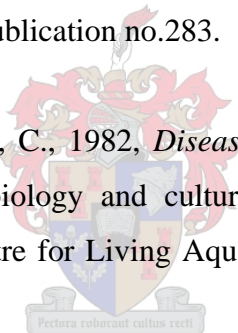
Pieters, J.G. and Deltour, J.M., 1999, *Modelling solar energy input in greenhouses*, Solar Energy, vol.67, no.1-3, pp. 119-130.

Pollet, I.V. and Pieters, J.G., *Laboratory measurements of PAR transmittance of wet and dry greenhouse cladding materials*, Agric. For. Meteorol., 93, 149-152

Popma, T. and Lovshin, L.L., 1994, *Worldwide prospects for commercial production of tilapia*, Department of Fisheries and Allied Aquaculture, Auburn University, Alabama, 43 pp.

Popma, T. and Masser, M., 1999, *Tilapia – Life history and biology*, Southern Regional Aquaculture Centre (SRAC), Publication no.283.

Roberts, R.J. and Sommerville, C., 1982, *Diseases of tilapias*, In: R.S.V. Pullen and R.H. McConnel (eds.), *The biology and culture of tilapias*, ICLARM Conference Proceedings, International Centre for Living Aquatic Resources Management, Manila, 247-263.



Sartori, E, 1996, *Solar still versus solar evaporator: A comparative study between their thermal behaviours*, Solar Energy, vol. 56, no. 2, pp. 199-206.

Sartori, E., 2000, *A critical review on equations employed for the calculation of the evaporation rate from free water surfaces*, Solar Energy, vol. 68, No.1, pp. 77-89.

Shah, M.M., 2002, *Evaluation of available correlations for rate of evaporation from undisturbed water pools to quiet air*, HVAC & R. Research 8(1): 125-31.

United Nations Food and Agriculture Organisation (FAO), 2003.

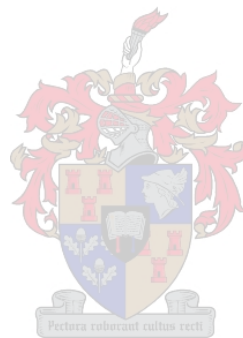
Schneider, P.J., *Conduction Heat Transfer*, Addison-Wesley Publ. Co. Inc., Reading, Mass, 1955.

Tang, Y., Etzion, I.A. and Meir, I.A., *Estimates of clear night sky emissivity in the Negev Highlands*, Israel, Energy Conversion and Management, Vol. 45, 2004, pp. 1831 – 1843.

Westdyk, D. and Kroger, D.G., 2003, *Evapotranspiration of grass growing under glass and subject to radiation and convective heat transfer*, 2<sup>nd</sup> International Conference on Heat Transfer, Fluid Mechanics and Thermodynamics, no. WD1.

Yilmaz, T.P. and Aybar, H.S., 1999, *Evaluation of correlations for predicting evaporative loss from water bodies*, ASHRAE Transaction 105(2): 185-90.

Zhu, S., Deltour, J. and Wang, S., 1998, *Modeling the thermal characteristics of greenhouse pond systems*, Elsevier Science, Aquacultural Engineering 18, 201-217.



## APPENDIX A

# Solar radiation

A.1 Direction of beam radiation

A.2 Ratio of beam radiation on tilted surface to that on horizontal surface

---

### A.1 Direction of beam radiation

The relationship between any particular surface orientated relative to the earth, and the position of the sun at any time can be described in terms of several angles. This is apparent if figure A.1 is considered.

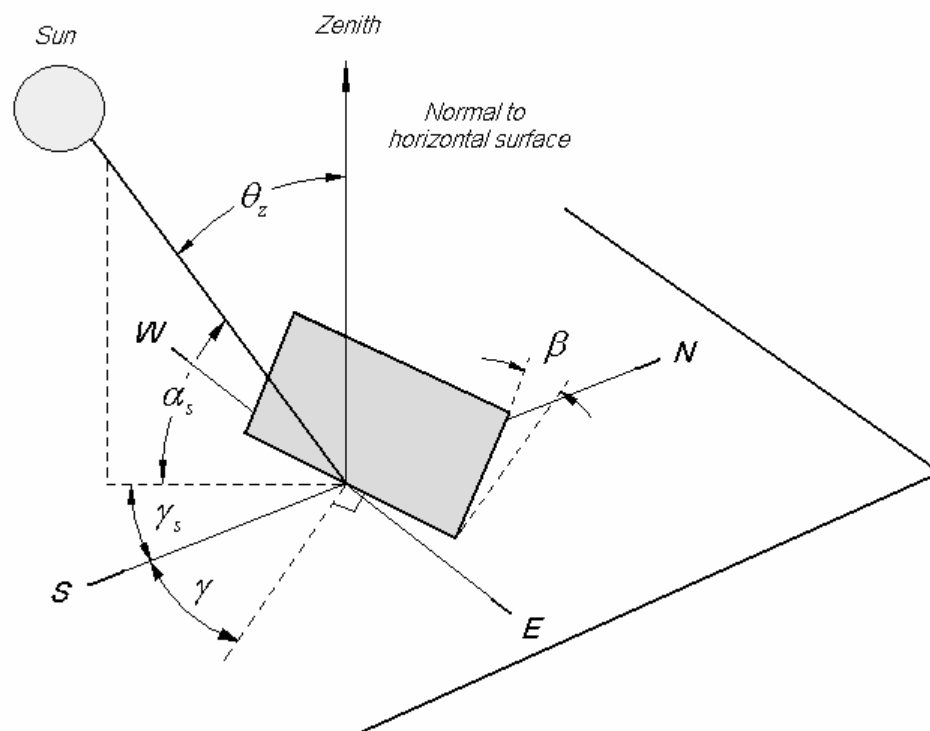


Figure A.1: Randomly orientated surface in direct sunlight with associated angles.

The angles listed in the figure are described below:

$\beta$  *Slope*, this is the angle between the surface of interest and the horizontal plane,  
 $0^\circ < \beta < 180^\circ$ .

- $\theta_z$  *Zenith angle*, the angle between the vertical and the line to the sun.
- $\alpha_s$  *Solar altitude angle*, the angle between the horizontal and the line to the sun.
- $\gamma_s$  *Solar azimuth angle*, the angular displacement from south of the projection of beam radiation on the horizontal plane. Note that displacements east of south are considered negative.
- $\gamma$  *Surface azimuth angle*, the deviation of the projection on a horizontal plane of the normal to the surface from the local meridian. Due south equals zero, with east negative.

It is often necessary to calculate the angle formed by the beam radiation on a surface and the normal to that surface, this is known as the angle of incidence,  $\theta$ . This angle is described by the following equations:

$$\begin{aligned} \cos \theta = & \sin \delta \sin \phi \cos \beta - \sin \delta \cos \phi \sin \beta \cos \gamma + \cos \delta \cos \phi \cos \beta \cos \omega \\ & + \cos \delta \sin \phi \sin \beta \cos \gamma \cos \omega + \cos \delta \sin \beta \sin \gamma \sin \omega \end{aligned} \quad (\text{A.1})$$

$$\cos \theta = \cos \theta_z \cos \beta + \sin \theta_z \sin \beta \cos(\gamma_s - \gamma) \quad (\text{A.2})$$

However, by definition the incidence angle for a horizontal surface is the zenith angle. Thus equation (A.1) can be rewritten as shown in equation (A.3) if the surface is horizontal.

$$\cos \theta_z = \sin \delta \sin \phi + \cos \delta \cos \phi \cos \omega \quad (\text{A.3})$$

The undefined terms in the above equations are the latitude angle  $\phi$ , hour angle  $\omega$  and the declination angle  $\delta$ . The latitude angle is a measure of the angular position of the specific location north or south of the equator, while the hour angle is the angular displacement of the sun east or west of the local meridian. The hour angle is measured in degrees and can be determined according to equation (A.4).

$$\omega = 15 (\text{Solar time} - \text{Solar noon}) \quad (\text{A.4})$$

The declination angle is defined as the angular position of the sun at solar noon with respect to the equator. The *South African Weather Bureau* suggests that the following equation be used to determine the declination angle (measured in radians).

$$\delta = 0.00661 + 0.40602 \sin(P - 1.4075) + 0.00665 \sin(2P - 1.4789) + 0.00298 \sin(3P - 1.0996) \quad (\text{A.5})$$

The  $P$  symbol is the annual phase angle (measured in radians) and is a function of the day of the year and the number of the specific year.

$$P = 0.0172028(DOY + YADJ + 0.417) \quad (\text{A.6})$$

$DOY$  represents the day of the year and  $YADJ$  is a leap year adjustment given by the *South African Weather Bureau*, and can be determined as follows:

$$YADJ = 0.25[2.5 - (Y - 4(\text{int}((Y - 1)/4)))] \quad (\text{A.7})$$

where  $Y$  indicates the number of the specific year.

Thus with the use of equations (A.4) through (A.7), the inclination angle in either equation (A.1) or (A.3) can be evaluated. The utilisation of equation (A.2) however still requires that the solar- and surface azimuth angles be correctly defined.

The solar azimuth angle (measured in degrees) is represented by the following expression, where  $\gamma_s'$  is introduced as a pseudo solar azimuth angle:

$$\gamma_s = C_1 \cdot C_2 \cdot \gamma_s' + C_3 \cdot \left( \frac{1 - C_1 \cdot C_2}{2} \right) \cdot 180 \quad (\text{A.8})$$

where  $\sin \gamma_s' = \frac{\sin \omega \cdot \cos \delta}{\sin \theta_z}$ .

The values of  $C_1$ ,  $C_2$  and  $C_3$  are determined according to the criteria below.

$$\begin{aligned}
 C_1 &= 1 && \text{if } |\omega| < \omega_{ew} \\
 C_1 &= -1 && \text{otherwise}
 \end{aligned}
 \quad \text{where} \quad \cos \omega_{ew} = \frac{\tan \delta}{\tan \phi}$$

$$\begin{aligned}
 C_2 &= 1 && \text{if } \phi (\phi - \delta) \geq 0 \\
 C_2 &= -1 && \text{otherwise}
 \end{aligned}$$

$$\begin{aligned}
 C_3 &= 1 && \omega \geq 0 \\
 C_3 &= -1 && \text{otherwise}
 \end{aligned}$$

## A.2 Ratio of beam radiation on tilted surface to that on horizontal surface

Solar performance calculations often require that the quantity of solar radiation on an oblique surface be calculated. This is given in terms of a ratio known as the geometric factor  $R_b$ , which can be expressed as shown in equation (A.9).

$$R_b = \frac{I_\theta}{I_h} = \frac{\cos \theta}{\cos \theta_z} \tag{A.9}$$

All equations supplied in section (A.1) and (A.2) were obtained from *Duffie and Beckman* (1991).

## APPENDIX B

# Evaporation

- B.1 Analysis – Evaporation from a water surface
  - B.2 Analysis – Temperature gradient within water layer
  - B.3 Evaporation pan photograph
  - B.4 Numerical example (section 2.3)
- 

### B.1 Analysis - Evaporation from a water surface

The problem of evaporation from a horizontal water surface that is exposed to the natural environment is analysed for cases where the water surface temperature is measurably higher than that of the ambient air. An empirical equation is recommended in the case where the temperature difference is relatively small and for application at night.

Consider a stationary fluid (binary mixture consisting of air and water vapour) in which the concentration  $c_{vi}$  of the species of interest (water vapour) is initially uniform. Beginning with the time  $t = 0$ , the concentration at the  $z = 0$  boundary or surface is maintained at a greater level  $c_{vo}$  as shown in figure B.1 (a).

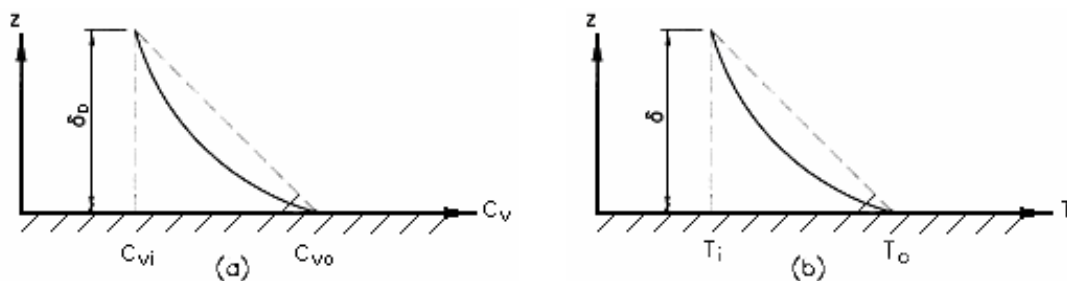


Figure B.1: Concentration or temperature distribution.

Water vapour will diffuse into the medium to form a concentration boundary layer, the thickness of which increases with time. The mathematical equation of time dependent

diffusion in a binary mixture, expressed in terms of the molar concentration  $c$  is as follows:

$$D \frac{\partial^2 c}{\partial x^2} = \frac{\partial c}{\partial t} \quad (\text{B.1})$$

The diffusion flux is driven solely by the concentration gradient strictly in an isothermal and isobaric medium. Equation (B.1) is however a good approximation in many non-isothermal systems, where temperature differences are relatively small. If changes in temperature are small the diffusion coefficient  $D$  can be assumed to be constant.

Equation (B.1) is analogous to the time-dependent equation for heat conduction into a semi-infinite body i.e.

$$\alpha \frac{\partial^2 T}{\partial z^2} = \frac{\partial T}{\partial t} \quad (\text{B.2})$$

If the temperature of a semi-infinite solid is initially uniform at  $T_i$  and a sudden increase in temperature to  $T_o$  occurs at  $z = 0$  as shown in figure B.1 (b), *Schneider* (1955) shows that the temperature gradient at  $z = 0$  is given by

$$\frac{\partial T}{\partial z} = (T_o - T_i) / (\pi \alpha t)^{1/2} \quad (\text{B.3})$$

The corresponding heat flux is

$$q_T = -k \frac{\partial T}{\partial z} = \frac{k(T_o - T_i)}{(\pi \alpha t)^{1/2}} \quad (\text{B.4})$$

An effective heat transfer coefficient can be expressed in terms of this heat flux i.e.

$$h_{T_i} = q_T / (T_o - T_i) = k / (\pi \alpha t)^{1/2} \quad (\text{B.5})$$

By solving equation (B.2) for the case where the solid at an initial uniform temperature  $T_i$  is suddenly exposed to a constant surface heat flux  $q_q$ , the latter can, according to *Holman* (1986), be expressed in terms of an effective surface temperature  $T_{oq}$  as

$$q_q = k(T_{oq} - T_i) / [2(\alpha t / \pi)^{1/2}] \quad (\text{B.6})$$

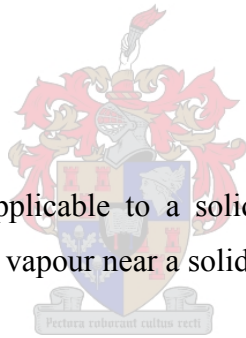
The corresponding effective heat transfer coefficient is defined as

$$h_{qt} = q_q / (T_{oq} - T_i) = k / [2(\alpha t / \pi)^{1/2}] \quad (\text{B.7})$$

It follows from equations (B.5) and (B.7) that for the same temperature difference i.e. for

$$\begin{aligned} (T_{oq} - T_i) &= (T_o - T_i) \\ h_{qt} / h_{Tt} &= \pi / 2 = h_q / h_T \end{aligned} \quad (\text{B.8})$$

Although equation (B.2) is applicable to a solid, it is a good approximation when applied to a thin layer of gas or vapour near a solid surface.



Due to the analogy between mass and heat transfer the solution of equation (B.1) gives the following relations corresponding to equations (B.3) to (B.8) respectively:

If the initial concentration at  $z = 0$  is suddenly increased to  $c_{vo}$

$$\frac{\partial c_v}{\partial z} = (c_{vi} - c_{vo}) / (\pi D t)^{1/2} \quad (\text{B.9})$$

The corresponding vapour mass flux is

$$m_v = -D \frac{\partial c}{\partial z} = (c_{vo} - c_{vi}) [D / (\pi t)]^{1/2} \quad (\text{B.10})$$

An effective mass transfer coefficient can be expressed in terms of this mass flux i.e.

$$h_{Dt} = m_v / (c_{vo} - c_{vi}) = [D / (\pi t)]^{1/2} \quad (\text{B.11})$$

If vapour is generated uniformly at a rate  $m_{vm}$  at  $z = 0$ , this mass flux can be expressed in terms of an effective concentration  $c_{vom}$  to give analogous to equation (B.6)

$$m_{vm} = D(c_{vom} - c_{vi}) / [2(Dt / \pi)^{1/2}] = (c_{vom} - c_{vi})(\pi D / t)^{1/2} / 2 \quad (\text{B.12})$$

The corresponding effective mass transfer coefficient is defined as

$$h_{Dmt} = m_{vm} / (c_{vom} - c_{vi}) = (\pi D / t)^{1/2} / 2 \quad (\text{B.13})$$

It follows from equations (B.11) and (B.13) that for the same effective difference in concentration i.e. for

$$\begin{aligned} (c_{vom} - c_{vi}) &= (c_{vo} - c_{vi}) \\ h_{Dmt} / h_{Dt} &= \pi / 2 = h_{Dm} / h_D \end{aligned} \quad (\text{B.14})$$

These latter equations are applicable in the region of early developing concentration distribution in a semi-infinite region of air exposed to a water or wet surface. According to *Merker* (1987) for a Rayleigh number  $Ra \geq 1101$ , unstable conditions prevail with the result that water vapour is transported upwards away from the wetted surface by means of “thermals” as shown in figure B.2.

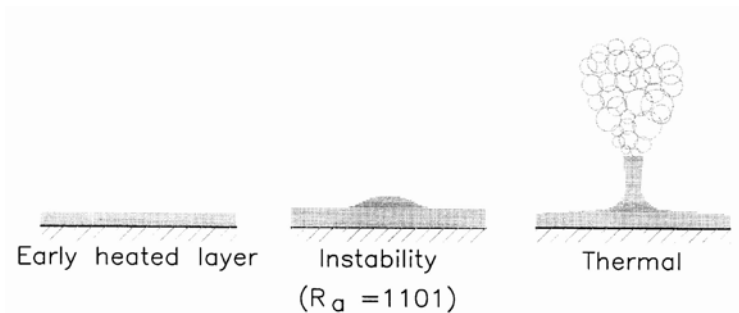


Figure B.2: Flow development on surface.

The generation of such thermals is periodic in time, and both spatial frequency and rate of production are found to increase with an increase in heating rate.

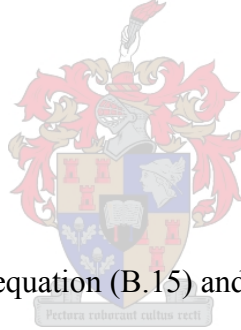
For an analysis of the initial developing vapour concentration distribution near the suddenly wetted surface at  $z = 0$ , consider figure B.1 (a).

The approximate magnitude of the curvature of the concentration profile is the same as the change in slope  $dc_v/\partial z$  across the relatively small concentration layer thickness or height  $\delta_D$  i.e.

$$\frac{\partial^2 c_v}{\partial z^2} \approx \frac{(\partial c_v / \partial z)_{z=\delta_D} - (\partial c_v / \partial z)_{z=0}}{\delta_D - 0} \quad (\text{B.15})$$

Figure B.1 (a) suggests the following concentration gradient scales:

$$\begin{aligned} (\partial c_v / \partial z)_{z=\delta_D} &= 0, \\ (\partial c_v / \partial z)_{z=0} &\approx (c_{vi} - c_{vo}) / \delta_D \end{aligned}$$



Substitute these gradients into equation (B.15) and find

$$\partial^2 c_v / \partial z^2 \approx -(c_{vi} - c_{vo}) / \delta_D^2 \quad (\text{B.16})$$

The approximate magnitude of the term on the right-hand side of equation (B.1) can be deduced by arguing that the average concentration of the  $\delta_D$ -thick region increases from the initial value  $c_{vi}$  by a value of  $(c_{vo} - c_{vi})/2$  during the time interval of length  $t$ .

$$\partial c_v / \partial t = (c_{vo} - c_{vi}) / (2t) \quad (\text{B.17})$$

According to equations (B.1), (B.16) and (B.17) find

$$-(c_{vi} - c_{vo}) / \delta_D^2 \approx (c_{vo} - c_{vi}) / (2Dt)$$

or

$$\delta_D = (2Dt)^{1/2} \quad (\text{B.18})$$

The concentration layer becomes unstable when

$$\text{Ra} = g\delta_{Du}^3 (\rho_{avi} - \rho_{avo}) \rho_{av} c_p / (k\mu) = 1101 \quad (\text{B.19})$$

where  $\rho_{av} = (\rho_{avo} + \rho_{avi})/2$

At this condition

$$\delta_{Du} = 10.33 [k\mu / \{g(\rho_{avi} - \rho_{avo}) \rho_{av} c_p\}]^{1/3} \quad (\text{B.20})$$

From equations (B.18) and (B.20) find

$$t_u = 53.31 [k\mu / \{g(\rho_{avi} - \rho_{avo}) \rho_{av} c_p\}]^{2/3} / D \quad (\text{B.21})$$

Substitute equation (B.21) into equation (B.11) to find

$$h_{Dt} [k\mu / \{g(\rho_{avi} - \rho_{avo}) \rho_{av} c_p\}]^{1/3} / D = 0.0773 \quad (\text{B.22})$$

The average mass transfer coefficient during the period  $t$  is found by integrating equation (B.11) i.e.

$$h_D = 2[D / (\pi t_u)]^{1/2} = 2h_{Dt}$$

or upon substitution of equation (B.22)

$$h_{Dt} [k\mu / \{g(\rho_{avi} - \rho_{avo}) \rho_{av} c_p\}]^{1/3} / D = 0.155 \quad (\text{B.23})$$

If the surface generates vapour at a uniform rate it follows from equation (B.14) that

$$h_{Dm} = \pi h_D / 2$$

or

$$h_{Dm} [k\mu / \{g(\rho_{avi} - \rho_{avom})\rho_{av}c_p\}]^{1/3} / D = 0.243 \quad (\text{B.24})$$

It is stressed that these equations are only applicable to the first phase of the heat or mass transfer process (growth of concentration layer) and do not include the second phase during which thermals exist (breakdown of concentration layer). No simple analytical approach is possible during this latter phase, although the mean mass transfer coefficient during the breakdown of the concentration layer will probably not differ much from the first phase. This would mean that the mean mass transfer coefficient over the cycle of conduction or concentration layer growth and breakdown is of approximately the same value as that obtained during the first phase of the cycle.

By following a procedure similar to the above, the analogous problem of heat transfer during natural convection above a heated horizontal surface for a constant surface temperature of  $T_o$  can be analysed to find according to *Kröger* (2002)

$$h_T [\mu T / \{g(T_o - T_i)c_p k^2 \rho^2\}]^{1/3} = h_T [k\mu / \{g(\rho_i - \rho_o)c_p \rho\}]^{1/3} / k = 0.155 \quad (\text{B.25})$$

and for the case of uniform heat flux  $q$

$$h_q [\mu T / \{g(T_{oq} - T_i)c_p k^2 \rho^2\}]^{1/3} = h_q [k\mu / \{g(\rho_i - \rho_{oq})c_p \rho\}]^{1/3} / k = 0.243 \quad (\text{B.26})$$

where  $\rho = (\rho_i + \rho_o) / 2$

Note the similarity between equations (B.23), (B.24) and (B.25), (B.26) respectively. These equations are applicable to natural convection mass and heat transfer respectively.

In the absence of winds, effective values of  $\rho_{avi}$  in equations (B.23) and (B.24) and  $\rho_i$  in equation (B.25) and (B.26) respectively, change with time ( $t > t_u$ ).

During windy periods (forced convection) evaporation rates generally increase with increasing wind speed. According to the Reynolds-Colburn analogy and the analogy between mass and heat transfer, the following relations exist (*Holman 1986*)

$$\frac{h_w Pr^{2/3}}{\rho c_p v_w} = \frac{C_f}{2} = \frac{h_{Dw} Sc^{2/3}}{v_w}$$

or

$$h_{Dw} = C_f v_w / (2 Sc^{2/3}) \quad (\text{B.27})$$

In general the rate of mass transfer or evaporation from a horizontal wetted surface at a uniform concentration  $c_{vo}$  is thus

$$m_{vo} = [h_D + h_{Dw}] (c_{vo} - c_{vi}) \quad (\text{B.28})$$

If the vapour is generated uniformly at  $z = 0$  find the rate of evaporation according to equations (B.24), (B.27) and (B.28). For relatively small temperature differences, the concentrations can be replaced by the partial vapour pressures i.e.  $c_v = p_v / R_v T_{oi}$  where  $T_{oi} = (T_o + T_i)/2$  and  $R_v = 461.52 \text{ J/kg K}$ . Furthermore, for air-water vapour mixtures  $Sc \approx 0.6$ .

$$m_{vom} = 8.78 \times 10^{-4} \left[ \left\{ g \mu^2 (\rho_{avi} - \rho_{avom}) c_p / (k \rho_{av}^2) \right\}^{1/3} + 1.735 C_f v_w \right] (p_{vo} - p_{vi}) / T_{oi} \quad (\text{B.29})$$

Since the thermal conductivity of water is not negligible, it is not possible to achieve a truly uniform heat flux situation. The value of the dimensionless mass transfer coefficient as given by equation (B.24) may thus be less than 0.243, i.e. it will be some value between 0.243 and 0.155 as given by equation (B.23). *Burger and Kröger (2004)* report the results of experiments conducted during analogous heat transfer tests between a low thermal conductivity horizontal surface and the environment. They obtain a value of 0.2106 instead of the theoretical value of 0.243 given in equation (B.26) and the analogous equation (B.24). They furthermore obtain a value of  $C_f = 0.0052$  based on a wind speed measured 1 m above the test surface. With these values equation (B.26) applied over a wetted surface can be extended to become

$$h_q \left[ \mu / \left\{ g c_p \rho_{av} k^2 (\rho_{avi} - \rho_{avom}) \right\} \right]^{1/3} = 0.2106 + 0.0026 v_w \left[ \rho_{av}^2 / \left\{ \mu g (\rho_{avi} - \rho_{avom}) \right\} \right]^{1/3} \quad (B.30)$$

If the above values (0.2106 and  $C_f = 0.0052$ ) are substituted into equation (B.29) find

$$m_{vom} = 7.61 \times 10^{-4} \left[ \left\{ g \mu^2 (\rho_{avi} - \rho_{avom}) c_p / (k \rho_{av}^2) \right\}^{1/3} + 0.0104 v_w \right] (p_{vo} - p_{vi}) / T_{oi} \quad (B.31)$$

When density differences are very small and conditions relatively stable or at night when  $T_{oq} < T_i$  and the heat flux is uniform *Burger and Kröger* (2004) recommend

$$h_q = 3.87 + 0.0022 \frac{v_w \rho_{av} c_p}{(\mu c_p / k)^{2/3}} \quad (B.32)$$

A mass transfer coefficient that is analogous to equation (B.32) is given by

$$h_{Dm} = \frac{h_q}{\rho_{av} c_p} \left( \frac{Pr}{Sc} \right)^{2/3} = \frac{3.87}{\rho_{av} c_p Sc} \left( \frac{Pr}{Sc} \right)^{2/3} + \frac{0.0022 v_w}{Sc^{2/3}} \quad (B.33)$$

The corresponding uniform mass transfer rate is

$$m_{vom} = \left( \frac{3.87}{\rho \cdot c_p} + \frac{0.0022 v_w}{Pr^{2/3}} \right) \cdot \left( \frac{c_p \cdot \rho \cdot D}{k} \right)^{2/3} \cdot \frac{(p_{vo} - p_{vi})}{R_v T_m} \quad (B.34)$$

This expression is applicable at night and during the day when the value for  $m_{vom}$  is found to be larger than that given by equation (B.32).

## B.2 Analysis - Temperature gradient within water layer

According to *Holman* (1986) the intensity of solar radiation in clear water at a distance  $z$  from the surface is given by

$$I_z = 0.6 I_h e^{-0.16 \cdot z} \quad (B.35)$$

For a thin film of thickness  $z \approx 0.0015$  m the heat flux near the surface of the film is thus approximately

$$k \frac{dT}{dz} \approx I_z \approx 0.6 I_h \quad (\text{B.36})$$

or the surface temperature can be described by

$$T_{oq} \approx T_{o \text{ measured}} - 0.6 \frac{I_h z}{k} \approx T_{o \text{ measured}} - 0.0015 I_h \quad (\text{B.37})$$

### B.3 Evaporation pan

A photograph of the evaporation pan employed in section 2.3 is shown below. Note the thick polystyrene plate painted black and maintained as level as practically possible, with the associated weather station is just out of picture on the right.



Figure B.3: Photograph of evaporation pan.

## B.4 Numerical example

The numerical example that follows makes use of experimental data between the times of 12.419 and 12.585 solar time on April 14<sup>th</sup> 2005. Take note that all numerical values listed from this point onwards would have been averaged over a period of ten minutes. All related experimental data and physical parameters are listed in Table B.1 below.

Table B.1: Evaporation pan experimental data on April 14<sup>th</sup> 2005 at 12.494 h.

Water surface temperature	$T_w$	31.12 °C	(304.27 K)
Ambient air temperature	$T_a$	27.83 °C	(300.98 K)
Dew point temperature	$T_{dp}$	14.70 °C	
Wind speed	$v_w$	1.13 m.s <sup>-1</sup>	
Atmospheric pressure	$p_a$	100990 Pa	
Total incident solar radiation	$I_h$	742.10 W.m <sup>-2</sup>	
Evaporation pan surface area	$A$	0.97 m <sup>2</sup>	
Long-wave emissivity of water	$\epsilon_w$	0.9	
Evaporation rate - Measured	$m_{exp}$	0.000 218 kg.s <sup>-1</sup>	
Evaporation rate – Equation (2.4)	$m_{en}$	0.000 231 kg.s <sup>-1</sup>	
Evaporation rate – Equation (2.7)	$m_{vom}$	0.000 179 kg.s <sup>-1</sup>	
Evaporation rate – Equation (2.9)	$m_{mon}$	0.000 239 kg.s <sup>-1</sup>	
Time interval - local		13h10 – 13h19	
Average time - local	$\Psi$	13.242	
Average time - solar		12.494 h	
Location latitude angle	$\Phi$	33.98 °S	
Location longitude angle	$\Phi_l$	18.85 °E	
South African standard meridian	$\Phi_m$	30.00 °E	

As described in section 2.3, 500 ml quantities of water were added in successive periods to the evaporation pan, where the time taken to evaporate the water was recorded and in turn converted into an evaporation rate. The period applicable to the current numerical example is between 12.035 h and 12.668 h, 38 minutes in length. The density of the water was considered constant for each period; with the temperature at 12.035 h a

density of  $994.6 \text{ kg}\cdot\text{m}^{-3}$  was used. Therefore the measured evaporation rate for this period of time could be calculated to be

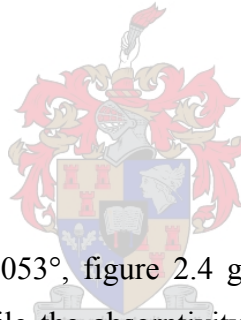
$$m_{\text{exp}} = \frac{0.5}{38 \cdot 60} \cdot \frac{994.6}{1000} = 0.000218 \text{ kg}\cdot\text{s}^{-1} \quad (\text{B.38})$$

The next evaporation rate to be evaluated is that predicted by the energy balance  $m_{\text{en}}$ . This equation however requires that the incidence angle be determined to evaluate the absorptivity of the water surface with the aid of figure 2.4.

Utilising equations (A.3) to (A.7), the incidence angle at 12.494 h on the 14<sup>th</sup> of April 2005 can be determined.

$$\cos\theta_z = \sin(0.16584)\sin(-0.593) + \cos(0.16584)\cos(-0.593)\cos(-0.1292)$$

$$\begin{aligned} \theta_z &= 0.7689 \text{ rad} \\ &= 44.053^\circ \end{aligned}$$



For an incidence angle of  $44.053^\circ$ , figure 2.4 gives an approximate absorptivity for beam radiation of 0.9467, while the absorptivity for diffuse radiation is 0.9207. The solar radiation absorbed by the horizontal water surface can now be determined under the assumption that all radiation not reflected from the water surface is absorbed.

Diffuse solar radiation was measured to be approximately 8% of the total incident radiation.

$$\alpha_w \cdot I_h = 0.9467 \cdot 742.10 \cdot 0.92 + 0.9207 \cdot 742.10 \cdot 0.08 = 700.99 \text{ W}$$

The average temperature between the ambient air,  $T_a$  and the saturated air just above the water,  $T_w$  is

$$T_m = \frac{(T_w + T_a)}{2} = \frac{(304.27 + 300.98)}{2} = 302.63 \text{ K}$$

The following thermophysical properties of the air are evaluated at the mean temperature,  $T_m$  according to *Kröger* (1998).

Density, $\rho$	1.16243 kg.m <sup>-3</sup>
Specific heat capacity, $c_p$	1007.05 J.kg <sup>-1</sup> .K <sup>-1</sup>
Thermal conductivity, $k$	0.026424 W.m <sup>-1</sup> .K <sup>-1</sup>
Dynamic viscosity, $\mu$	1.85894 · 10 <sup>-5</sup> kg.m <sup>-1</sup> .s <sup>-1</sup>

From these values it is then possible to determine the Prandtl number

$$\text{Pr} = \frac{\mu \cdot c_p}{k} = \frac{1.85894 \cdot 10^{-5} \cdot 1007.05}{0.026424} = 0.708449$$

Now the convective component from equation (2.4) can be evaluated.

$$\begin{aligned}
 h_a \cdot (T_w - T_a) &= \left[ \frac{0.2106 + 0.0026 v_w \left[ \frac{\rho T_m}{\mu g (T_w - T_a)} \right]^{1/3}}{\left[ \frac{\mu T_m}{g (T_w - T_a) c_p k^2 \rho^2} \right]^{1/3}} \right] \cdot (T_w - T_a) \\
 &= \left[ \frac{0.2106 + 0.0026 \cdot 1.13 \left[ \frac{1.16243 \cdot 302.63}{1.85894 \cdot 10^{-5} \cdot 9.81 (304.27 - 300.98)} \right]^{1/3}}{\left[ \frac{1.85894 \cdot 10^{-5} \cdot 302.63}{9.81 \cdot (304.27 - 300.98) \cdot 1007.05 \cdot 0.026424^2 \cdot 1.16243^2} \right]^{1/3}} \right] \\
 &\quad \cdot (304.27 - 300.98) \\
 &= 26.323 \text{ W}
 \end{aligned}$$

Similarly, the radiative component in equation (2.4) can be evaluated

$$\begin{aligned}
 \varepsilon_w \sigma (T_w^4 - (0.727 + 0.006 T_{dp}) T_a^4) &= 0.9 \cdot 5.67 \cdot 10^{-8} \cdot (304.27^4 - (0.727 \\
 &\quad + 0.006 \cdot 14.7) \cdot 300.98^4) \\
 &= 96.021 \text{ W}
 \end{aligned}$$

If the latent heat of vaporization of water at 304.27 K is determined as shown below

$$\begin{aligned}
 i_{fg} &= 3483181.4 - 5867.703 \cdot T_s + 12.139568 \cdot T_s^2 - 0.01402090431 \cdot T_s^3 \\
 &= 3483181.4 - 5867.703 \cdot 304.27 + 12.139568 \cdot 304.27^2 - 0.01402090431 \cdot 304.27^3 \\
 &= 2426499 \text{ J.kg}^{-1}
 \end{aligned} \tag{B.39}$$

Now with all the terms necessary to complete equation (B.42), the predicted evaporation rate  $m_{en}$  can be determined.

$$\begin{aligned}
 m_{en} &= \frac{\alpha_w \cdot I_h - h \cdot (T_w - T_a) - \varepsilon_s \cdot \sigma \left[ T_w^4 - \left[ (0.727 + 0.0060 T_{dp}) \cdot T_a^4 \right] \right]}{i_{fg}} \\
 &= \frac{700.99 - 26.323 - 96.021}{2426499} \\
 &= 0.000238 \text{ kg.s}^{-1}
 \end{aligned} \tag{B.40}$$

But this is applicable to an area of 1 m<sup>2</sup>, for an area of 0.97 m<sup>2</sup> the predicted evaporation rate  $m_{en}$  becomes 0.000231 kg.s<sup>-1</sup>.

To determine the evaporation rate according to equation (2.7) it is first necessary to calculate the following values.

The vapour pressure,  $p_{vi}$  in the air can be determined with the aid of the following equation.

$$\begin{aligned}
 p_{vi} &= 2.368745 \cdot 10^{11} \cdot e^{\left( \frac{-5406.1915}{T_{dp}} \right)} = 2.368745 \cdot 10^{11} \cdot e^{\left( \frac{-5406.1915}{287.85} \right)} \\
 &= 1651.63 \text{ N.m}^{-2}
 \end{aligned} \tag{B.41}$$

The humidity ratio,  $w_i$  of the ambient air is given by

$$w_i = \frac{0.622 \cdot p_{vi}}{p_a - p_{vi}} = \frac{0.622 \cdot 1651.63}{100990 - 1651.63} \tag{B.42}$$

$$= 0.010342 \text{ kg } H_2O / \text{ kg dry air}$$

With the aid of these two values, the density of the ambient air can be determined.

$$\begin{aligned} \rho_{avi} &= (1 + w_i) \cdot \left[ 1 - \frac{w_i}{(w_i + 0.622)} \right] \cdot \left( \frac{p_a}{287.08 \cdot T_a} \right) \\ &= (1 + 0.010342) \cdot \left[ 1 - \frac{0.010342}{(0.010342 + 0.622)} \right] \cdot \left( \frac{100990}{287.08 \cdot 300.98} \right) \\ &= 1.161561 \text{ kg} \cdot \text{m}^{-3} \end{aligned} \quad (\text{B.43})$$

The partial vapour density of the ambient air,  $\rho_{vi}$  is determined below.

$$\begin{aligned} \rho_{vi} &= \frac{p_{vi}}{R_w \cdot T_a} = \frac{1651.63}{461.5 \cdot 300.98} \\ &= 0.01189 \text{ kg} \cdot \text{m}^{-3} \end{aligned} \quad (\text{B.44})$$

Similarly, these equations can be applied to the saturated air at the surface of the water.

The vapour pressure,  $p_{vo}$  is

$$\begin{aligned} p_{vo} &= 2.368745 \cdot 10^{11} \cdot e^{(-5406.1915/T_w)} = 2.368745 \cdot 10^{11} \cdot e^{(-5406.1915/304.27)} \\ &= 4552.045 \text{ N} \cdot \text{m}^{-2} \end{aligned} \quad (\text{B.45})$$

The humidity ratio of the saturated air at  $T_w$  is

$$\begin{aligned} w_o &= \frac{0.622 \cdot p_{vo}}{p_a - p_{vo}} = \frac{0.622 \cdot 4552.045}{100990 - 4552.045} \\ &= 0.029360 \text{ kg } H_2O / \text{ kg dry air} \end{aligned}$$

Then the density of the air at the surface of the water can be calculated as follows:

$$\rho_{avo} = (1 + w_o) \cdot \left[ 1 - \frac{w_o}{(w_o + 0.622)} \right] \cdot \left( \frac{p_a}{287.08 \cdot T_w} \right)$$

$$\begin{aligned}
 &= (1 + 0.029360) \cdot \left[ 1 - \frac{0.029360}{(0.029360 + 0.622)} \right] \cdot \left( \frac{100990}{287.08 \cdot 304.27} \right) \\
 &= 1.136439 \text{ kg.m}^{-3}
 \end{aligned}$$

The partial vapour density of the saturated air,  $\rho_{vo}$  can be found according to the equation that follows:

$$\begin{aligned}
 \rho_{vo} &= \frac{p_{vo}}{R_w \cdot T_w} = \frac{4552.045}{461.5 \cdot 304.27} \\
 &= 0.032417 \text{ kg.m}^{-3}
 \end{aligned}$$

The average density of the moist air between the water surface and the ambient is

$$\rho_{av} = \frac{(\rho_{avi} + \rho_{avo})}{2} = \frac{(1.161561 + 1.136439)}{2} = 1.149 \text{ kg.m}^{-3}$$

Equation (2.7) can now be evaluated

$$\begin{aligned}
 m_{vom} &= 7.6053 \cdot 10^{-4} \cdot ((9.81 \cdot (1.85894 \cdot 10^{-5})^2) \cdot (1.161561 - 1.136439)) \\
 &\quad \times 1007.05 / ((0.026424 \cdot 1.149^2))^{1/3} + 2.002 \cdot 0.0052 \cdot 1.13 \times \frac{(4552.045 - 1651.63)}{302.63} \\
 &= 0.000179 \text{ kg.s}^{-1} \tag{B.46}
 \end{aligned}$$

Lastly, if the evaporation rate predicted by equation (2.9) is to be evaluated, it is first necessary to determine the values that follow.

$$\begin{aligned}
 c_{pv} &= 1.3605 \cdot 10^3 + 2.31334 \cdot T_a - 2.46784 \cdot 10^{-10} \cdot T_a^5 + 5.91332 \cdot 10^{-13} \cdot T_a^6 \\
 &= 1.3605 \cdot 10^3 + 2.31334 \cdot 300.98 - 2.46784 \cdot 10^{-10} \cdot 300.98^5 + 5.91332 \cdot 10^{-13} \cdot 300.98^6 \\
 &= 1886.83 \text{ J.kg}^{-1} \cdot \text{K}^{-1}
 \end{aligned}$$

$$\begin{aligned}
 c_{pma} &= c_{pa} + w_i \cdot c_{pv} \\
 &= 1007.05 + 0.010342 \cdot 1886.83
 \end{aligned}$$

$$= 1026.50 \text{ J.kg}^{-1}.\text{K}^{-1}$$

Now if the latent heat of vaporization at the wet-bulb temperature ( $T_{wb} = 293.31 \text{ K}$ ) is to be determined equation (B.39) can be used to find

$$\begin{aligned} i_{fg} &= 3483181.4 - 5867.703 \cdot 293.31 + 12.139568 \cdot 293.31^2 - 0.01402090431 \cdot 293.31^3 \\ &= 2452488 \text{ J.kg}^{-1} \end{aligned}$$

then the adjusted psychrometric constant can be expressed as shown below

$$\begin{aligned} \gamma^* &= Le^{2/3} \cdot \gamma = \left( \frac{k}{D \cdot \rho \cdot c_p} \right)^{2/3} \cdot \left( \frac{c_{pma} \cdot P_{atm}}{0.622 \cdot i_{fg}(T_{wb})} \right) \\ &= \left( \frac{0.026424}{0.26 \cdot 10^{-4} \cdot 1.16878 \cdot 1007.05} \right)^{2/3} \cdot \left( \frac{1026.50 \cdot 100990}{0.622 \cdot 2452488} \right) \\ &= 61.433 \end{aligned} \tag{B.47}$$

The slope of the saturated vapour pressure line  $\Delta$ , can be calculated with the aid of the following equation

$$\Delta = \frac{i_{fg} \cdot p_{sat}(T)}{T^2 \cdot R_v} \tag{B.48}$$

where all properties are evaluated at the temperature  $T$ , which is the average between the surface-  $T_s$  and wet-bulb temperatures  $T_{wb}$ .

$$T = \frac{T_s + T_{wb}}{2} = \frac{304.27 + 293.31}{2} = 298.79 \text{ K}$$

With equation (B.39) the latent heat of vaporization at this temperature is

$$\begin{aligned} i_{fg} &= 3483181.4 - 5867.703 \cdot 298.79 + 12.139568 \cdot 298.79^2 - 0.01402090431 \cdot 298.79^3 \\ &= 2439506 \text{ J.kg}^{-1} \end{aligned}$$

The saturation vapour pressure  $p_{sat}(T)$  at this temperature can be determined according to equation (B.41)

$$\begin{aligned} p_{sat} &= 2.368745 \cdot 10^{11} \cdot e^{(-5406.1915/T)} = 2.368745 \cdot 10^{11} \cdot e^{(-5406.1915/298.79)} \\ &= 3292.54 \text{ N.m}^{-2} \end{aligned}$$

$$\Delta = \frac{2439506 \cdot 3292.54}{298.79^2 \cdot 461.5} = 194.95 \text{ Pa.K}^{-1}$$

Lastly the difference between the vapour pressure of the air at the ambient condition  $p_{vi}$  and the saturated vapour pressure at that same dry-bulb temperature  $p_{vsi}$  is given by

$$\begin{aligned} p_{vsi} - p_{vi} &= 3747.84 - 1651.63 \\ &= 2096.21 \text{ Pa} \end{aligned}$$

Now it is possible for the evaporation rate according to equation (2.9) to be evaluated.

$$\begin{aligned} m_{mon} &= \left( \frac{194.95 \cdot 700.99 + 2096.21 \cdot 8}{194.95 + 61.43} \right) \cdot \left( \frac{0.97}{2426499} \right) \\ &= 0.000239 \text{ kg.s}^{-1} \end{aligned} \tag{B.49}$$

## APPENDIX C

# Water tank experiments

- C.1 Open water tank photograph and spindle drawing
  - C.2 Numerical example (section 3.2)
  - C.3 Solar collector with plastic-covered water tank: Photograph and analysis
  - C.4 Numerical example (section (3.3))
- 

### C.1 Open water tank

A photograph of the open water tank is shown below. The tank is in the centre of the picture with the weather station to the left and the pyranometer to the right.



Figure C.1: Photograph of open water tank.

Observation of the above figure shows that the “thermocouple spindle” used to determine the water temperature profile is located in the centre of the tank, with the upper portion visible above the water level. It is shown in detail in the figure C.2.

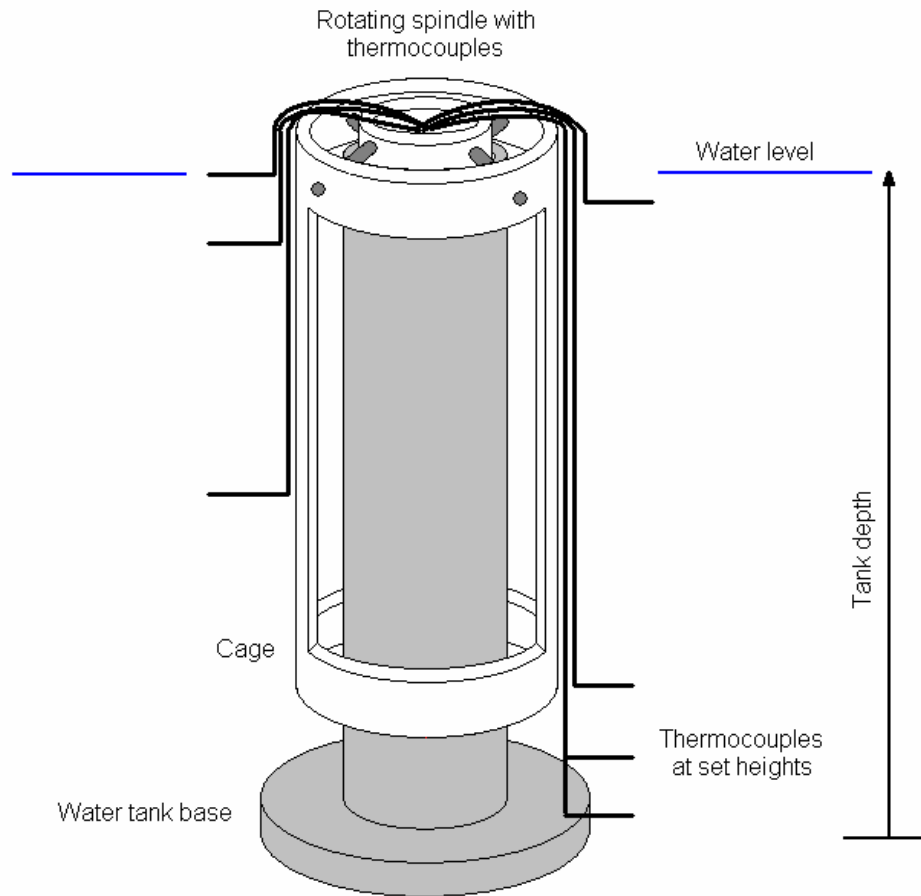


Figure C.2: Thermocouple spindle used to determine water temperature profile.

## C.2 Numerical example

Table C.1 supplies the measured experimental data and apparatus parameters applicable to the water tank between 12.301 and 12.451 solar time on the 29<sup>th</sup> of April 2005. As before, all numerical data listed has been averaged over a period of ten minutes.

Table C.1: Experimental data and physical parameters of water tank.

Water surface temperature	$T_w$	23.62 °C	(296.77 K)
Ambient air temperature	$T_a$	33.20 °C	(306.35 K)

Dew-point temperature	$T_{dp}$	11.66 °C	
Wind speed	$v_w$	0.28 m.s <sup>-1</sup>	
Atmospheric pressure	$p_a$	100830 Pa	
Total incident solar radiation	$I_h$	729.77 W.m <sup>-2</sup>	
Water tank surface area	$A$	1 m <sup>2</sup>	
Depth of water tank	$t_w$	0.190 m	
Long-wave emissivity of water	$\varepsilon_w$	0.9	
Evaporation rate – Measured	$m_{exp}$	0.000 096 kg.s <sup>-1</sup>	
Evaporation rate – Equation (3.2)	$m_{en}$	0.000 093 kg.s <sup>-1</sup>	
Evaporation rate – Equation (2.8)	$m_{vom}$	0.000 052 kg.s <sup>-1</sup>	
Evaporation rate – Equation (2.9)	$m_{mon}$	0.000 231 kg.s <sup>-1</sup>	
Time interval - local		13h00 – 13h09	
Average time - local	$\Psi$	13.075 h	
Average time - solar		12.376 h	
Mean water temperature (12.209 h)	$T_{wm}^i$	23.423 °C	(296.573 K)
Mean water temperature (12.376 h)	$T_{wm}^{i-1}$	23.071 °C	(296.221 K)
Location latitude angle	$\Phi$	33.98 °S	
Location longitude angle	$\Phi_l$	18.85 °E	
South African standard meridian	$\Phi_m$	30.00 °E	

As in section 2.3, a quantity of water was added to the water tank and the period of time taken for that particular quantity of water to evaporate was recorded and converted into the measured evaporation rate  $m_{exp}$ . In this case 750 ml of water was evaporated within a period of 130 minutes at an average density of 997.4 kg.m<sup>-3</sup>. The measured evaporation rate is then

$$m_{exp} = \frac{0.75}{130 \cdot 60} \cdot \frac{997.4}{1000} = 0.000\ 096\ kg.s^{-1} \quad (C.1)$$

The solar absorptivity of water is a function of the position of the sun in the sky and thus it is important that the incidence angle be determined. The same procedure is followed as in Appendix A and the result is that the incidence angle is found to be 48.823°.

This means that the solar altitude at this time of the day was  $41.177^\circ$ , which with the aid of figure 2.4 gives a solar absorptivity for water under clear skies to be 0.9392.

$$\begin{aligned}\alpha_w \cdot I_h &= 0.9392 \cdot 729.77 \cdot 0.92 + 0.9207 \cdot 729.77 \cdot 0.08 = 684.333 \text{ W} \\ &= 684.333 \text{ W}\end{aligned}$$

The average temperature between the ambient air,  $T_a$  and the saturated air just above the water,  $T_w$  is

$$T_m = \frac{(T_w + T_a)}{2} = \frac{(296.77 + 306.35)}{2} = 301.56 \text{ K}$$

The following thermophysical properties of the air are evaluated at the mean temperature  $T_m$  according to Kröger (1998).

Density, $\rho$	1.16469 kg.m <sup>-3</sup>
Specific heat capacity, $c_p$	1007.01 J.kg <sup>-1</sup> .K <sup>-1</sup>
Thermal conductivity, $k$	0.026342 W.m <sup>-1</sup> .K <sup>-1</sup>
Dynamic viscosity, $\mu$	$1.85404 \cdot 10^{-5}$ kg.m <sup>-1</sup> .s <sup>-1</sup>



Then with the use of these three values, the Prandtl number can be determined.

$$\text{Pr} = \frac{\mu \cdot c_p}{k} = \frac{1.85404 \cdot 10^{-5} \cdot 1007.01}{0.026342} = 0.708765$$

Now the convective component from equation (3.2) can be evaluated with the use of equation (2.2)

$$\begin{aligned}h_a(T_a - T_w) &= \left[ 3.87 + 0.0022 \frac{v_w \cdot \rho \cdot c_p}{(\mu \cdot c_p / k)^{2/3}} \right] \cdot (T_a - T_w) \\ &= \left[ 3.87 + 0.0022 \frac{0.28 \cdot 1.16469 \cdot 1007.01}{(1.85404 \cdot 10^{-5} \cdot 1007.01 / 0.026342)^{2/3}} \right] \cdot (306.35 - 296.77)\end{aligned}$$

$$= 45.772 \text{ W}$$

Similarly, the radiative component in equation (3.3) can be evaluated as shown below.

$$\begin{aligned} \varepsilon_w \sigma (T_w^4 - T_{sky}^4) &= \varepsilon_w \sigma (T_w^4 - (0.727 + 0.006 T_{dp}) T_a^4) \\ &= 0.9 \cdot 5.67 \cdot 10^{-8} \cdot (296.77^4 - (0.727 + 0.006 \cdot 11.66) \cdot 306.35^4) \\ &= 37.628 \text{ W} \end{aligned}$$

Evaluating the stored energy within the water tank requires that the following properties be determined at the mean temperature of the water tank (296.573 K). The density of water at this temperature according to *Kröger* (1998) is

$$\begin{aligned} \rho_{wm} &= (1.49343 \cdot 10^{-3} - 3.7164 \cdot 10^{-6} \cdot T_{wm} + 7.09782 \cdot 10^{-9} \cdot T_{wm}^2 \\ &\quad - 1.090321 \cdot 10^{-20} \cdot T_{wm}^6)^{-1} \\ &= (1.49343 \cdot 10^{-3} - 3.7164 \cdot 10^{-6} \cdot 296.573 + 7.09782 \cdot 10^{-9} \cdot 296.573^2 \\ &\quad - 1.090321 \cdot 10^{-20} \cdot 296.573^6)^{-1} \\ &= 997.42 \text{ kg} \cdot \text{m}^{-3} \end{aligned}$$

The specific heat capacity of water at 296.573 K according to *Kröger* (1998) is

$$\begin{aligned} c_{pwm} &= 8.15599 \cdot 10^3 - 2.80627 \cdot 10 \cdot T_{wm} + 5.11283 \cdot 10^{-2} \cdot T_{wm}^2 \\ &\quad - 2.17582 \cdot 10^{-13} \cdot T_{wm}^6 \\ &= 4182.32 \text{ J} \cdot \text{kg}^{-1} \cdot \text{K}^{-1} \end{aligned}$$

and the change in mean water temperature over a period of 10 minutes is

$$\begin{aligned} \frac{dT_{wm}}{dt} &= \frac{T_{wm}^i - T_{wm}^{i-1}}{60 \cdot 10} \\ &= \frac{296.573 - 296.221}{600} \\ &= 0.000587 \text{ K} \cdot \text{s}^{-1} \end{aligned}$$

The change in internal energy can then be evaluated as shown below

$$\begin{aligned}\rho_{wm} \cdot t_w \cdot c_{pm} \cdot \frac{dT_{wm}}{dt} &= 997.42 \cdot 0.190 \cdot 4182.32 \cdot 0.000587 \\ &= 465.054 \text{ W}\end{aligned}$$

The evaporative heat flux leaving the water surface and is represented by

$$q_{ev} = m_{ev} \cdot i_{fg}$$

If the latent heat of vaporization of water at 296.77 K is determined by equation (B.39) to be 2 444 300 J.kg<sup>-1</sup>, then the evaporation rate as predicted by the energy balance  $m_{en}$  is represented by

$$\begin{aligned}m_{en} &= \frac{\alpha_w \cdot I_h - h \cdot (T_w - T_a) - \varepsilon_s \cdot \sigma \left[ T_s^4 - \left[ (0.727 + 0.0060 T_{dp}) \cdot T_a^4 \right] \right] - \rho_{wm} \cdot t_w \cdot c_{pm} \cdot \frac{dT_{wm}}{dt}}{i_{fg}} \\ &= \frac{684.333 + 45.772 - 37.628 - 465.054}{2\,444\,300} \\ &= 0.000\,093 \text{ kg.s}^{-1}\end{aligned}\tag{C.2}$$

If the evaporation rate according to equation (2.8) is to be evaluated

$$\begin{aligned}m_{vom} &= \left[ 3.87 + 0.0022 \cdot \frac{0.28 \cdot 1.16469 \cdot 1007.01}{(1.85404 \cdot 10^{-5} \cdot 1007.01 / 0.026342)^{2/3}} \right] \cdot \left( \frac{1}{1.16469 \cdot 1007.01} \right) \\ &\quad \times \left( \frac{1007.01 \cdot 1.16469 \cdot 0.00026}{0.026342} \right)^{2/3} \cdot (0.021209 - 0.00956) \\ &= 0.000\,052 \text{ kg.s}^{-1}\end{aligned}\tag{C.3}$$

The evaporation rate predicted by equation (2.9) can be evaluated with the calculation of the following values.

The specific heat capacity of the vapour is

$$\begin{aligned}
 c_{pv} &= 1.3605 \cdot 10^3 + 2.31334 \cdot 300.98 - 2.46784 \cdot 10^{-10} \cdot 300.98^5 \\
 &\quad + 5.91332 \cdot 10^{-13} \cdot 300.98^6 \\
 &= 1892.10 \text{ J.kg}^{-1} \cdot \text{K}^{-1}
 \end{aligned}$$

The vapour pressure of the air  $p_{vi}$  can be determined with equation (B.41)

$$\begin{aligned}
 p_{vi} &= 0.45 \cdot 2.368745 \cdot 10^{11} \cdot e^{(-5406.1915/284.81)} \\
 &= 1351.61 \text{ Pa}
 \end{aligned}$$

Then with the use of the above result it is possible to find the humidity ratio  $\omega_i$  of the air with equation (B.42).

$$\begin{aligned}
 \omega_i &= \frac{0.622 \cdot 1351.61}{100830 - 1351.61} \\
 &= 0.008451 \text{ kg H}_2\text{O} / \text{kg dry air}
 \end{aligned}$$

The following relationship is used to calculate the specific heat capacity of the moist air

$$\begin{aligned}
 c_{pma} &= 1007.01 + 0.008451 \cdot 1892.10 \\
 &= 1023.19 \text{ J.kg}^{-1} \cdot \text{K}^{-1}
 \end{aligned}$$

Now if the latent heat of vaporization at the wet-bulb temperature ( $T_{wb} = 289.30 \text{ K}$ ) is to be determined with equation (B.39).

$$\begin{aligned}
 i_{fg} &= 3483181.4 - 5867.703 \cdot 289.30 + 12.139568 \cdot 289.30^2 - 0.01402090431 \cdot 289.30^3 \\
 &= 2461984 \text{ J.kg}^{-1}
 \end{aligned}$$

then the adjusted psychrometric constant can be expressed as in equation (B.47)

$$\gamma^* = \left( \frac{0.026342}{0.26 \cdot 10^{-4} \cdot 1.16469 \cdot 1007.01} \right)^{\frac{2}{3}} \cdot \left( \frac{1023.19 \cdot 100830}{0.622 \cdot 2461984} \right) = 62.325$$

The slope of the saturated vapour pressure line  $\Delta$ , can be calculated with the aid of the equation (B.48), where  $T$  is defined by

$$T = \frac{T_s + T_{wb}}{2} = \frac{296.77 + 289.30}{2} = 293.04 \text{ K}$$

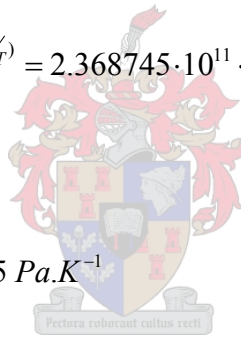
With equation (B.39) the latent heat of vaporization at this temperature is

$$\begin{aligned} i_{fg} &= 3483181.4 - 5867.703 \cdot 293.04 + 12.139568 \cdot 293.04^2 - 0.01402090431 \cdot 293.04^3 \\ &= 2453145 \text{ J.kg}^{-1} \end{aligned}$$

The saturation vapour pressure  $p_{sat}(T)$  at this temperature can be determined according to equation (B.41)

$$\begin{aligned} p_{sat} &= 2.368745 \cdot 10^{11} \cdot e^{(-5406.1915/T)} = 2.368745 \cdot 10^{11} \cdot e^{(-5406.1915/293.04)} \\ &= 2322.16 \text{ N.m}^{-2} \end{aligned}$$

$$\Delta = \frac{2453145 \cdot 2322.16}{293.04^2 \cdot 461.5} = 143.75 \text{ Pa.K}^{-1}$$



Lastly the difference between the vapour pressure of the air at the ambient condition  $p_{vi}$  and the saturated vapour pressure at that same dry-bulb temperature  $p_{vsi}$  is given by

$$p_{vsi} - p_{vi} = 5134.25 - 1351.61 = 3782.64 \text{ Pa}$$

It is now possible for the evaporation rate according equation (2.9) to be evaluated.

$$\begin{aligned} m_{mon} &= \left( \frac{143.75 \cdot 684.33 + 3782.64 \cdot 4.779}{143.75 + 62.33} \right) \cdot \left( \frac{1}{2444300} \right) \\ &= 0.000231 \text{ kg.s}^{-1} \end{aligned} \tag{C.4}$$

### C.3 Solar collector with plastic-covered water tank: Photograph and analysis

The solar collector is analysed with the intention of obtaining a set of equations that can be solved simultaneously to accurately predict the measured glass cover- and mean water temperatures.

As shown schematically in figure 3.7, the solar collector is simply comprised of a volume of water covered by a plastic film that is exposed to solar radiation through a glass cover. The purpose of the plastic film is to prevent the condensation of water on the lower face of the glass lid and thus the effects of evaporation, condensation and the influence of condensation on light transmission can be omitted in this analysis.

Applying an energy balance to the glass cover shown in figure 3.7 and find

$$Ih_b + Ih_d + q_{cw} + q_{rw} = \rho'_{bc} Ih_b + \rho'_{dc} Ih_d + \tau'_{bc} Ih_b + \tau'_{dc} Ih_d + q_{ca} + q_{ra} + \rho_c t_c c_{pc} \frac{dT_c}{dt} \quad (C.5)$$

The terms with  $b$  and  $d$  subscripts represent the beam and diffuse components as discussed previously, while  $\rho'$  and  $\tau'$  are the effective reflectivity and transmissivity of the glass cover as defined in Appendix D. The terms  $q_{cw}$  and  $q_{rw}$  represent the convective and radiative heat transfer respectively between the cover and the water tank. Similarly,  $q_{ca}$  and  $q_{ra}$  are the convective and radiative heat transfer between the cover and the environment.

It is important to note that the solar collector is well insulated and thus losses through conduction are considered negligible, while highly reflective sides used in the solar collector ensure very little radiation heat exchange between the glass cover and the sides, or the water surface and the sides.

Equation (C.5) can be rewritten in the following format

$$(1 - \rho'_{bc} - \tau'_{bc})Ih_b + (1 - \rho'_{dc} - \tau'_{dc})Ih_d + q_{cw} + q_{rw} = q_{ca} + q_{ra} + \rho_c t_c c_{pc} \frac{dT_c}{dt} \quad (C.6)$$

As mentioned in Appendix D, *Mills* (1992) states that  $\rho' + \tau' + \alpha' = I$ , which means that equation (C.6) can be rewritten as

$$\alpha'_{bc} Ih_b + \alpha'_{dc} Ih_d + q_{cw} + q_{rw} = q_{ca} + q_{ra} + \rho_c t_c c_{pc} \frac{dT_c}{dt} \quad (C.7)$$

The beam and diffuse cover absorptivities can now be substituted into equation (C.7) from equation (D.6). This results in the cover energy balance as given by equation (C.8)

$$\frac{(1 - \rho_{bc})(1 - \tau_{abc})}{1 - \rho_{bc}\tau_{abc}} \cdot Ih_b + \frac{(1 - \rho_{dc})(1 - \tau_{adc})}{1 - \rho_{dc}\tau_{adc}} \cdot Ih_d + q_{cw} + q_{rw} = q_{ca} + q_{ra} \quad (C.8)$$

Note that the last term representing the change in stored energy of the glass cover  $\rho_c t_c c_{pc} dT_c/dt$ , has been omitted since it will be shown that the magnitude of this term is negligible under all conditions. Also note the addition of the cover subscripts c in the absorptivity terms from equation (D.6).

Now it remains for the convective and radiative terms associated with equation (C.8) to be evaluated.

The convective losses to the environment  $q_{ca}$  will be determined according to equation (2.1) and (2.2) as given by *Burger and Kröger* (2004). Note that the surface temperatures  $T_s$  from equation (2.1) have simply been replaced by the cover temperatures  $T_c$ . This equation is only applicable when the cover temperature exceeds that of the ambient air, otherwise equation (2.2) would have been used instead.

The radiative heat transfer to the environment  $q_{ra}$  is also evaluated in same manner as in Appendix B, with the use of either equation (2.5) or (2.6) as recommended by *Berdahl and Fromberg* (1982).

The appropriate convective heat transfer coefficient between the water surface and the glass cover, when the water surface is at a greater temperature than the glass, is supplied by *Holland et al. (1975)* as shown below

$$h_e = \left[ 1 + 1.44 \left[ 1 - \frac{1708}{Gr_{cw} Pr_{cw}} \right] + \left[ \left( \frac{Gr_{cw} Pr_{cw}}{5830} \right)^{1/3} - 1 \right] \right] \frac{k_{cw}}{t_a} \quad (C.9)$$

Note that the Prandtl and Grashof numbers are determined at the mean temperature between the water and glass cover.

Lastly, if the water surface and the glass cover are considered as two infinite parallel plates then the radiative heat exchange between the two can be calculated according to *Mills (1992)*.

$$q_{rw} = \sigma \left( \frac{1}{\varepsilon_c} + \frac{1}{\varepsilon_w} - 1 \right)^{-1} (T_w^4 - T_c^4) \quad (C.10)$$

where the cover and water emissivities are given by  $\varepsilon_c$  and  $\varepsilon_w$ .



If the appropriate equations are substituted into equation (C.8), it is possible for the energy balance on the cover to be fully expanded for steady-state conditions as shown below

$$\begin{aligned} & \frac{(1 - \rho_{bc})(1 - \tau_{abc})}{1 - \rho_{bc}\tau_{abc}} \cdot I_{hb} + \frac{(1 - \rho_{dc})(1 - \tau_{adc})}{1 - \rho_{dc}\tau_{adc}} \cdot I_{hd} + \sigma \left( \frac{1}{\varepsilon_c} + \frac{1}{\varepsilon_f} - 1 \right)^{-1} (T_w^4 - T_c^4) \\ & + \left[ 1 + 1.44 \left[ 1 - \frac{1708}{Gr_{cw} Pr_{cw}} \right] + \left[ \left( \frac{Gr_{cw} Pr_{cw}}{5830} \right)^{1/3} - 1 \right] \right] \frac{k_{cw}}{t_a} (T_w - T_c) \quad (C.11) \\ & = \left[ \frac{0.2106 + 0.0026v_w \left[ \frac{\rho T_m}{\mu g (T_c - T_a)} \right]^{1/3}}{\left[ \frac{\mu T_m}{g (T_c - T_a) c_p k^2 \rho^2} \right]^{1/3}} \right] \cdot (T_c - T_a) + \varepsilon_c \sigma (T_c^4 - (0.727 + 0.006 T_{dp}) T_a^4) \end{aligned}$$

Note that the emissivity of the water  $\varepsilon_w$  has simply been replaced with that of the plastic film  $\varepsilon_f$ . It is assumed that good contact exists between the plastic film and the water surface, and since the film is very thin ( $t_f \approx 0.0002$  m) it is assumed to be at the same temperature as that of the water.

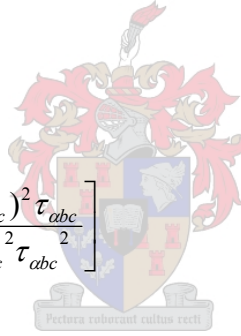
Now if an energy balance is applied to the water tank as shown in figure 3.7 then the following equation is produced

$$(\tau'_{bc} \alpha_w)_b I_{hb} + (\tau'_{dc} \alpha_w)_d I_{hd} = q_{cw} + q_{rw} + \rho_w t_w c_{pw} \frac{dT_w}{dt} \quad (C.12)$$

The transmittance-absorptance product can be determined from equation (D.16), but since the transmittance of the water tank is zero then the sum of the effective reflectivity and absorptivity must add up to unity.

Equation (D.16) then becomes

$$(\tau' \alpha_w) = \left( \frac{(1 - \rho'_{bf})}{1 - \rho'_{bf} \cdot \rho_{dc}} \right) \cdot \left[ \frac{(1 - \rho_{bc})^2 \tau_{abc}}{1 - \rho_{bc}^2 \tau_{abc}^2} \right] \quad (C.13)$$



Then if equation (D.4) is substituted into equation (C.13) for the effective reflectivity, which is in turn substituted into equation (C.12), then the energy balance on the water tank becomes

$$\begin{aligned} & \left[ \frac{(1 - \rho_{bc})^2 \tau_{abc}}{(1 - \rho_{bc}^2 \tau_{abc}^2)} \right] \left[ 1 - \frac{\rho_{baf} + (1 - 2\rho_{baf})\rho_{bfw}\tau_{abf}^2}{1 - \rho_{baf}\rho_{bfw}\tau_{abf}^2} \right] \left[ 1 - \rho_{dc} \frac{\rho_{baf} + (1 - 2\rho_{baf})\rho_{bfw}\tau_{abf}^2}{1 - \rho_{baf}\rho_{bfw}\tau_{abf}^2} \right]^{-1} \cdot I_{hb} \\ & + \left[ \frac{(1 - \rho_{dc})^2 \tau_{adc}}{(1 - \rho_{dc}^2 \tau_{adc}^2)} \right] \left[ 1 - \frac{\rho_{daf} + (1 - 2\rho_{daf})\rho_{dfw}\tau_{adf}^2}{1 - \rho_{daf}\rho_{dfw}\tau_{adf}^2} \right] \left[ 1 - \rho_{dc} \frac{\rho_{daf} + (1 - 2\rho_{daf})\rho_{dfw}\tau_{adf}^2}{1 - \rho_{daf}\rho_{dfw}\tau_{adf}^2} \right]^{-1} I_{hd} \\ & = \left[ 1 + 1.44 \left[ 1 - \frac{1708}{Gr_{cw} Pr_{cw}} \right] + \left[ \left( \frac{Gr_{cw} Pr_{cw}}{5830} \right)^{1/3} - 1 \right] \right] \cdot \frac{k_{cw}}{t_a} (T_w - T_c) \\ & + \sigma \left( \frac{1}{\varepsilon_c} + \frac{1}{\varepsilon_f} - 1 \right)^{-1} (T_w^4 - T_c^4) + \rho_w t_w c_{pw} \frac{dT_w}{dt} \quad (C.14) \end{aligned}$$

Equation (C.14) presented above is the water tank's steady-state energy equation and is based on the assumption that good contact exists between the plastic film and the water surface. However it was found in practice that while exposed to the sun, a small layer of air developed between the plastic film and the water. This occurred because the solubility of oxygen in water is decreased with an increase in temperature and thus the cumulative result of the oxygen being released from solution would be the air gap that formed.

The presence of this air gap changes the above analysis slightly, such that the effective transmissivity of the plastic film needs to incorporate the air layer that has formed. The result is equation (C.15) below.

$$\begin{aligned}
 & \left[ \frac{(1 - \rho_{bc})^2 \tau_{abc}}{(1 - \rho_{bc}^2 \tau_{abc}^2)} \right] \left[ 1 - \frac{\rho_{baf} + (1 - 2\rho_{baf})\rho_{bfw}\tau_{abf}^2}{1 - \rho_{baf}\rho_{bfw}\tau_{abf}^2} \right] \left[ 1 - \rho_{dc} \frac{\rho_{baf} + (1 - 2\rho_{baf})\rho_{bfw}\tau_{abf}^2}{1 - \rho_{baf}\rho_{bfw}\tau_{abf}^2} \right]^{-1} \\
 & \cdot (1 - \rho_{bw})I_{hb} + \left[ \frac{(1 - \rho_{dc})^2 \tau_{adc}}{(1 - \rho_{dc}^2 \tau_{adc}^2)} \right] \left[ 1 - \frac{\rho_{daf} + (1 - 2\rho_{daf})\rho_{dfw}\tau_{adf}^2}{1 - \rho_{daf}\rho_{dfw}\tau_{adf}^2} \right] \\
 & \cdot \left[ 1 - \rho_{dc} \frac{\rho_{daf} + (1 - 2\rho_{daf})\rho_{dfw}\tau_{adf}^2}{1 - \rho_{daf}\rho_{dfw}\tau_{adf}^2} \right]^{-1} (1 - \rho_{dw})I_{hd} \\
 & = \left[ 1 + 1.44 \left[ 1 - \frac{1708}{Gr_{cw} Pr_{cw}} \right] + \left[ \left( \frac{Gr_{cw} Pr_{cw}}{5830} \right)^{1/3} - 1 \right] \right] \frac{k_{cw}}{t_a} (T_w - T_c) \\
 & + \sigma \left( \frac{1}{\varepsilon_c} + \frac{1}{\varepsilon_f} - 1 \right)^{-1} (T_w^4 - T_c^4) + \rho_w t_w c_{pw} \frac{dT_w}{dt} \tag{C.15}
 \end{aligned}$$

The change in plastic film transmissivity is employed by simply multiplying the solar terms by a factor of  $(1 - \rho_w)$ .

Note that in the above equations the *af* and *fw* subscripts refer to the air-film and film-water interfaces respectively.

Lastly it needs to be stated that a number of assumptions were made regarding the derivation of equations (C.11) and (C.15). It was mentioned previously that the thermal

capacitance of the plastic film was considered negligible and that conductive losses through the sides of the well-insulated water tank were also ignored, however it also needs to be mentioned that the changes in thermal capacity of the enclosed air is ignored. This assumption is based on the fact that under steady-state conditions, the natural convective heat transfer between the water surface and the air is the same as that between the enclosed air and the glass cover.

The other assumption made is that the water temperature predicted will be compared to the measured mean water temperature. Stored energy is a function of mean water temperature and convection and radiation a function of water surface temperature; it will be shown at a later stage that the stored energy term in equation (C.15) has a much larger influence on the predicted temperatures than the radiative or convective terms and thus more accurate results are expected with this approach.

Figure C.3 shows a photograph of the solar collector with plastic-covered water tank during daytime operation.

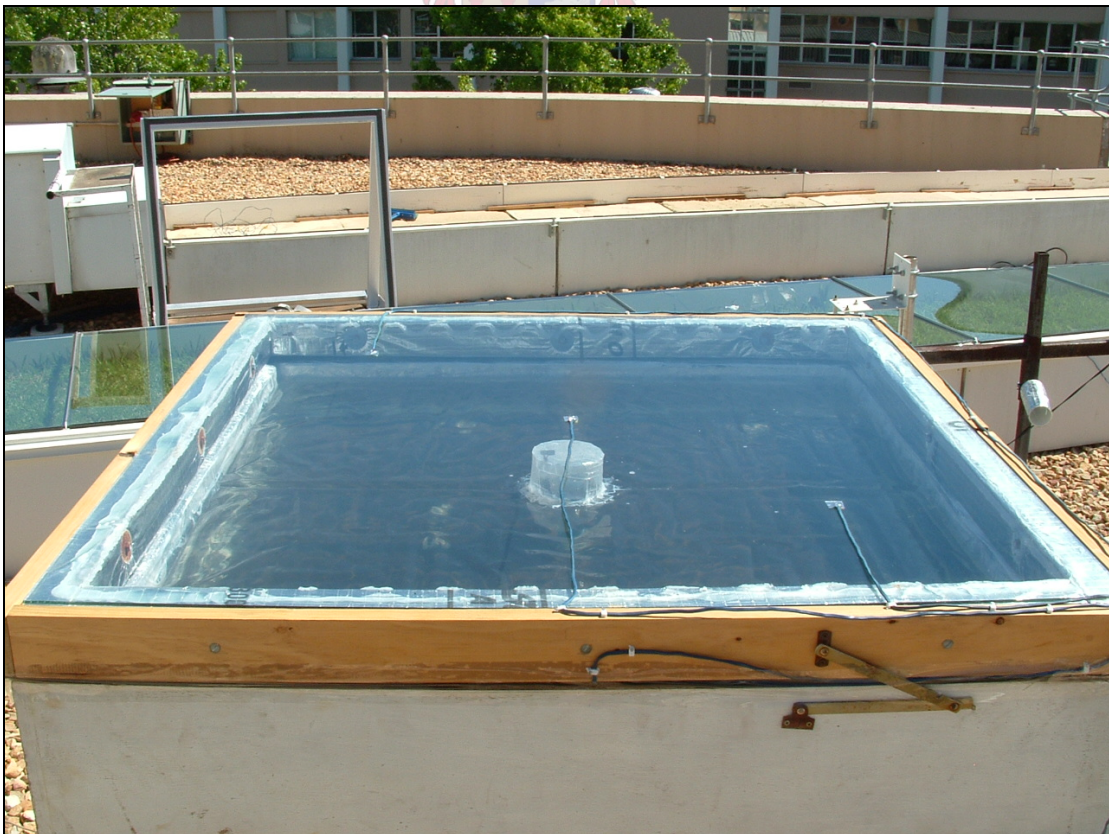


Figure C.3: Solar collector with plastic-covered water tank.

## C.4 Numerical example (section 3.3)

Table C.2 supplies the measured experimental data and apparatus parameters applicable to the water tank between 11.500 and 11.650 solar time on the 12<sup>th</sup> of January 2005. The predicted mean water temperature and glass cover temperature were found to be 329.3403 K and 310.8348 K respectively. As before, all numerical data listed has been averaged over a period of ten minutes.

Table C.2: Experimental data and physical parameters of plastic covered water tank.

Predicted glass cover temperature	$T_c$	37.6848 °C (310.8348 K)
Predicted mean water temperature	$T_w^i$	56.1903 °C (329.3403 K)
Predicted previous mean water temperature	$T_w^{i-1}$	55.5806 °C (328.7306 K)
Ambient air temperature	$T_a$	30.81 °C (303.96 K)
Dew-point temperature	$T_{dp}$	16.03 °C
Wind speed	$v_w$	2.09 m.s <sup>-1</sup>
Atmospheric pressure	$p_a$	100550 Pa
Total incident solar radiation	$I_h$	1057.757 W.m <sup>-2</sup>
Water tank surface area	$A$	1 m <sup>2</sup>
Air gap height	$t_a$	0.100 m
Depth of water tank	$t_w$	0.170 m
Long-wave emissivity of plastic film	$\epsilon_f$	0.88
Long-wave emissivity of glass cover	$\epsilon_c$	0.9
Time interval - local		11h23 – 11h32
Average time - local	$\Psi$	12.458 h
Average time - solar		11.575 h
Measured glass cover temperature	$T_{cm}$	42.5869 °C (315.7369 K)
Measured mean water temperature	$T_{wm}$	54.8409 °C (327.9909 K)
Location latitude angle	$\Phi$	33.98 °S
Location longitude angle	$\Phi_l$	18.85 °E
South African standard meridian	$\Phi_m$	30.00 °E

Employing the method described in section 3.3.2, the measured diffuse radiation was found to be roughly 6.5% of the total solar radiation, ie.

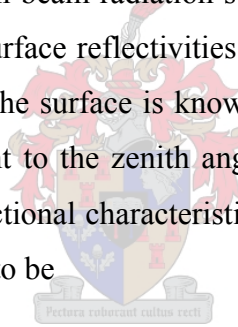
$$I_{hd} = 0.065 I_h = 0.065 \cdot 1057.757 = 68.754 \text{ W.m}^{-2}$$

This means that the rest of the total solar radiation was represented by the beam component.

$$I_{hb} = I_h - I_{hd} = 1057.757 - 68.754 = 989.003 \text{ W.m}^{-2}$$

However, since the surface of the glass cover is  $1\text{m}^2$  the above radiation components could simply be written as 68.754 W and 989.003 W respectively.

Determining the angle at which beam radiation strikes a surface is critical, particularly when calculations regarding surface reflectivities are considered. This angle, measured with respect to the normal of the surface is known as the incidence angle, which for a horizontal surface is equivalent to the zenith angle. Appendix A contains all relevant information regarding the directional characteristics of sunlight. The angle of incidence in this particular case is found to be



$$\theta_z = 13.605^\circ$$

It is now possible the numerical value of the incidence angle to be used in conjunction with equation (D.9) from Appendix D to determine the appropriate interface reflectivities.

The beam reflectivity for the air-glass interface is

$$\begin{aligned} \rho_{bc} &= \frac{1}{2} \left[ \frac{\tan^2(13.605 - \sin^{-1}(\sin 13.605/1.526))}{\tan^2(13.605 + \sin^{-1}(\sin 13.605/1.526))} + \frac{\sin^2(13.605 - \sin^{-1}(\sin 13.605/1.526))}{\sin^2(13.605 + \sin^{-1}(\sin 13.605/1.526))} \right] \\ &= 0.043418 \end{aligned}$$

while the beam reflectivity of the air-plastic film interface can be found to be

$$\begin{aligned}\rho_{baf} &= \frac{1}{2} \left[ \frac{\tan^2(13.605 - \sin^{-1}(\sin 13.605/1.6))}{\tan^2(13.605 + \sin^{-1}(\sin 13.605/1.6))} + \frac{\sin^2(13.605 - \sin^{-1}(\sin 13.605/1.6))}{\sin^2(13.605 + \sin^{-1}(\sin 13.605/1.6))} \right] \\ &= 0.053316\end{aligned}$$

The beam reflectivity for the air-water interface is determined below for evaluating the influence of the air layer beneath the plastic film.

$$\begin{aligned}\rho_{bw} &= \frac{1}{2} \left[ \frac{\tan^2(13.605 - \sin^{-1}(\sin 13.605/1.333))}{\tan^2(13.605 + \sin^{-1}(\sin 13.605/1.333))} + \frac{\sin^2(13.605 - \sin^{-1}(\sin 13.605/1.333))}{\sin^2(13.605 + \sin^{-1}(\sin 13.605/1.333))} \right] \\ &= 0.020410\end{aligned}$$

Similarly, the reflectivity of the film-water interface can be calculated with the aid of equation (D.11) and the incidence angle.

$$\begin{aligned}\rho_{bfw} &= \frac{1}{2} \left[ \frac{\tan^2(\sin^{-1}(\sin 13.605/1.6) - \sin^{-1}(\sin 13.605/1.333))}{\tan^2(\sin^{-1}(\sin 13.605/1.6) + \sin^{-1}(\sin 13.605/1.333))} \right] \\ &+ \frac{1}{2} \left[ \frac{\sin^2(\sin^{-1}(\sin 13.605/1.6) - \sin^{-1}(\sin 13.605/1.333))}{\sin^2(\sin^{-1}(\sin 13.605/1.6) + \sin^{-1}(\sin 13.605/1.333))} \right] \\ &= 0.008293\end{aligned}$$



Now to determine the diffuse reflectivities, the same equations are used with an effective incidence angle of  $60^\circ$ .

$$\begin{aligned}\rho_{dc} &= \frac{1}{2} \left[ \frac{\tan^2(60 - \sin^{-1}(\sin 60/1.526))}{\tan^2(60 + \sin^{-1}(\sin 60/1.526))} + \frac{\sin^2(60 - \sin^{-1}(\sin 60/1.526))}{\sin^2(60 + \sin^{-1}(\sin 60/1.526))} \right] \\ &= 0.093468\end{aligned}$$

$$\begin{aligned}\rho_{daf} &= \frac{1}{2} \left[ \frac{\tan^2(60 - \sin^{-1}(\sin 60/1.6))}{\tan^2(60 + \sin^{-1}(\sin 60/1.6))} + \frac{\sin^2(60 - \sin^{-1}(\sin 60/1.6))}{\sin^2(60 + \sin^{-1}(\sin 60/1.6))} \right] \\ &= 0.105240\end{aligned}$$

$$\rho_{dw} = \frac{1}{2} \left[ \frac{\tan^2(60 - \sin^{-1}(\sin 60/1.333))}{\tan^2(60 + \sin^{-1}(\sin 60/1.333))} + \frac{\sin^2(60 - \sin^{-1}(\sin 60/1.333))}{\sin^2(60 + \sin^{-1}(\sin 60/1.333))} \right]$$

$$= 0.059690$$

$$\begin{aligned} \rho_{dfw} &= \frac{1}{2} \left[ \frac{\tan^2(\sin^{-1}(\sin 60/1.6) - \sin^{-1}(\sin 60/1.333))}{\tan^2(\sin^{-1}(\sin 60/1.6) + \sin^{-1}(\sin 60/1.333))} \right] \\ &\quad + \frac{1}{2} \left[ \frac{\sin^2(\sin^{-1}(\sin 60/1.6) - \sin^{-1}(\sin 60/1.333))}{\sin^2(\sin^{-1}(\sin 60/1.6) + \sin^{-1}(\sin 60/1.333))} \right] \\ &= 0.010742 \end{aligned}$$

The transmissivity due to absorptance of the cover and the plastic film, due to beam radiation can be calculated as follows according to equation (D.13).

$$\tau_{abc} = e^{-C_{ect_c} / \cos(\sin^{-1}(n_a \sin \theta_b / n_c))} = e^{-13 \cdot 0.004 / \cos(\sin^{-1}(\sin 13.605 / 1.526))} = 0.948732$$

$$\tau_{abf} = e^{-C_{ef t_f} / \cos(\sin^{-1}(n_a \sin \theta_b / n_f))} = e^{-200 \cdot 0.0002 / \cos(\sin^{-1}(\sin 21.252 / 1.6))} = 0.960367$$

As in the case of the diffuse reflectivities, the transmissivity due to absorptance for diffuse solar radiation is calculated in the same manner as the beam transmissivities, but with an incidence angle of  $60^\circ$ .

$$\tau_{adc} = e^{-C_{ect_c} / \cos(\sin^{-1}(n_a \sin 60 / n_c))} = e^{-13 \cdot 0.004 / \cos(\sin^{-1}(\sin 60 / 1.526))} = 0.938798$$

$$\tau_{adf} = e^{-C_{ef t_f} / \cos(\sin^{-1}(n_a \sin 60 / n_f))} = e^{-200 \cdot 0.0002 / \cos(\sin^{-1}(\sin 60 / 1.6))} = 0.953543$$

The extinction coefficients used in the above calculations were determined by *Lombaard* (2002) and were confirmed by the author with experimental tests.

To evaluate the convective heat transfer from the glass cover to the environment, the thermophysical properties of the air at a mean cover / ambient temperature are required.

$$T_{am} = \frac{(T_c + T_a)}{2} = \frac{(310.8348 + 303.96)}{2} = 307.3974 \text{ K}$$

Density,  $\rho$  1.139407 kg.m<sup>-3</sup>

Specific heat capacity,  $c_p$  1007.243 J.kg<sup>-1</sup>.K<sup>-1</sup>

Thermal conductivity,  $k$        $0.026792 \text{ W.m}^{-1}.\text{K}^{-1}$

Dynamic viscosity,  $\mu$     $1.880767 \cdot 10^{-5} \text{ kg.m}^{-1}.\text{s}^{-1}$

Similarly it is necessary that the same thermophysical properties be determined to calculate the natural convective heat transfer between the water surface and the glass plate. These properties are determined at the mean temperature between the two surfaces as shown below.

$$T_{cm} = \frac{(T_c + T_w)}{2} = \frac{(310.8348 + 329.3403)}{2} = 320.0876 \text{ K}$$

Density,  $\rho$                        $1.094234 \text{ kg.m}^{-3}$

Specific heat capacity,  $c_p$      $1007.858 \text{ J.kg}^{-1}.\text{K}^{-1}$

Thermal conductivity,  $k$        $0.027762 \text{ W.m}^{-1}.\text{K}^{-1}$

Dynamic viscosity,  $\mu$     $1.938320 \cdot 10^{-5} \text{ kg.m}^{-1}.\text{s}^{-1}$

Then with the use of these three values, the Prandtl number can be determined.

$$\text{Pr} = \frac{\mu \cdot c_p}{k} = \frac{1.938320 \cdot 10^{-5} \cdot 1007.858}{0.027762} = 0.703667$$

The natural convective heat transfer within the enclosed air space requires that the Grashof number be calculated. According to *Mills* (1992), the effective length used in the calculation of the Grashof number in the case of a thin air enclosure can be taken as the distance between the two opposing surfaces.

$$\begin{aligned} Gr_{cw} &= \frac{2(T_w - T_c)g t_a^3 \rho_{cw}^2}{(T_w + T_c)\mu_{cw}^2} && \text{(C.16)} \\ &= \frac{2 \cdot (329.3403 - 310.8348) \cdot 9.81 \cdot 0.1^3 \cdot 1.094234^2}{(329.3403 + 310.8348) \cdot (1.938320 \cdot 10^{-5})^2} = 1807468.057 \end{aligned}$$

The density and specific heat capacity of the water at the mean temperature,  $T_w$  are provided below, as determined according to *Kröger* (1998).

Water density  $\rho_w = 985.174 \text{ kg.m}^{-3}$

Water specific heat capacity  $c_{pw} = 4181.798 \text{ J.kg}^{-1}.\text{K}^{-1}$

It is now possible to substitute all the necessary values into the energy balance on the glass cover given by equation (3.3).

$$\begin{aligned} & \frac{(1-0.043418)(1-0.948732)}{1-0.043418 \cdot 0.948732} \cdot 989.003 + \frac{(1-0.093468)(1-0.938798)}{1-0.093468 \cdot 0.938798} \cdot 68.754 \\ & + 5.67 \cdot 10^{-8} \left( \frac{1}{0.9} + \frac{1}{0.88} - 1 \right)^{-1} (T_w^4 - T_c^4) \\ & + \left[ 1 + 1.44 \left[ 1 - \frac{1708}{1807468.057 \cdot 0.703667} \right] + \left[ \left( \frac{1807468.057 \cdot 0.703667}{5830} \right)^{\frac{1}{3}} - 1 \right] \right] \frac{0.027762}{0.1} \\ & (T_w - T_c) = \frac{\left[ \frac{0.2106 + 0.0026 \cdot 2.09 \left[ \frac{1.139407 \cdot 307.3974}{1.880767 \cdot 10^{-5} \cdot 9.81 \cdot (310.8348 - 303.96)} \right]^{\frac{1}{3}}}{\left[ \frac{1.880767 \cdot 10^{-5} \cdot 307.3974}{9.81 \cdot (310.8348 - 303.96) \cdot 1007.243 \cdot 0.026792^2 \cdot 1.139407^2} \right]^{\frac{1}{3}}} \right]}{\cdot (T_c - 303.96) + 0.9 \cdot 5.67 \cdot 10^{-8} (T_c^4 - (0.727 + 0.006 \cdot 16.03) \cdot 303.96^4)} \end{aligned}$$

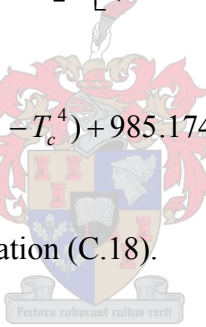
This equation can then be further simplified to

$$\begin{aligned} & 50.5884 + 4.1814 + 4.5452 \cdot 10^{-8} (T_w^4 - T_c^4) + 2.0675 \cdot (T_w - T_c) = 12.4627 \cdot (T_c - 303.96) \\ & + 5.1030 \cdot 10^{-8} (T_c^4 - 289.5277^4) \end{aligned} \quad (\text{C.17})$$

Similarly, equation (3.4) representing the energy balance on the water tank can be completed as shown below.

$$\begin{aligned}
 & \left[ \frac{(1-0.043418)^2 \cdot 0.948732}{(1-0.043418^2 \cdot 0.948732^2)} \right] \left[ 1 - \frac{0.053316 + (1-2 \cdot 0.053316) \cdot 0.008293 \cdot 0.960367^2}{1-0.053316 \cdot 0.008293 \cdot 0.960367^2} \right] \\
 & \cdot \left[ 1 - 0.093468 \frac{0.053316 + (1-2 \cdot 0.053316) \cdot 0.008293 \cdot 0.938798^2}{1-0.053316 \cdot 0.008293 \cdot 0.938798^2} \right]^{-1} \cdot (1-0.020410) \cdot 989.003 \\
 & + \left[ \frac{(1-0.093468)^2 \cdot 0.938798}{(1-0.093468^2 \cdot 0.938798^2)} \right] \left[ 1 - \frac{0.105240 + (1-2 \cdot 0.105240) \cdot 0.010742 \cdot 0.953543^2}{1-0.105240 \cdot 0.010742 \cdot 0.953543^2} \right] \\
 & \cdot \left[ 1 - 0.093468 \cdot \frac{0.105240 + (1-2 \cdot 0.105240) \cdot 0.010742 \cdot 0.953543^2}{1-0.010742 \cdot 0.953543^2} \right]^{-1} (1-0.059690) \cdot 68.754 \\
 & = \left[ 1 + 1.44 \left[ 1 - \frac{1708}{1807468.057 \cdot 0.703667} \right] + \left[ \left( \frac{1807468.057 \cdot 0.703667}{5830} \right)^{1/3} - 1 \right] \right] \frac{0.027762}{0.1} (T_w - T_c) \\
 & + 5.67 \cdot 10^{-8} \left( \frac{1}{0.9} + \frac{1}{0.88} - 1 \right)^{-1} (T_w^4 - T_c^4) + 985.174 \cdot 0.170 \cdot 4181.798 \frac{(T_w - 328.7306)}{60 \cdot 10}
 \end{aligned}$$

Which can be simplified into equation (C.18).



$$812.8616 + 47.9190 = 2.0675 \cdot (T_w - T_c) + 4.5452 \cdot 10^{-8} \cdot (T_w^4 - T_c^4) \quad (C.18)$$

$$+ 1167.2765 \cdot (T_w - 328.7306)$$

Solving equations (C.17) and (C.18) simultaneously produces predicted glass cover- and mean water temperatures of 310.8348 K and 329.3403 K. Unfortunately these temperatures are found to differ by quite a substantial margin from the measured glass and water temperatures of 315.7369 K and 327.9909 K.

## APPENDIX D

# Water tank solar characteristics

### D.1 Cover solar characteristics

### D.2 Absorber plate effective absorptivity

---

If the water tank is to be accurately modelled, it is necessary that the behaviour of the solar radiation be fully understood. The components into which the solar radiation that strikes the solar collector is divided will be explained in detail in the section that follows.

### D.1 Cover solar characteristics.

The literature provides two alternate sets of equations for determining the solar characteristics of a non-opaque cover. *Duffie and Beckman* (1991) provide equations that are only applicable to a cover that has the same media at the upper and lower interfaces, while *Modest* (1993) provides similar equations without the afore-mentioned limitation.

*Mills* (1992) states that the sum of the effective reflectivity, transmissivity and absorptivity of a transparent medium is equal to one. Summing the two sets of equations given in the literature (*Duffie and Beckman* (1991) and *Modest* (1993)), it was found that those provided by the latter added up to one. Thus, the equations provided by *Modest* (1993) will be used to determine the solar characteristics of the glass cover.

Figure D.1 shows the behaviour of solar radiation that strikes a cover of thickness  $t_c$ . Note that  $\rho$  represents the interface reflectivity between the cover and the air, and  $\tau_a$  the transmittance due to absorptance. The symbols  $n_1$ ,  $n_2$  and  $n_3$  represent the medium at the upper interface, the material from which the cover is constructed and the medium at the lower interface. Equations (D.1), (D.2) and (D.3) are recommended by *Modest* (1993)

for determining the effective reflectivity  $\rho'$ , effective transmissivity  $\tau'$  and effective absorptivity  $\alpha'$  of a transparent cover.

$$\rho' = \rho_{12} + \frac{\rho_{23} \cdot (1 - \rho_{12})^2 \cdot \tau_\alpha^2}{1 - \rho_{12} \cdot \rho_{23} \cdot \tau_\alpha^2} \quad (\text{D.1})$$

$$\tau' = \frac{(1 - \rho_{12}) \cdot (1 - \rho_{23}) \cdot \tau_\alpha}{1 - \rho_{12} \cdot \rho_{23} \cdot \tau_\alpha^2} \quad (\text{D.2})$$

$$\alpha' = \frac{(1 - \rho_{12}) \cdot (1 + \rho_{23} \cdot \tau_\alpha) \cdot (1 - \tau_\alpha)}{1 - \rho_{12} \cdot \rho_{23} \cdot \tau_\alpha^2} \quad (\text{D.3})$$

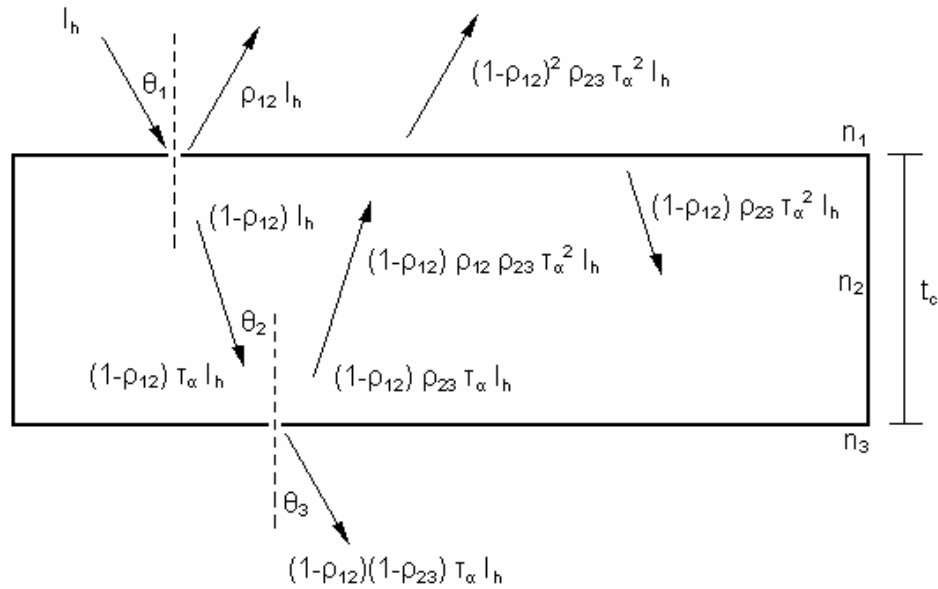


Figure D.1: Solar radiation striking a cover of thickness  $t_c$  and being either transmitted, absorbed or reflected.

However, if the media above and below the cover is the same then these equations simplify to those given below in equations (D.4), (D.5) and (D.6).

$$\rho' = \rho \left[ 1 + \frac{(1 - \rho)^2 \cdot \tau_\alpha^2}{1 - \rho^2 \cdot \tau_\alpha^2} \right] \quad (\text{D.4})$$

$$\tau' = \frac{(1 - \rho)^2 \cdot \tau_\alpha}{1 - \rho^2 \cdot \tau_\alpha^2} \quad (\text{D.5})$$

$$\alpha' = \frac{(1-\rho) \cdot (1-\tau_a)}{1-\rho \cdot \tau_a} \quad (\text{D.6})$$

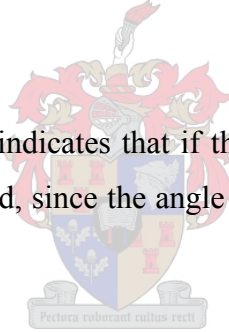
Now if these values are to be determined it is first necessary for the reflectivities and transmissivity due to absorption to be determined. Both are functions of incidence angle  $\theta_2$  and the refraction indices.

*Modest* (1993) recommends the use of Fresnel's equation to determine the interface reflectivities as given by equation (D.7).

$$\rho_{12} = \frac{1}{2} \left[ \frac{\tan^2(\theta_1 - \theta_2)}{\tan^2(\theta_1 + \theta_2)} + \frac{\sin^2(\theta_1 - \theta_2)}{\sin^2(\theta_1 + \theta_2)} \right] \quad (\text{D.7})$$

The incidence is given by  $\theta_1$  in this case, while  $\theta_2$  represents the refractive angle of the interface.

Observation of equation (D.7) indicates that if the refractive angle is determined, then the reflectivity can be calculated, since the angle of incidence has already been defined in Appendix A.



With the aid of Snell's law and the incidence angle and refractive indices, the angle of refraction can be determined.

$$\theta_2 = \arcsin\left(\frac{n_1 \sin \theta_1}{n_2}\right) \quad (\text{D.8})$$

Equation (D.8) can be substituted into (D.7) with the result below

$$\rho_{12} = \frac{1}{2} \left[ \frac{\tan^2(\theta_1 - \arcsin(n_1 \sin \theta_1 / n_2))}{\tan^2(\theta_1 + \arcsin(n_1 \sin \theta_1 / n_2))} + \frac{\sin^2(\theta_1 - \arcsin(n_1 \sin \theta_1 / n_2))}{\sin^2(\theta_1 + \arcsin(n_1 \sin \theta_1 / n_2))} \right] \quad (\text{D.9})$$

Similarly at the lower surface interface, the refractive angle  $\theta_3$  is

$$\theta_2 = \arcsin\left(\frac{n_2 \sin \theta_2}{n_3}\right) = \arcsin\left(\frac{n_1 \sin \theta_1}{n_3}\right) \quad (\text{D.10})$$

which results in a lower interface reflectivity of

$$\rho_{12} = \frac{1}{2} \left[ \frac{\tan^2(\arcsin(n_1 \sin \theta_1 / n_2) - \arcsin(n_1 \sin \theta_1 / n_3))}{\tan^2(\arcsin(n_1 \sin \theta_1 / n_2) + \arcsin(n_1 \sin \theta_1 / n_3))} \right] + \frac{1}{2} \left[ \frac{\sin^2(\arcsin(n_1 \sin \theta_1 / n_2) - \arcsin(n_1 \sin \theta_1 / n_3))}{\sin^2(\arcsin(n_1 \sin \theta_1 / n_2) + \arcsin(n_1 \sin \theta_1 / n_3))} \right] \quad (\text{D.11})$$

Now if equations (D.4), (D.5) and (D.6) are to be evaluated it remains for the transmissivity due to absorptance to be determined. This can be found according to Bouguer's law for a partially transparent medium with an extinction coefficient  $C_e$  and thickness  $t_c$ .

$$\tau_\alpha = e^{-C_e t_c / \cos(\theta_2)} \quad (\text{D.12})$$

This can be rewritten with the use of Snell's law as in equation (D.8) to give the following result.

$$\tau_\alpha = e^{-C_e t_c / \cos(\arcsin(n_1 \sin \theta_1 / n_2))} \quad (\text{D.13})$$

It has been shown in Appendix A how to determine the incidence angle, then with the use of the equations listed above it is possible to calculate the effective reflectivity, transmissivity and absorptivity of any non-opaque cover of thickness  $t_c$ .

## D.2 Absorber plate effective solar absorptivity.

Since the solar properties of a solar collector cover have been discussed in section D.2, it only remains for the solar absorptivity of the absorber plate to be evaluated.

Figure D.2 shown below presents the incident solar radiation penetrating the cover and being absorbed and reflected numerous times from both the absorber plate and solar collector cover.

If the assumption is made that the reflected energy is diffuse and if multiple reflections are taken into consideration, then according to *Duffie and Beckman* (1991) the transmittance-absorptance product for the absorber plate shown in figure D.2 is

$$(\tau' \alpha_p) = \alpha_p \left( \frac{\tau'}{1 - (1 - \alpha_p) \cdot \rho_d} \right) \quad (D.14)$$

However, if the definition of the effective transmissivity as given by *Modest* in equation (D.5) is substituted into equation (D.14) then the transmittance-absorptance product can be rewritten as

$$(\tau' \alpha_p) = \left( \frac{\alpha_p}{1 - (1 - \alpha_p) \cdot \rho_d} \right) \cdot \left[ \frac{(1 - \rho)^2 \tau_a}{1 - \rho^2 \tau_a^2} \right] \quad (D.15)$$

Note that  $\alpha_p$  is the absorptance of the absorber plate and that is  $\rho_d$  the diffuse reflectivity of the underside of the cover.

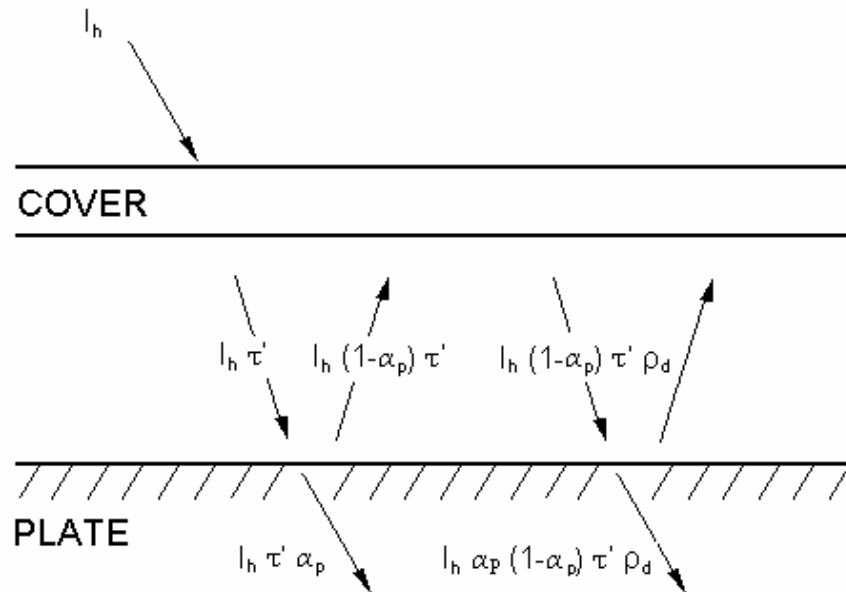


Figure D.2: Effective transmittance-absorptance product.

## APPENDIX E

# Greenhouse sunlight properties

### E.1 Area of transmitted sunlight

---

In Chapter 4 it is stated that for the total solar input to a panel of an all-glass structure to be calculated, it becomes necessary to determine what portion of the sunlight indirectly incident on a particular window has been transmitted through which window in direct sunlight. Consider figure E.1.

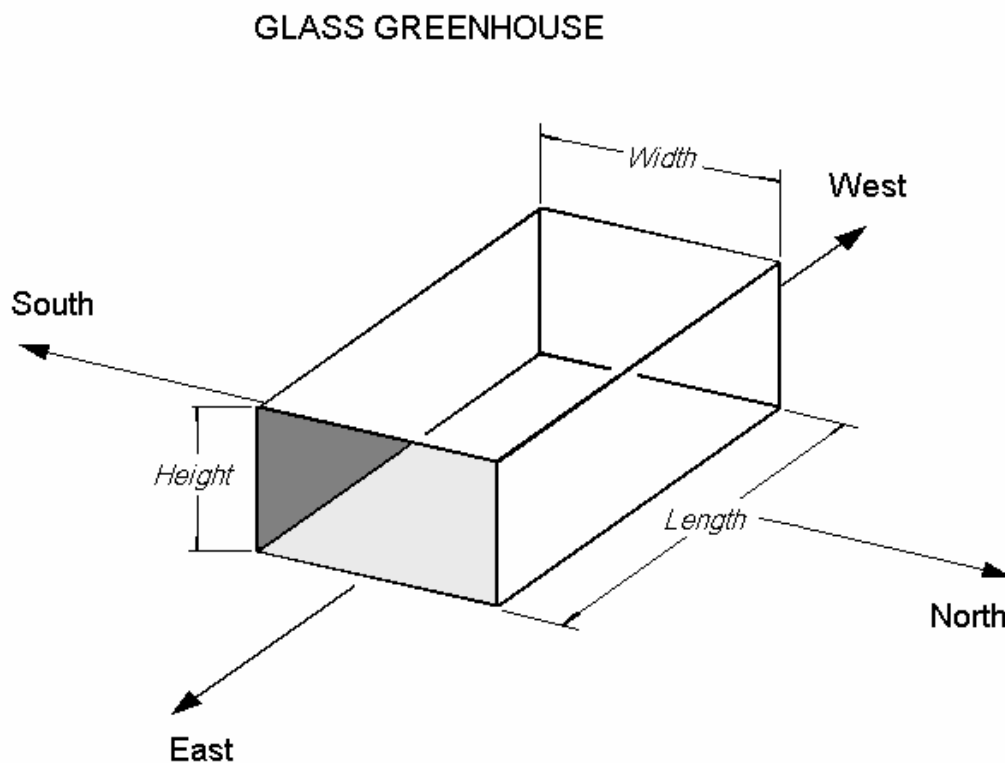


Figure E.1: Relative orientation of glass greenhouse.

The above statement is explained in the following manner: All four walls, the roof and floor receive sunlight in the above structure. However, if the sun is shining in the line of sight then the eastern- and northern walls and roof will receive direct sunlight, while the floor, southern- and western walls receive light that has been transmitted

through the other surfaces. The total sunlight incident on a surface in indirect sunlight can be evaluated by equation (E.1). It means that the total effective transmissivity is the sum of the transmissivity of each window multiplied by the associated area, the sum is then divided by the total area of the window in indirect sunlight.

$$\tau' = \frac{\sum_1^n \tau_n \cdot A_n}{A_{tot}} \quad (E.1)$$

### E.1 Area of transmitted sunlight.

#### Condition 1:

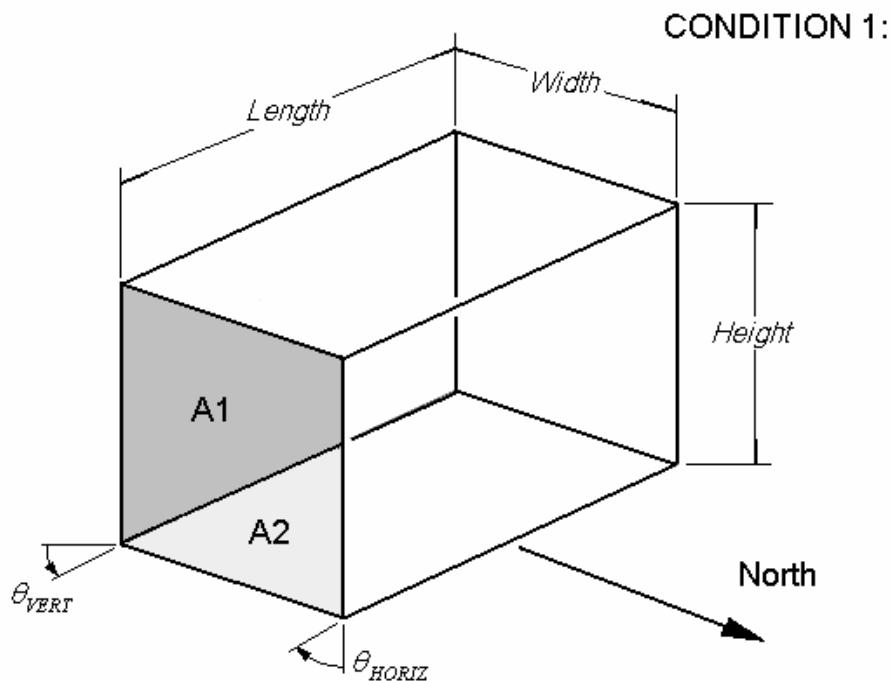


Figure E.2: Sketch of condition 1.

Light passes through the eastern wall and strikes the floor and south wall of the greenhouse. If the incident light on the eastern wall is broken up into horizontal and vertical components, as shown in the sketch, then case 1 is applicable between the following limits.

- $\tan^{-1}(\text{width}/\text{length}) < \theta_{HORIZ} < 90^\circ$

- $0^\circ < \theta_{VERT} < \tan^{-1} ((\text{height}/\text{width}) \tan \theta_{HORIZ}) < \theta_{HORIZ} < 90^\circ$

While the appropriate areas are:

$$A1 = (\text{height width}) / \tan \theta_{HORIZ} - 0.5 \text{ width}^2 \tan \theta_{VERT} / (\tan \theta_{HORIZ})^2$$

$$A2 = 0.5 \text{ width}^2 / \tan \theta_{HORIZ}$$

**Condition 2:**

Light strikes the eastern wall as in condition 1, however different limits are now applicable.

- $0^\circ < \theta_{HORIZ} < \tan^{-1} ((\text{width}/\text{height}) \tan \theta_{VERT})$
- $\tan^{-1}(\text{height}/\text{length}) < \theta_{VERT} < 90^\circ$

The appropriate areas are:

$$A1 = 0.5 \text{ height}^2 / \tan \theta_{VERT}$$

$$A2 = (\text{height width}) / \tan \theta_{VERT} - 0.5 \text{ height}^2 \tan \theta_{HORIZ} / (\tan \theta_{VERT})^2$$

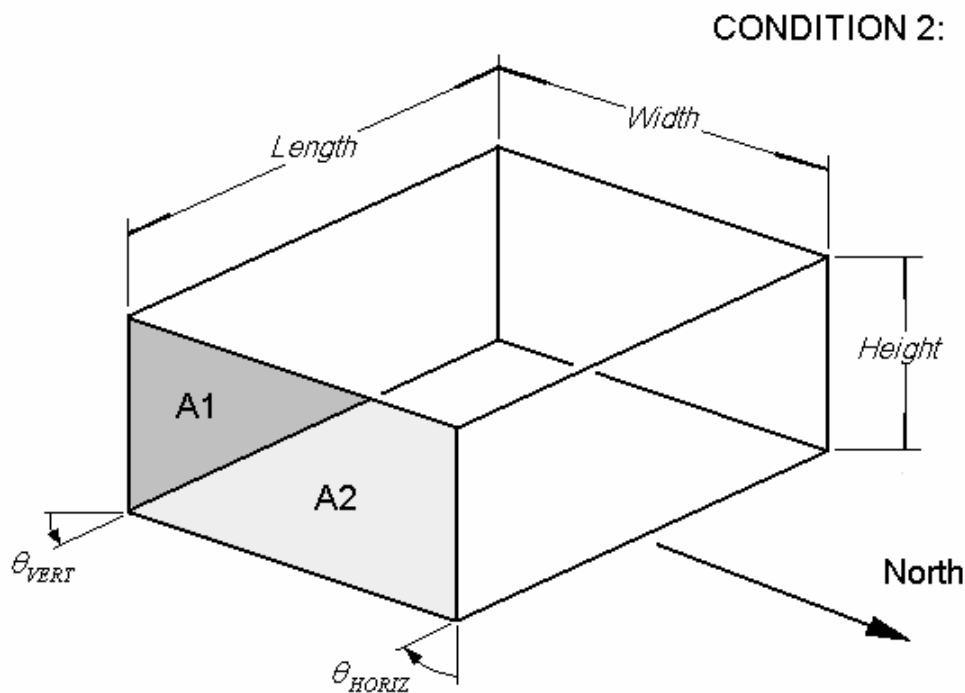


Figure E.3: Sketch of condition 2.

Condition 3:

Light passing through the eastern window now strikes the floor, south window and western window. This condition occurs under the following limitations.

- $0^\circ < \theta_{HORIZ} < \tan^{-1}(\text{width}/\text{length})$
- $0^\circ < \theta_{VERT} < \tan^{-1}(\text{height}/\text{length})$

The appropriate areas are:

$$A1 = \text{length} (\text{height} - 0.5 \text{ length} \tan \theta_{VERT})$$

$$A2 = \text{length} (\text{width} - 0.5 \text{ length} \tan \theta_{HORIZ})$$

$$A3 = (\text{width} - \text{length} \tan \theta_{HORIZ}) (\text{height} - \text{length} \tan \theta_{VERT})$$

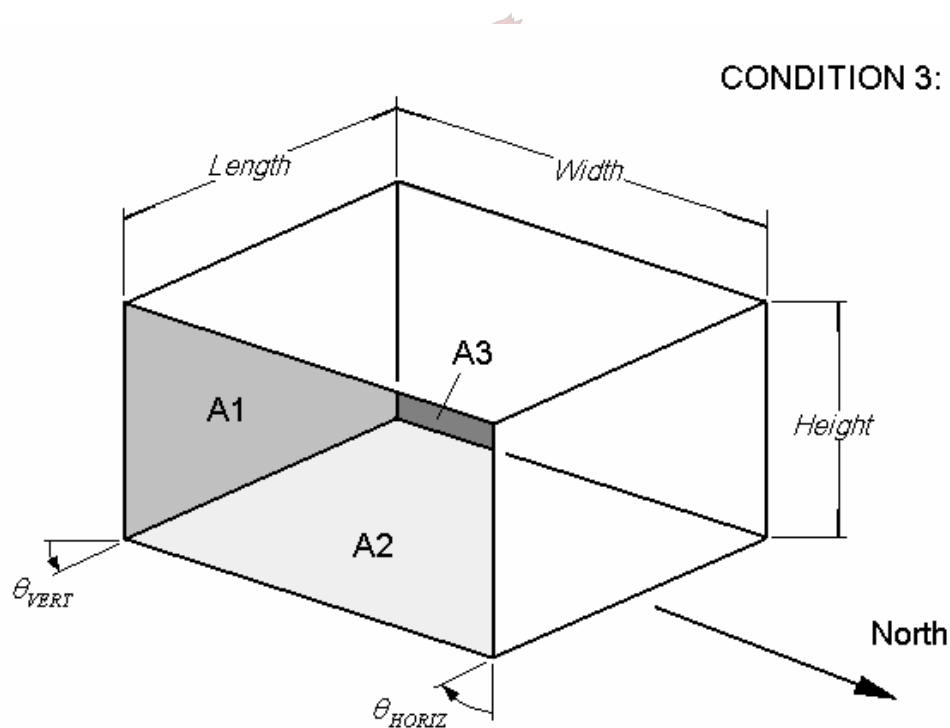


Figure E.4: Sketch of condition 3.